UCRL-18145

cy. 2

University of California

Ernest O. Lawrence Radiation Laboratory

SEMICONDUCTOR ELECTROCHEMISTRY

Heinz Gerischer

October 1968

DISCLAIMER

Submitted as chapter in
Advances in High Temperature
Chemistry

UCRL-18145
Preprint

UNIVERSITY OF CALIFORNIA

Lawrence Radiation Laboratory
Berkeley, California

AEC Contract No. W-7405-eng-48

SEMICONDUCTOR ELECTROCHEMISTRY

Heinz Gerischer°

October 1968

TABLE OF CONTENTS

I. GENERAL

A. Differences Between Metal and Semiconductor Electrodes

The thermodynamics of galvanic cells are similar for metal or semiconductor electrodes. But, in the kinetics of the electrode reactions, the type of electronic conductance found in the electrode changes considerably the basic concepts for describing charge-transfer processes at the electrode surface. Emphasis, therefore, is given in this chapter to the electrode kinetics and closely related problems. It will be seen that there are some unique potentialities for the understanding of the role of electron energy states in heterogeneous electrode reactions.

Phenomenologically, the striking difference between a semiconductor and a metal lies in the much lower concentration of mobile electrons available for electric conduction in semiconductors. Two kinds of mobile electronic charge carriers can be distinguished, electrons in the conduction band and holes in the valence band, the latter behaving like positively charged particles of about the electron mass. These two differences cause the main distinctions in the electrode behavior of semiconductors.

Because of the lower carrier concentrations, the semiconductor cannot be treated in electrostatics like a conductor of infinite conductivity. This restricts the possible accumulation of charge carriers in the surface of the crystal when the electrode is charged by means of an external counter charge in the adjacent electrolyte as one does in polarizing an electrolytic cell. The interior remains charge free in a metal; in a semiconductor however, the excess charge extends fairly far into the interior over the so-called "space charge layer" and the electrical forces (field strength) drop to much lower values than in a metal-electrolyte interface.

The charge distribution just under a semiconductor surface is very similar to that of a diffuse double layer in a dilute electrolyte. Carrier concentrations of 10^{13} to $10^{17}/cm^3$ are quite normal in semiconductors compared with $10^{19}/cm^3$ for a 0.01-molar electrolyte solution. Since the extension of a diffuse double layer, according to the Gouy-Chapman theory, is proportional to the inverse square root of the carrier concentration, this numerical relation indicates that the electrolyte at a semiconductor-electrolyte interface is usually much closer to an infinitely good conductor than the semiconductor, and, therefore the charge distribution is inverted to that of a metal electrode. Figure 1 shows a comparison between the course followed by the electrical potential for a semiconductor and for a metal electrode at the same potential difference between electrode and electrolyte.

At a metal electrode, the electrical field strength in the interface varies for a 1-volt change in the applied voltage by an order of 10^7 volt/cm or more. These enormous electrostatic forces change the energy barrier in shape and height and lead to a variation of rate constants for anodic and cathodic processes, as was discussed in Chapter III of this volume.

The variation of field strength in the surface of a semiconductor is normally much smaller. Therefore, the influence of electrostatic forces on the energy barriers for charge-transfer processes are usually negligible. In place of this, the concentration of electronic charge carriers in the surface itself, which varies by orders of magnitude with changing voltage, becomes the important factor for the rate of all reactions in which these charge carriers take part directly. And only processes in which the electronic carriers are involved as reactants can be influenced by the applied voltage.

In other words, the applied voltage at a semiconductor electrode controls the probability factor (entropy factor) of a surface reaction primarily and not, as at metal electrodes, the energy factor.

This direct participation of the mobile electronic charge carriers leads to the other important aspect of semiconductor electrochemistry. Since we have two types of electronic carriers, electrons and holes, the question arises whether these carriers behave differently or not. Experimental evidence has shown that there are indeed extreme differences in the reaction behavior of electrons and holes, or more precisely, since holes are fictitious particles, between electrons in the conduction and in the valence band. This can be well understood from theoretical reasons based on the great difference in binding energy for these separate energy states in the crystal.

Electrons and holes represent excited electronic states of the crystal. This leads to a close connection between electrode reactions and photochemical processes at semiconductors, which can be seen in the fact that illumination of the electrode surface is one of the most important ways of qualifying the type of electronic interaction in charge-transfer reactions.

B. Experimental Problems and Special Techniques

In general, semiconductor electrode reactions are rather irreversible. Equilibrium data, therefore, must usually be derived from thermodynamic calculations.

For studying kinetics, all the various techniques developed for metal electrode investigations can be employed. Stationary or cyclic

current voltage curves, as well as transients of current or voltage under controlled conditions, are among the most generally applied modes of investigation. Because the carrier distribution in the space-charge layer is one of the most important factors for any analysis of the reaction mechanism, impedance measurements or relaxation analyses of short pulses play a key role in many experiments.

In analyzing correlations between current and voltage, unavoidable ohmic resistances in the electrode itself can cause serious errors if not corrected to sufficient accuracy. Contacts between metals and the semiconducting electrode used for current supply must be controlled for ohmic behavior or, better, the potential must be measured with the help of an auxiliary connection which is not loaded with the current for electrolysis.

The properties of semiconductors depend to an enormous extent on impurity concentrations and must be controlled as well as possible. Since crystal size, surface orientation, and grain boundaries strongly influence the properties of semiconductors, reliable studies of semiconductor electrodes should be carried out with single crystals cut in definite orientations. After mechanical surface treatment, however, the damaged surface layers have to be removed by chemical or electrochemical etching, which gives reproducible surfaces although their real structures are not known in any detail.

The electronic characteristics of a semiconductor have to be known under working conditions. Normal semiconductor technology and research have made available a great number of techniques for defining the electronic properties under static and transient behavior. Such techniques -- like carrier concentration modulation by means of p-n junctions or illumination,

surface conductance studies, or photovoltage measurements -- can and must be combined with electrochemical techniques to obtain all necessary information. Examples are given later in connection with special problems.

As this chapter is merely a survey of fundamentals, many details must be omitted. The interested reader, therefore, may be referred to some more comprehensive reviews [Dewald (1959); Green (1959); Gerischer (1961); Holmes (1961); and Myamlin and Pleskov (1965)]. The physical concepts which have to be applied to semiconductor surfaces are comprehensively reviewed by Many et al., (1965) and Frankl (1967).

II. ELECTRICAL DOUBLE LAYER AT SEMICONDUCTOR-ELECTROLYTE INTERFACE

A. Charge Distribution and Differential Capacity

At a semiconductor-electrolyte interface, the conductance type changes from electronic to ionic. If no electrochemical reaction is available to act in the interface as a transmuter for the conductance mechanism, the interface represents a barrier for the flow of electric current. Electrical charges can then be accumulated at both sides of the interface and the electrode behaves like a condenser. This accumulation of charge is limited by leakage, i.e., electrochemical reactions which finally start when the electrical forces at the electrode surface exceed the respective critical values for the particular electrode reactions. As long as this leakage current is negligible or small compared with the rate of exchange of charge carriers between the space charge layer and the bulk, the charge distribution at both sides of the phase boundary can be described in terms of a condensor model with equilibrium charge distribution in both phases separately. The laws of electrostatics then control the course of electrical potential from one phase to the other. The model that fits best this situation is shown in Fig. 2 [compare also Boddy (1965), Harten (1964), and Memming and Schwandt(1967)].

This model represents the main different types of charges which contribute to the double layer:

(a) space charge of electrons and holes and of fixed, immobile donor or acceptor states in the lattice, q_{sc}.

(b) trapped charge in surface states, of both possible signs, q_{ss} (the sign of the surface-state charge can be opposite to the space charge).

(c) charges of adsorbed ions or ionized surface groups on the crystal, again of both possible signs, of amount q_{ad}.

(d) the ionic counter charge in the electrolyte, q_{el}.

Electroneutrality demands

$$q_{sc} + q_{ss} + q_{ad} + q_{el} = 0 \quad . \tag{1}$$

The spatial distribution of carriers in the semiconductor follows Boltzmann statistics for the mobile carriers, electrons and holes, as long as their concentration does not approach the range of degeneracy. The occupation of the donor or acceptor states as well as of surface states is described by Fermi statistics, compare, e.g., Hanney (1959), Shockley (1963), Spenke (1965). For ions adsorbed from the electrolyte, or surface groups that react with electrolyte components, again Boltzmann statistics have to be applied, modified by the restrictions due to a limited number of surface sites. By these basic laws, the correlations between charge density and electrostatic potential can be derived and compared with experimental data. Since the electrostatic potential cannot be measured directly, the most valuable information has been obtained from capacity measurements, to which we refer later.

1. Space-charge layer

We denote the electrostatic potential in the charge-free interior of the semiconductor with ϕ_i, and the equilibrium concentrations of electrons and holes in the interior may be n_0 and p_0, respectively. Between n_0 and p_0, we have the equilibrium correlation

$$n_0 \cdot p_0 = n_i^2 = N_C \cdot N_V \cdot \exp\left(-\frac{E_{gap}}{kT}\right), \tag{2}$$

where n_i = intrinsic concentration of electrons and holes,

N_C = effective density of states for the bottom of the conductance band,

N_V = effective density of states for the top of the valence band,

E_{gap} = energy gap between conductance and valence band.

When the distance from the surface is denoted by x, the charge distribution is given by

$$n(x) = n_0 \cdot \exp\left(+\frac{e_0(\phi_{(x)}-\phi_i)}{kT}\right), \tag{3a}$$

$$p(x) = p_0 \cdot \exp\left(-\frac{e_0(\phi_{(x)}-\phi_i)}{kT}\right), \tag{3b}$$

with e_0 = elementary charge of the electron. The charges in donor or acceptor states depend on the position of the respective energy level to the Fermi level, locally. Let us assume that there is in the crystal a donor with a single energy level E_D, and with a concentration, c_D. Then the concentration of ionized donors, c_{D+}, is given by

$$c_{D+} = c_D \cdot \frac{1}{1 + g_D \exp\left(\frac{E_F - E_D + e_0(\phi_{(x)}-\phi_i)}{kT}\right)} \tag{4}$$

where g_D is the degeneracy of the donor energy level and E_F is the Fermi energy in the semiconductor.

The corresponding expression for ionized acceptors, with a single energy level E_A of degeneracy, g_A, and bulk concentration, c_A, is

$$c_{A^-} = c_A \cdot \frac{1}{1+\frac{1}{g_A}\exp\left(\frac{E_A - e_0(\phi_{(x)} - \phi_i) - E_F}{kT}\right)} \qquad (5)$$

The Fermi energy of the semiconductor bulk is correlated with the concentration of electron and holes there by the equations,

$$n_0 = n_i \cdot \exp\left(\frac{E_F - {}_iE_F}{kT}\right), \qquad (6a)$$

$$p_0 = n_i \cdot \exp\left(\frac{{}_iE_F - E_F}{kT}\right), \qquad (6b)$$

where ${}_iE_F$ is the Fermi level of an intrinsic semiconductor, with $n_0 = p_0 = n_i$, for which one finds [for these fundamentals compare Hanney, (1959); Shockley (1963); Spenke (1965)]

$${}_iE_F = \frac{1}{2}(E_C + E_V) - kT \ln \frac{N_C}{N_V} . \qquad (7)$$

As N_C and N_V are in the same order of magnitude, usually, the Fermi level of an intrinsic semiconductor is close to the middle of the band gap.

From these basic equations, the whole charge q_{sc} can be correlated with the change of potential ϕ from bulk, ϕ_i, to the surface, ϕ_s, with help of Poisson's equation, which reads, for the one-dimensional case,

$$\frac{d^2\phi}{dx^2} = -\frac{1}{\epsilon\epsilon_0}\rho(x), \qquad (8)$$

where ϵ_0 = dielectric constant of the vacuum $\left(\frac{\text{coulomb}}{\text{volt}}\ \text{cm}^{-1}\right)$,

ϵ = dimensionless dielectric constant of the medium relative to the vacuum.

The density of electric charge, ρ, is given by

$$\rho(x) = e_0[p(x) - n(x) + c_{D^+}(x) - c_{A^-}(x)] \, . \qquad (9)$$

After integration of Poisson's equation with respect to x, and using the boundary condition, $\frac{d\phi}{dx} = 0$, in the bulk, one can correlate the field strength in the surface with the net charge by

$$\left(\frac{d\phi}{dx}\right)_s = + \frac{1}{\epsilon \, \epsilon_0} \int_{x_s}^{\infty} \rho(x) \, dx = + \frac{1}{\epsilon\epsilon_0} \cdot q_{sc} \, . \qquad (10)$$

This equation can be combined with another integrated form of Poisson's equation, namely,

$$\left(\frac{d\phi}{dx}\right)^2_{x_s} = + \frac{2}{\epsilon\epsilon_0} \int_{x_s}^{\infty} \rho(x) \left(\frac{d\phi}{dx}\right) dx = + \frac{2}{\epsilon\epsilon_0} \int_{\phi_s}^{\phi_i} \rho(\phi) \, d\phi, \quad (11)$$

to give a correlation between the excess charge in the space-charge layer and the potential difference between surface and bulk,

$$q^2_{sc} = 2\epsilon\epsilon_0 \int_{\phi_s}^{\phi_i} \rho(\phi) \, d\phi \, . \qquad (12)$$

From Eqs. (9) and (3), (4) and (5), $\rho(\phi)$ can be obtained, and then Eq. (12) can be integrated for the particular conditions, which gives a relation between q_{sc} and the potential drop in the space charge layer, $(\phi_s - \phi_i) \equiv \Delta\phi_s$.

Absolute excess charges are much harder to measure than differential changes. Therefore, the differential capacity $C_{sc} = \frac{-dq_{sc}}{d(\phi_s - \phi_i)}$ is the more interesting magnitude. From Eq. (12) one derives:

$$C_{sc} = \frac{-dq_{sc}}{d\Delta\phi_s} = \left(\frac{\epsilon\epsilon_0}{2}\right)^{1/2} \frac{|\rho(\phi_s)|}{\left(\int_{\phi_s}^{\phi_i} \rho(\phi)d\phi\right)^{1/2}} \cdot \qquad (13)$$

This equation has been solved for various conditions [for more details compare Brattain and Bardeen (1953), Kingston and Neustadter (1955), Green (1959a), Seiwatz and Green (1958), Dewald (1960), Green (1959b), Myamlin and Pleskov (1965), Many, Goldstein, and Grover (1965)]. Simplest situations are found where the ionized acceptor and donor states have constant concentration over the whole space-charge range or are negligible, as in intrinsic semiconductors. For the latter case, the capacity is symmetrical around $\phi_s = \phi_i$, the so-called "flat band situation,"

$$C_{sc} = \left(\frac{2\epsilon\epsilon_0 e_0^2 n_i}{kT}\right)^{1/2} \cdot \cosh\left(\frac{e_0(\Delta\phi_s)}{2kT}\right) \qquad (14)$$

$$= \frac{\epsilon\epsilon_0}{L} \cosh\left(\frac{V_s}{2}\right),$$

with $L = \sqrt{\frac{\epsilon\epsilon_0 kT}{2n_i e_0^2}}$ the Debye length for an intrinsic semiconductor, and $V_s = \frac{e_0\Delta\phi_s}{kT}$. Figure 3 shows the space-charge capacitance of an intrinsic germanium surface according to this relation. In reality, the range of applicability of this equation is limited by the width of the band gap. If $e_0(\Delta\phi_s)$ approaches $E_{gap}/2$, further accumulation of charges becomes restricted by the density of states, and degeneracy begins, which slows down the further increase of the capacity (Green, 1959). In Fig. 3, the

influence of degeneracy is also shown.

The capacity of n- or p-type specimens follows a more complex correlation, which shall be given for a semiconductor in which the doping and acceptor impurities have energy levels very close to the band edges and are therefore fully ionized. The space charge capacity then has the values [compare Myamlin and Pleskov (1965), Boddy (1965)]

$$C_{sc} = \frac{\epsilon\epsilon_0}{L} \cdot \frac{\left| y\,(e^{-V_s}-1) - y^{-1}(e^{+V_s}-1) \right|}{\sqrt{\left[y(e^{-V_s}-1) + y^{-1}(e^{+V_s}-1) + (y-y^{-1})V_s \right]}} , \qquad (15)$$

with $y = \frac{p_0}{n_i} = \frac{n_i}{n_0} = \sqrt{p_0/n_0}$. This relationship goes through a minimum also, as shown in Fig. 3 for an n-type specimen.

It is worthwhile to summarize qualitatively the three main situations to be found in the double layer of a semiconductor:

(a) enrichment layer, where the excess charge has the same sign as the majority carrier of the bulk and is constituted mainly by these carriers;

(b) depletion layer, where the excess charge has opposite sign to the majority carrier in the bulk, and consists mainly of ionized donors or acceptors for n- or p-type specimens, respectively;

(c) inversion layer, in which the excess charge of opposite sign to the majority carriers increases near the surface so much that the minority carriers of the bulk become the excess carriers in a space adjacent to the surface. The excess charge is constituted in this case by ionized donors or acceptors and the minority carriers.

These three situations are shown in Fig. 4 for an n-type semiconductor. It must be noted that inversion layers often cannot be formed at semiconductors with wide band gap when the equilibrium between electrons and holes cannot be inverted because of too slow thermal generation of electron-hole pairs. In this case withdrawing the majority carriers from the surface results in a depletion layer, for which the capacity at potential differences $|\Delta\phi_s| > 10 \frac{kT}{e_0}$ (≈ 250 mV) for an n-type specimen is given by the Schottky-Mott equation, [Schottky (1942), Mott (1939)].

$$\left(\frac{1}{C_{sc}}\right)^2 = \frac{2}{\epsilon\epsilon_0 e_0 c_D} \cdot \left(|\Delta\phi_s| - \frac{kT}{e_0}\right). \qquad (16)$$

For a p-type semiconductor, where this situation would be found at negative excess charge, c_D has to be replaced by c_A.

If the electronic levels of donor or acceptor states cannot be represented by a single energy, the capacity follows more complex relations, which are not discussed here [Green (1959)].

2. Surface States

Surface states can be of the donor or acceptor type. They are localized electronic quantum states, and can be characterized by their energy level and degeneracy. [Compare Many et al., (1965) or Myamlin and Pleskov (1965).] The occupation by electrons is controlled by Fermi statistics. For an acceptor surface state with a single energy term, ${}_sE_A$, the number of negatively charged states N_{A^-} is given as

$$N_{A^-} = N_A \cdot \frac{1}{1 + \frac{1}{{}_sg_A} \exp\left(\frac{{}_sE_A - e_0\Delta\phi_s - E_F}{kT}\right)} , \qquad (17a)$$

and the number of positively charged donor states, N_{D^+}, with an energy level ${}_sE_D$ as

$$N_{D^+} = N_D \cdot \frac{1}{1 + {}_sg_D \exp\left(\frac{E_F - {}_sE_D + e_0\Delta\phi_s}{kT}\right)} . \qquad (17b)$$

The resulting differential capacitance is

$$C_{ss} = -\frac{dq_{ss}}{d\Delta\phi_s} = +\frac{e_0^2}{kT} \left\{ N_D \cdot \frac{{}_sg_D \cdot \exp\left(\frac{E_F - {}_sE_D + e_0\Delta\phi_s}{kT}\right)}{\left[1 + {}_sg_D \exp\left(\frac{E_F - {}_sE_D + e_0\Delta\phi_s}{kT}\right)\right]^2} + \right.$$

$$\left. + N_A \cdot \frac{\frac{1}{{}_sg_A} \cdot \exp\left(\frac{{}_sE_A - E_F - e_0\Delta\phi_s}{kT}\right)}{\left[1 + \frac{1}{{}_sg_A} \exp\left(\frac{{}_sE_A - E_F - e_0\Delta\phi_s}{kT}\right)\right]^2} \right\} \qquad (18)$$

$$= {}_DC_{ss} + {}_AC_{ss} .$$

The minus sign accounts for the inversion in sign of $\Delta\phi_s$ and q_{ss}.

This capacity has two maxima for the conditions

(a) ${}_oE_F + e_o\,\Delta\phi_s = {}_sE_D$ kT ln ${}_sq_D$, with

$$C_{ss} \approx \frac{e_0^2}{4kT} \cdot N_D \cdot \qquad (19a)$$

and (b) $$ {}_0E_F + {}_0e\Delta\phi_s = {}_sE_A - kT \ln {}_sq_A, \text{ with} $$

$$ C_{ss} \approx \frac{e_0^2}{4kT} N_A \quad . \tag{19b} $$

These are the conditions under which the Fermi level of the semiconductor just passes the effective energy level, ${}_sE - kT \ln {}_sq$, of one of the surface states due to the bending of bands with changing $\Delta\phi_s$. For a density of surface states of the order of $10^{13}/cm^2$, which is equivalent to about 1% of the surface sites per cm^2, these capacities have values in the order of 20 $\mu F/cm^2$. In Fig. 5, an example is given for the surface-state capacity as a function of $\Delta\phi_s$.

The capacity of these surface states is in parallel to the space charge layer capacity and can be detected therefore, only if a maximum is found in the range where C_{sc} is not much larger than the maximum of C_{ss}.

3. Counter charge in the electrolyte and in ionized surface groups.

For the reason of electroneutrality, the net charge in the semiconductor must be compensated by a charge of opposite sign in the electrolyte. These charges can be so closely attached to the surface of the semiconductor by chemical interaction that, in some cases, it is impossible to make any distinction between charges in surface states and in bonded ionic groups on the surface. But in our conception, the distinction is based not on the location but on the origin. If the charge is formed by electron exchange with the semiconductor we speak of a surface state; if by chemical reaction with the electrolyte we denote this charge as an ionic surface group or adsorbed ion.

As already mentioned in the introduction, the electric field strength on semiconductor electrode surfaces is usually much less than at metal electrodes. This has the result that, in the absence of ionized surface groups and surface states, the electrostatic potential in the electrolyte, ϕ_{el}, is very close to ϕ_s, the difference being

$$-\Delta\phi_H = \phi_{el} - \phi_s \approx -\delta_H \frac{\epsilon}{\epsilon_H} \left(\frac{d\phi}{dx}\right)_s + \chi_{dipole} \,, \qquad (20)$$

where δ_H, the thickness of the Helmholtz double layer, is in the order of a few Å units controlled by the size of ions, and ϵ, ϵ_H are the effective dielectric constants of the semiconductor and of the Helmholtz double layer, respectively; χ_{dipole} is the contribution of oriented dipoles in the Helmholtz layer and of the electrical momentum in the surface of the semiconductor to the difference in electrostatic potential.

$\left(\frac{d\phi}{dx}\right)_s$ is correlated to $\Delta\phi_s$ by Eq. (10) and will not range, except for the case of degeneracy in the surface, above about 10^6 volt/cm. With a value of $\delta_H \approx 2$ Å, the difference between ϕ_{el} and ϕ_s remains then on the order of 20 mV or below if we do not count χ_{dipole}. The unknown electrical momentum of the surface can certainly amount to larger values but will remain very little influenced by the charging state of the surface. We can conclude that the potential difference between the interior of the semiconductor and the electrolyte, $|\Delta\phi| = |\phi_i - \phi_{el}|$, will be very close to $|\Delta\phi_s|$ minus a constant:

$$\Delta\phi = \phi_i - \phi_{el} = (\phi_i - \phi_s) + (\phi_s - \phi_{el}) \approx -\Delta\phi_s - \chi_{dipole} \,.$$

The sign of $\Delta\phi$ is opposite to $\Delta\phi_s$ because in electrochemistry one

is used to take the electrolyte as reference point for the potential, whereas in semiconductor physics the bulk of the crystal has usually this function. The differential change of the net charge in the semiconductor with the potential drop in the Helmholtz double layer can be derived from Eqs. (10) and (20) as

$$C_H = \frac{\partial q_{sc}}{\partial \Delta\phi_H} = \frac{\epsilon_0 \cdot \epsilon_H}{\delta_H} \quad . \tag{22}$$

In the presence of electronic surface states, Eq. (22) has to be replaced by the relation

$$C_H = \frac{\partial(q_{sc} + q_{ss})}{\partial\Delta\phi H} \tag{23}$$

This relation indicates that, only if $q_{ss} \gg q_{sc}$, the potential difference in the Helmholtz layer may reach a usual magnitude for metal electrodes. In such a case, the Helmholtz double layer becomes controlled by the surface states and changes to some extent with $\Delta\phi$.

A different situation is found in the presence of ionized groups in the surface which are formed by reaction with the electrolyte, e.g. by a process like

$$X^-_{solv} \rightleftharpoons X^-_{ads} \tag{24a}$$

or

$$R\text{-}Y_s \rightleftharpoons R^- + Y^+_{solv} \quad , \tag{24b}$$

attaching a negative charge to the surface. In this case the equilibrium

charge is mainly controlled by the chemical interaction, and the potential difference in the Helmholtz layer can become fully fixed, if enough ions are adsorbed or formed.

The equilibrium conditions for reactions of the type of Eq. (24) are

$$z_{ad} \cdot e_0 \cdot \Delta\phi H = {}^{\circ}\mu_{sol} - {}^{\circ}\mu_{ad} + kT \ln \frac{c_{sol} \left({}^{\circ}N_{ad} - N_{ad} \right)}{{}^{\circ}c_{sol} \cdot N_{ad}} \quad , \qquad (25)$$

where z_{ad} is the net charge of a surface group, ${}^{\circ}\mu_{sol}$ and ${}^{\circ}\mu_{ad}$ are the standard chemical potentials for the species in solution and on the surface; c_{sol} and ${}^{\circ}c_{sol}$ are the concentration in solution and that in the standard state; N_{ad} and ${}^{\circ}N_{ad}$ are the surface concentrations of adsorbed charged species for the equilibrium state and for maximal coverage.

In the presence of ionic groups on the surface, a yet larger amount of charge is necessary to change $\Delta\phi_H$, therefore increasing the effective capacity of the Helmholtz layer. This increase can be derived from Eq. (25) by assuming that the additional charge is given by $z_{ad} \cdot e_0 \cdot N_{ad}$ and is located practically in the surface at x_s; this means

$$C_H = \frac{\partial}{\partial \Delta\phi_H} \cdot (q_{sc} + q_{ss} + z_{ad} \cdot e_0 \cdot N_{ad}) \quad , \qquad (26)$$

or

$$\frac{\partial (q_{sc} + q_{ss})}{\partial \Delta\phi_H} = \frac{\epsilon_0 \cdot \epsilon_H}{\delta_H} - \frac{\partial}{\partial \Delta\phi_H} (z_{ad} \cdot e_0 \cdot N_{ad}) \quad ,$$

which, from Eq. (22), results in

$$\frac{\partial(q_{sc} + q_{ss})}{\partial \Delta\phi_H} = C_H + C_{ad} \quad , \tag{27}$$

with $C_{ad} = - \frac{\partial}{\partial\Delta\phi_H} \quad (z_{ad} \, e_0 \, N_{ad})$

This gives, from Eq. (25),

$$C_{ad} = \frac{z_{ad}^2 \, e_0^2}{kT} \cdot N_{ad} \cdot \frac{^{\circ}N_{ad} - N_{ad}}{^{\circ}N_{ad}} \quad . \tag{28}$$

Equation (27) indicates that the charges in the electrolyte and in ionized surface groups act in parallel as counter charges for the semiconductor net charge. Therefore, the whole charge distribution can be described by a model of two pairs of parallel capacitors in series, as shown in Fig. 6, and the net capacity of the electrode double layer, C_D, is given by a combination of Eq. (13), (18), and (26), namely

$$\frac{\partial\Delta\phi}{\partial q} = \frac{1}{C_D} = \frac{1}{C_{sc} + C_{ss}} + \frac{1}{C_H + C_{ad}} \quad . \tag{29}$$

This net double-layer capacity describes the variation of $\phi_i - \phi_{el} = \Delta\phi$ with the net charge $q = q_{sc} + q_{ss}$. The relation between the variations of the potential difference in the semiconductor and in the Helmholtz double layer is given by

$$- \frac{\partial\Delta\phi_s}{\partial\Delta\phi_H} = \frac{\partial(\phi_i - \phi_s)}{\partial(\phi_s - \phi_{el})} = \frac{C_H + C_{ad}}{C_{sc} + C_{ss}} \quad , \tag{30}$$

which is an important result although the absolute values of ϕ remain unknown.

B. Relaxation Phenomena and Effect of Illumination

In Section IIA we have discussed equilibrium of charge distribution, disregarding the time for establishing equilibrium. Some of the processes involved, however, can be rather slow, and give additional information on the double layer. Equilibrium in the space-charge layer is established very fast if the mobility of the majority carrier is not unusually small. But electron exchange between bulk and surface states is often much slower and does not follow fast changes. The same might be found for the adsorption of ions or the formation of ionized groups in the surface and for reactions which change the dipole momentum in the surface.

Furthermore, if the equilibrium is disturbed by external forces, like illumination or high electric fields, a charge distribution can be obtained which is rather different from equilibrium. A few typical examples are discussed in the following. A detailed analysis is given in the book by Myamlin and Pleskov (1965).

1. Relaxation at high frequencies

If an ac voltage is applied externally to a semiconductor electrode in a galvanic cell with an unpolarizable counter electrode, the potential drop $\Delta\phi_s$ in the space charge will follow the external signal with a time constant given by $R_{ext}C_{sc}$, this means that for a frequency $\omega = 2\pi\nu = 1/R_{ext} \cdot C_{sc}$ the phase shift will reach 45 deg. R_{ext} is completely controlled by the ohmic resistance in the semiconductor and the electrolyte.

The real relaxation time of the space-charge layer would be smaller by a factor of $\frac{R_{sc}}{R_{ext}}$, where R_{sc} is the ohmic resistance in the space-charge layer, that is the resistance over a distance L in the semiconductor. Since the Debye length, L, is normally small compared with the distance at which an ohmic contact can be made, the response of the space-charge layer is controlled by the external conditions. Only in some extreme cases, where the space-charge layer is formed not so much by charge movement as by generation or recombination processes, as in the formation of a depletion or an inversion layer, the relaxation of space-charge formation can become an observable process.

Such relaxation phenomena, though very important for semiconductor technology and theory, are not interesting for electrochemical processes. But the relaxation of the charge in surface states can be very important for electrochemical problems and must be discussed in some detail.

2. Relaxation in surface states

The electron transfer reaction for an acceptor surface state can occur in two possible ways:

(a) strong coupling with the conduction band,

$$A_s + e^- \underset{C^k_{neutr}}{\overset{C^k_{ion}}{\rightleftharpoons}} A_s^- \quad , \tag{31a}$$

with a rate of

$$\frac{dN_{A^-}}{dt} = C^k_{ion} \cdot n_s \cdot (N_A - N_{A^-}) - C^k_{neutr} N_{A^-} \quad ; \tag{32a}$$

(b) strong coupling with the valence band,

$$A_s \underset{V^k_{neutr}}{\overset{V^k_{ion}}{\rightleftharpoons}} A_s^- + h^+ \qquad (31b)$$

with the rate

$$\frac{dN_{A^-}}{dt} = V^k_{ion}\,(N_A - N_{A^-}) - V^k_{neutr} \cdot p_s \cdot N_A \quad . \qquad (32b)$$

The relaxation process for any deviation in N_{A^-} from the equilibrium value ${}_0N_{A^-}$, at constant n_s of p_s, follows the time law,

$$\Delta N_{A^-} = (N_{A^-} - {}_0N_{A^-}) \propto \exp\left(-\frac{t}{\tau_A}\right),$$

where τ_A is the relaxation time,

${}_C\tau_A$ for process a)

$${}_C\tau_A = \frac{1}{C^k_{ion} \cdot n_s + C^k_{neutr}} \quad , \qquad (33a)$$

${}_V\tau_A$ for process b)

$${}_V\tau_A = \frac{1}{V^k_{ion} + V^k_{neutr} \cdot p_s} \quad . \qquad (33b)$$

Analogous relations are found for the respective charging process of a donor state,

$$D_s \underset{C^k_{neutr}}{\overset{C^k_{ion}}{\rightleftharpoons}} D_s^+ + e^- \qquad (34a)$$

or

$$D_s + h^+ \underset{V^k_{neutr}}{\overset{V^k_{ion}}{\rightleftharpoons}} D_s^+ \quad , \qquad (34b)$$

where the relaxation times are

$$C^{\tau}D = \frac{1}{C^{k}neutr \cdot n_s + C^{k}ion} \quad , \tag{35a}$$

$$V^{\tau}D = \frac{1}{V^{k}neutr + V^{k}ion \cdot p_s} \quad . \tag{35b}$$

If a surface state is coupled as well to the conduction band as to the valence band, the effective relaxation time contains all the rate constants in the denominator and is given, for an acceptor state, for example, by

$$\tau_A = \frac{1}{C^{k}ion \cdot n_s + V^{k}ion + C^{k}neutr + V^{k}neutr \cdot p_s} = \frac{C^{\tau}A \cdot V^{\tau}A}{C^{\tau}A + V^{\tau}A} \quad . \tag{36}$$

The surface state capacity becomes frequency-dependent if ω approaches $1/\tau_A$ or $1/\tau_D$. This time dependence can be described (Myamlin and Pleskov, 1965) by a complex capacitance,

$$C_{ss}(\omega) = {}_{A}C_{ss}(\omega=0) \cdot \frac{1-i\omega\tau_A}{1+\omega^2\tau_A^2} + {}_{D}C_{ss}(\omega=0) \cdot \frac{1-i\omega\tau_A}{1+\omega^2\tau_D^2} \quad , \tag{37}$$

where ${}_{A}C_{ss}(\omega=0)$ and ${}_{D}C_{ss}(\omega=0)$ are the equilibrium values of Eq. (18) and i is the imaginary unit. Equation (37) shows that for frequencies $1/\tau_A$ or $1/\tau_D$ the capacity decreases rapidly, $\propto 1/\omega^2$, and also the then dominating resistive part decreases with $1/\omega$. Therefore, at high enough frequencies, C_{ss} can be neglected and only C_{sc} is left.

We have treated only the simplest case with single-energy-term surface states and one relaxation time for each separate state. Often the situation is more complicated because of a distribution of the energy levels over a wide-range. Then, the frequency response must be

represented by a relaxation spectrum, but this is outside the scope of this chapter.

The relaxation of a charge in ionized surface groups follows fully analogous relationships. The charge density in such groups, however, depends little on the applied voltage; the resulting relaxation is hardly detectable in the overall capacity. Only under special circumstances will this kind of relaxation process become obvious. One such case has been found at germanium surfaces, where a reaction occurs which varies the surface composition with the electron and hole concentration. [Turner (1956), Gobrecht, et al. (1966), Gerischer (1966).] This causes a change of the dipole momentum in the surface which must be compensated by a matching rearrangement of the excess charge [Gerischer, (1965)].

3. Effect of illumination

Illumination generates electron-hole pairs if the light energy exceeds the energy difference of the band gap. This generation of carriers causes an increase in their concentrations compared with the equilibrium values in the dark, and changes the carrier distribution in the double layer of a semiconductor electrode.

Light absorption is a process which usually extends nonuniformly over a crystal. The spatial distribution of absorbed light quanta is

therefore a crucial parameter for the distribution of carriers. Two limiting conditions will be discussed here for which the situation can most easily be described [compare, e.g., Bube (1960), Shockley (1963), Tauc (1962), Ryvkin (1965)] .

(a) Light absorption occurs practically homogeneously over a range of the mean diffusion length, ℓ, of the minority carrier, and this diffusion length is large compared with the Debye length, L, of the space-charge layer. This is the case for light of energy close below the absorption edge for which the absorption coefficient, κ, $\langle cm^{-1} \rangle$ is small. A characteristic parameter for the depth of penetration of light is $\frac{1}{\kappa}$.

(b) Most of the incident light is absorbed in a range $\frac{1}{\kappa}$ that is small compared with the space charge layer, L, the diffusion length being again large compared with L, as shown in Fig. 7.

In case a, the generation of electron-hole pairs by light is constant over the whole space of ℓ at a rate $\kappa \cdot I_0$, in pairs per volume unit where I_0 is the light intensity in suitable units. The recombination rate is given by $r \cdot n^* \cdot p^*$, where r is a rate constant and n^*, p^* are the electron and hole concentrations in the diffusion layer ℓ under illumination. In the dark, the recombination under equilibrium, $r \cdot n_0 \cdot p_0$, is compensated by thermal generation, g. The steady state under illumination is reached when the excess concentrations, $\Delta n^* = n^* - n_0$ and $\Delta p^* = p^* - p_0$, recombine at the same rate as light is absorbed, which means

$$\kappa \cdot I_0 = r(n^* \cdot p^* - n_0 \cdot p_0) = r(n_0 \, \Delta p^* + p_0 \, \Delta n^* + \Delta n^* \cdot \Delta p^*) \quad .$$

Because the stoichiometry of electron-hole pair formation demands

$\Delta p^* = \Delta n^*$, we obtain

$$\kappa \cdot I_0 = r(n_0+p_0) \cdot \Delta n^* + r \cdot \Delta n^{*2} \quad . \qquad (38)$$

Equation (38) indicates that Δn^* and Δp^* increase linearly with I_0 as long as Δn^* remains small compared with the majority carrier concentration. After illumination is suddenly interrupted, the excess concentration of electron-hole pairs Δn^* decays with $\exp\left(-\frac{t}{\tau}\right)$, where τ is the life-time of excess electron-hole pairs,

$$\tau = \frac{1}{r(n_0+p_0)} \qquad (39)$$

The excess concentration in the steady state, Eq. (38), can therefore be represented also by

$$\Delta n^* = \Delta p^* = \kappa \cdot I_0 \cdot \tau \quad . \qquad (40)$$

In case b, the generated electron hole pairs diffuse into the bulk, where they recombine. If the diffusion length is large enough, $\ell \gg L$, the recombination in the space-charge layer can be neglected in the absence of surface recombination. Then, the rate of diffusion is controlled by the flux of minority carriers into the bulk, and the steady-state distribution must fulfill the condition

$$D \cdot \frac{\partial^2 \Delta n^*}{\partial x^2} = \frac{\Delta n^*}{\tau} \quad , \qquad (41)$$

where D is the diffusion coefficient of the minority carrier and it is assumed that Δn^* remains small compared with the majority carrier

concentration; τ is given by Eq. (39). The solution, under the correct boundary conditions, for that part of electron-hole pairs which recombines outside the space-charge layer is

$$\Delta n^*(x) = \Delta n_L^* \cdot \exp\left(-\frac{x-L}{\ell}\right) , \qquad (42)$$

where Δn_L^* is the excess concentration at the end of the space-charge layer, $x = L$, and ℓ is the diffusion length of minority carriers, with

$$\ell = \sqrt{D\tau} . \qquad (43)$$

Using Fick's first law, a correlation between Δn_L^* and the light intensity can be obtained, which reads, after correction for surface recombination and recombination in the space charge layer itself,

$$\Delta n_L^* = \frac{I_0 - I_s}{D} = \sqrt{\tau/D}\ (I_0 - I_s) . \qquad (44)$$

Here I_s represents the current density consumed for surface recombination and by recombination in the space-charge layer.

We see that in both cases the concentration of electrons and holes increases proportionally to the intensity of incident light as long as the light intensity does not become too high. If the flux of electrons and holes produced in the space-charge layer does not reach the order of magnitude of the thermal exchange of carriers between the space-charge layer and the bulk, the carrier distribution over the space-charge layer remains in equilibrium with the steady-state carrier concentration in the adjacent bulk, that is, n^* and p^*. All space-charge layer properties can then be obtained from the same set of correlations as derived for the dark in the previous section, with the only difference of

replacing n_0 and p_0 in Eq. (15) by n^* and p^*.

The result of illumination is therefore an increase in capacity as long as equilibrium for both types of carriers is maintained, and an increase in the concentration of electrons and holes in the surface as well:

$$n_s^* = n^* \cdot \exp\left(\frac{e_0 \Delta\phi_s}{kT}\right), \tag{45a}$$

$$p_s^* = p^* \cdot \exp\left(-\frac{e_0 \Delta\phi_s}{kT}\right), \tag{45b}$$

The increase of capacity can be used to get information on the charge of the double layer, and the variation of carrier density is very important for testing the influence of electronic charge carriers on surface reactions, as we shall see later.

C. Selected Experimental Results

The capacity behavior of Ge, Si, GaAs, and ZnO single-crystal electrodes has been studied in some detail. Best known are the properties of germanium, which we shall use as an example for the demonstration of space-charge properties, [Bohnenkamp and Engell (1957), Boddy (1964)]. The influence of surface states can be excluded by using high enough frequencies [Bohnenkamp and Engell (1957), Gobrecht and Meinhardt (1963), Hofmann-Perez and Gerischer (1961)] or short enough pulses for the capacity measurements [Brattain and Boddy (1962)]. Frequencies above 50 kHz or pulses on the order of 10 μsec have given satisfactory results. To exclude changes in the voltage drop of the Helmholtz double layer, a

rapid sweep technique has to be applied for the variation of the electrode potential to obtain the correct capacity versus space-charge voltage dependence [Boddy and Sundburg (1963), Gerischer et al. (1965)].

If corrected for the increase of area by surface roughness, the results agree well with theory, as shown in Fig. 8. Because $\Delta\phi_s$, the theoretical parameter for C_{sc}, cannot be measured directly, the necessary information on the potential drop must be obtained from the externally applied cell voltage, U, measured against a suitable reference electrode. As long as $\Delta\phi_H$ in the Helmholtz double layer remains constant, U and $\Delta\phi_s$ move fully in parallel. Then, the most convenient reference potential for the analysis of the space-charge behavior is the flat band potential, i.e., the zero point of space charge. This point can be referred to the minimum in the theoretical capacity curves of Eq. (14) or (15) and the electrode potential at this point, U_{fb}, can be used to link the experimental capacity curves in terms of cell voltages with the potential drop in the space charge layer by the relation

$$U-U_{fb} = -|\Delta\phi_s| \quad . \tag{46}$$

This has been done for the capacity measurements referred to in Fig. 8.

For a highly doped specimen the theoretically expected minimum in the capacity is not found [Memming (1963)] because equilibrium distribution cannot be established for the minority carriers. The flat band potential must be determined in a different way. Equation (16) has shown that a plot of $(1/C_{sc})^2$ against U should give a straight line with an intersection on the abscissa at $|\Delta\phi_s| = \frac{kT}{e_0}$ for a depletion layer. Dewald (1960) has studied zinc oxide crystals, which are normally

n-type by an excess of metal atoms on interstitial lattice places, and gives a good example for this behavior under anodic load. The flat-band position of a ZnO electrode depends, as does that for germanium, on the pH of the electrolyte, which has been studied in detail by Lohmann (1966).

Another good example for the formation of a depletion layer at an electrode under anodic polarization is cadmium sulfide, which has been investigated by Tyagi (1963). A plot of capacity measurements for determining the flat-band position is represented in Fig. 9.

Photovoltage measurements have also been employed for testing the distribution of charge in the space.charge layer and are used as a convenient tool for finding the flat band potential [Dewald 1960), Lazorenko-Manevich (1962)].

The photovoltage under steady-state conditions depends to a large extent on the surface properties and on charge-transfer reactions in the surface. It is therefore much more conclusive for characterizing the space-charge situation to measure the photoeffects with short light pulses under such conditions that the surface charge remains unchanged. This so-called surface photovoltage comprehends only the change of potential drop in the space-charge layer, which is caused by electron-hole pair generation therein [Garrett and Brattain (1955), Brattain and Garrett (1955), Lazorenko-Manevich (1962), Pleskov and Tyagi (1961), Boddy and Brattain (1963), Boddy (1965)]. Following the existing potential gradients, these carriers will move in the opposite direction and create an electric field opposite in sign to the field present in the space-charge layer in the dark. As a result of this very fast process, the previously existing $\Delta\phi_s$ will be reduced in absolute value. If $\Delta\phi_s = 0$, i.e., at

the flat band position, no driving force exists for separating the charge carriers of opposite sign. Then, only a small potential difference is created by the different mobilities of electrons and holes, the so-called Dember potential, which is in principle the same phenomenon as the diffusion potential in electrolytes when ions of opposite charge have different mobilities [compare Many et al. (1965)]. In semiconductors the Dember potential is normally very small and can be neglected for most purposes. Therefore, the change in sign of the surface photovoltage, measured with short light pulses, indicates clearly the position of the flat-band situation. The exact theory of surface photovoltage has been worked out in detail by Garrett and Brattain (1955) and Brattain and Garrett (1955). Figure 10 shows some experimental results obtained by Boddy and Brattain (1963) for a Ge-electrode in comparison with a theoretical curve under the assumption that surface recombination is either negligible or constant over the whole range of potential.

It has been observed that the flat-band potential of a semiconductor electrode can be greatly shifted by varying the composition of the electrolyte [Bohnenkamp and Engell (1957), Boddy and Brattain (1963), Hofmann-Perez and Gerischer (1961), Gobrecht and Meinhardt (1964), Gobrecht et al. (1966)]. Most of the semiconductor electrode flat-band potentials are influenced by the pH of aqueous electrolytes in a very regular way. This is shown in Fig. 11 for an intrinsic Ge electrode.

A plausible explanation of this result is to assume that the surface of germanium in contact with aqueous solution is covered by a monolayer of OH groups, which are chemically bonded to Ge atoms in the surface [Turner (1956), Harvey et al. (1968), Beck and Gerischer (1959)]. This

"surface hydroxide" has some acidity, and the dissociation equilibrium is controlled by the pH of the solution according to the process [Hofmann-Perez and Gerischer (1961)]

$$Ge\text{-}OH + H_2O \leftrightharpoons GeO^- + H_3O^+ \quad . \qquad (47)$$

In this surface reaction, an electric charge is transferred from a place on the surface to a place in the outer Helmholtz layer of the electrolyte. This process is therefore controlled, at least partially, by the difference in the electrostatic potential between surface sites and the bulk of the electrolyte, denoted in the preceding section with $\Delta\phi_H$.

The thermodynamical discussion of this equilibrium leads to a correlation like

$$\Delta\phi_H = \text{const} - \frac{2{,}3 \cdot kT}{e_0}\,[pH] - \log\,(f_{GeO^-} \cdot x_{GeO^-}), \qquad (48)$$

where f_{GeO^-} and x_{GeO^-} are the activity coefficient and the mole fraction of GeO^- in the surface. As long as this mole fraction does not change to a larger extent by the variation in surface charges which are necessary to change $\Delta\phi_s$, a linear relation between the flat-band potential U_{fb} and pH sould be expected, as found in the experiments of Fig. 11. The deviation in the slope at low pH might indicate that the mole fraction, x_{GeO^-}, becomes so small there that the last term of Eq. (47) gains importance.

A similar influence of some anions in the electrolyte, especially J^-, has been attributed to an exchange of OH^- groups by J^- in the surface compounds [Boddy (1965), Brattain and Boddy (1966)]. This varies the dipole momentum of the surface and also the mole fraction of dissociable surface groups, which is reflected in a shift of the flat-band potential.

But the conditions are much more complex for such exchange reactions and have not yet been discussed quantitatively.

III. ELECTRON TRANSFER REACTIONS

A. Theory

1. Fundamental aspects

In an electron transfer reaction, the semiconductor acts only as donor or acceptor for electrons without chemical change of its constitution. This is possible if a suitable acceptor or donor is available in the electrolyte. The generally accepted concept for the theory of this process is based on the Franck-Condon principle, and takes the conversion of energy into account [Randles (1952), Hush (1958), Hush (1956), Marcus (1956) (1959) (1964) (1968), Dewald (1959), Dogonadze and Chizmadzhev (1962), Levich (1966), Gerischer (1960), (1960), (1961)]. Since the electron transfer is a fast process compared with atomic movements, the chemical arrangement of atoms is not changed during the transfer time. The conservation of energy demands further that the electron exchanges occur between electron states of the same energy level, within the range of $\pm kT$. Otherwise, a too great contribution of phonon support would be necessary for the electron transfer, which would make the process very improbable. The energy conservation principle permits radiationless electron transfer processes at a semiconductor electrode only on energy levels in the range of the conduction or of the valence band, excluding all donor or acceptor states in the solution with energy levels within the range of the band gap. This situation is represented in Fig. 12, and can be described by two different reaction paths:

$$A + e^- \rightleftharpoons D^- \qquad (49)$$

and

$$A \rightleftharpoons D^- + h^+ \ . \qquad (50)$$

What process is possible depends on the relative position between the energy levels of the redox components and the band edges of the semiconductor, with the vacuum level as the common reference energy.

The band model for solids give sufficient information about the electronic energy levels in a semiconductor. In the electrolyte, the electron energy levels are located at the donors and acceptors that are the reduced and oxidized components of a redox system in the solution. The energy levels of these states can be defined in a fully analogous way as energy levels in a solid, namely by the energy of electron emission from a donor state or electron attachment to an acceptor state [Gerischer, (1960), (1961)].

There is an important difference, however, between energy levels of delocalized electrons in a crystalline solid and those of localized states in a polarizable and polar solvent. Whereas, in the first case, no distinction can be made whether such a level is occupied or not, in the latter case this makes a great difference in the position of the energy level due to the strong interaction energies with the solvent. This can be demonstrated by the cycle

$$\text{(a)} \quad (\text{Red})_{\text{solv,R}} \rightarrow (\text{Ox}^+)_{\text{solv,R}} + e_\infty^- \qquad \text{for which } \Delta E = +\,{}^\circ I \qquad (51a)$$

$$\text{(b)} \quad (\text{Ox}^+)_{\text{solv,R}} \rightarrow (\text{Ox}^+)_{\text{solv,Ox}} \qquad \text{for which } \Delta E = -\lambda_{\text{Ox}} \qquad (51b)$$

$$\text{(c)} \quad (\text{Ox}^+)_{\text{solv,Ox}} + e_\infty^- \rightarrow (\text{Red})_{\text{solv,Ox}} \qquad \text{for which } \Delta E = -{}^\circ A \qquad (51c)$$

$$\text{(d)} \quad (\text{Red})_{\text{solv,Ox}} \rightarrow (\text{Red})_{\text{solv,R}} \qquad \text{for which } \Delta E = -\lambda_{\text{R}} \qquad (51d)$$

This describes (a) an ionization process from the most probable solvation state of the reduced component (index, solv,R) without change of solvation structure (Franck-Condon principle); (b) the formation of the most probable solvation structure of the oxidized component (index, solv,Ox); (c) electron attachment to the oxidized component without solvation shell rearrangement; (d) formation of the stable solvation shell for the reduced species.

The steps in free energy for this cycle are sketched in Fig. 13. Entropy changes occur only in processes (b) and (d), while for steps (a) and (c), which do not involve structural changes, standard free energy and enthalpy are equal.

The energy difference for step (a) represents the energy level of occupied electron states in the redox solution which will be found with the highest probability averaged over time at the reduced component; the energy difference in step (c) describes the most probable unoccupied level. Figure 13 shows that the levels having maximal statistical weight are different by the sum of the rearrangement energies of the solvation shells and that the occupied levels are deeper than the unoccupied ones.

At present there is no way for measuring the ionization energies or electron affinities under the restriction of the Franck-Condon principle directly. But the energy combinations

$$^{\circ}I - \lambda_{Ox} = {}^{\circ}A + \lambda_R = - \; {}^{\circ}E_{F,redox}, \qquad (52)$$

representing the change in free energy for a redox reaction of the type

$$(Red)_{solv,R} \rightleftharpoons (Ox^+)_{solv,Ox} + e^-_{\infty} , \qquad (53)$$

can be obtained from the standard redox potentials in a relative scale. At a redox electrode, the reaction for which equilibrium is obtained differs from Eq. (53) only in the state of the electron, which comes from the electrode where it has on the average the energy of the Fermi level, E_F,

$$(\mathrm{Red})_{\mathrm{solv,R}} \rightleftharpoons (\mathrm{Ox}^+)_{\mathrm{solv,Ox}} + e^-_{E_F} \quad . \tag{53a}$$

To balance the free-energy difference, the mean free energy of this electron in the metal must be a level that corresponds to ${}^{\circ}E_{F,\mathrm{redox}}$, the free energy in reaction (51). Since, under equilibrium conditions, the electrode potential difference is adjusting a situation in which $E_{F,\mathrm{electrode}} = {}^{\circ}E_{F,\mathrm{redox}}$, the value of ${}^{\circ}E_{F,\mathrm{redox}}$ is directly related to the standard redox potential (at equal concentration of oxidized and reduced species) of a redox system by

$${}^{\circ}E_{F,\,\mathrm{redox}} = \mathrm{const} - e_0 \cdot {}^{\circ}U_{\mathrm{redox}} \quad . \tag{54}$$

Here ${}^{\circ}U_{\mathrm{redox}}$ is the standard redox potential in the European scale.

This relation indicates that redox systems that are highly oxidizing have deeper ${}^{\circ}E_{F,\mathrm{redox}}$ values than reducing systems.

2. Kinetics

In the simplest approach, the rate of electron transfer, according to the preceding principle, will be proportional to the density of occupied energy states in the one phase and unoccupied states in the other phase that are on the same energy level. Because the energy states are distributed over a wide range of energies, an integration has to be executed

over all corresponding energy levels. This leads to an expression for the cathodic process, j^- = electron transfer from electrode to oxidized species in the solution of the type [Dogonadze and Chizmadzhev (1962), Levich (1966), Gerischer (1960), (1961)].

$$j^- \propto c_{Ox} \int_{-\infty}^{0} \kappa(E) \cdot D_{\Theta}(E) \cdot W_{Ox}(E)\, dE, \qquad (55a)$$

and for the anodic process, j^+ = electron transfer from reduced species in solution to the electrode

$$j^+ \propto c_R \int_{-\infty}^{0} \kappa(E)\, D_{\oplus}(E) \cdot W_R(E)\, dE \ . \qquad (55b)$$

In these equations c_{Ox} and c_R are the concentrations, and $D_{\Theta}(E)$ and $D_{\oplus}(E)$ are the densities of occupied and unoccupied states in the semiconductor on a particular energy level E. $W_{Ox}(E)$ and $W_R(E)$ denote the distribution functions for finding respectively an oxidized or a reduced component in a solvation state that corresponds to an energy level E. These distribution functions represent the average in time over all possible thermal fluctuations in energy caused by interaction with the solvent or directly bonded ligands. This probability function has a maximum at the most probable solvation state and decreases exponentially to both sides of these energies, which we shall denote (compare Fig. 13) by

$$^{\circ}E_{Ox} = - \,^{\circ}A \text{ and } ^{\circ}E_R = - \,^{\circ}I \ , \qquad (56)$$

$\kappa(E)$ is a factor that gives the transfer probability for a species

of the redox system during its "encounter time" with the surface; $\kappa(E)$ includes the quantum mechanical transfer probability summed over all distances. [Compare Levich (1966).]

Because the density-of-states function has a gap between the band edges, it is convenient to divide the integrals of Eq. (55) into two parts which cover the energy states in the valence or in the conduction band. [Gerischer (1961).] In this way, the currents in the conduction band and the valence band can be expressed separately:

$$j_C = j_C^+ - j_C^- = k_C^+ \cdot c_R \cdot \int_{E_C}^{0} \kappa(E) \cdot D_O(E) \cdot W_R(E)\, dE \qquad (57a)$$

$$-k_C^- \cdot c_{Ox} \int_{E_C}^{0} \kappa(E) \cdot D_O(E) \cdot W_{Ox}(E)\, dE,$$

$$j_V = j_V^+ - j_V^- = k_V^+ \cdot c_R \int_{-\infty}^{E_V} \kappa(E)\, D_O(E)\, W_R(E)\, dE \qquad (57b)$$

$$-k_C^- \cdot c_{Ox} \int_{-\infty}^{E_V} \kappa(D)\, D_O(E) \cdot W_{Ox}(D)\, dE \quad .$$

Figure 14 shows these functions and their products. The results of such an integration is indicated for two different redox systems, one in which ${}^{\circ}E_{F,redox}$ is close to E_C and another in which ${}^{\circ}E_{F,redox}$ is close to E_V. As seen in Fig. 14, electron transfer is possible only in the conduction band in the first case and in the valence band in the latter case.

As a general conclusion the following is obtained. Redox systems, which have a positive enough standard potential, that the surface of the semiconductor becomes p-type in contact with this system at equilibrium conditions, exchange electrons with the valence band. Redox systems with such a negative standard potential that the electrode becomes n-type at equilibrium exchange electrons with the conduction band.

Because the main electron transfer takes place in a narrow energy range above and below the band edge energies E_C and E_V, the situation

is well described by the approximations

$$j_C = k_C^+ \cdot \kappa(E_C) \cdot c_R \cdot W_R(E_C) \cdot N_C - k_C^+ \cdot \kappa(E_C) \cdot c_{Ox} \cdot W_{Ox}(E_C) \cdot n_s \,, \tag{58a}$$

$$j_V = k_V^+ \cdot \kappa(E_V) \cdot c_R \cdot W_R(E_V) \cdot p_s - k_V^+ \cdot \kappa(E_V) \cdot c_{Ox} \cdot W_{Ox}(E_V) \cdot N_V \,, \tag{58b}$$

where $\kappa(E_C)$, $\kappa(E_V)$, $W(E_C)$, and $W(E_V)$ are the values of these functions at the band edges. The densities of occupied and unoccupied electron states in the semiconductor are represented by the concentrations of electrons and holes in the surface and by the effective densities of states at the band edges.

The values of $\kappa(E)$ and $W(E)$ are independent of the applied voltage, as long as the potential jump in the Helmholtz layer does not change considerably with varying excess charge. Equations (58a) and (58b) indicate therefore that the variation of currents due to the applied potential can be attributed only to a variation of the concentrations of electrons and holes in the surface. This shows that electrode processes on semiconductors are much closer to normal reaction kinetics than those processes on metals where the activation energy varies so widely with the applied voltage.

This constancy of the energy correlations between the semiconductor electrode surface and the electrolyte has to be taken "cum grano salis" because chemical interaction can change the potential drop in the Helmholtz layer quite drastically as we discussed in the first section. Reliable comparisons between different redox reactions can be made, therefore, only at "constant chemical composition" of the solution, which means

constant insofar as the chemical state of the semiconductor surface is influenced by the components of the solution. Quantitative predictions can be made only under these restrictions, and have their value more in a relative than in an absolute scale.

Taking advantage of the equilibrium conditions for the charge transfer processes described in Eqs. (58a) and (58b), namely that $j_C = 0$ and $j_V = 0$ simultaneously if the concentrations of electrons and holes in the surface correspond to the equilibrium values $n_{s,0}$ and $p_{s,0}$ for the respective redox reaction, one can write the rate equation in another way which is more useful for experimental applications:

$$j_C = j_{C,0} \left[\frac{c_{R,s}}{c_{R,0}} - \frac{c_{Ox,s}}{c_{Ox,0}} \cdot \frac{n_s}{n_{s,0}} \right] , \tag{59a}$$

$$j_V = j_{V,0} \left[\frac{c_{R,s}}{c_{R,0}} \cdot \frac{p_s}{p_{s,0}} - \frac{c_{Ox,s}}{c_{Ox,0}} \right] , \tag{59b}$$

with the exchange currents at equilibrium $j_{C,0}$ and $j_{V,0}$ given by

$$j_{C,0} = k_C^+ \cdot \kappa(E_C) \cdot c_{R,0} \cdot W_R(E_C) \cdot N_C \tag{60a}$$

$$= k_C^- \cdot \kappa(E_C) \cdot c_{Ox,0} \cdot W_{Ox}(E_C) \cdot n_{s,0}$$

$$j_{V,0} = k_V^+ \cdot \kappa(E_V) \cdot c_{R,0} \cdot W_R(E_V) \cdot p_{s,0}$$

$$= k_V^- \cdot \kappa(E_V) \cdot C_{Ox,0} \cdot W_{Ox}(E_V) \cdot N_V , \tag{60b}$$

and $c_{R,s}$, $c_{Ox,s}$ the concentrations of the redox components in the range

of interaction with the electrode surface. The same set of equations has been derived by Dewald (1953) on the basis of the electron transfer theory of Marcus (1956, 1959, 1968). A more quantitative expression for the functions $\kappa(E)$ and $W(E)$ has been derived by Dogonadze and Chizmadzhev (1962, 1963) with the assumption that the distribution function $W(E)$ is strictly controlled by the electrostatic interaction between the central ion and the polarizable surroundings. These expressions are discussed by Levich in this volume (Chapter 8). Since the critical parameters needed in this treatment, like the rearrangement energies λ_{Ox} and λ_R from Fig. 13, are not accessible at present, we shall not use these formulas in this chapter.

If the variation of the electrode potential at varying polarizing voltage occurs fully over the space-charge layer, $\Delta\phi_H$ remaining constant, the surface concentrations of carriers follow the applied voltage exponentially [compare Eqs. (3) and (46)],

$$\frac{n_s}{n_{s,0}} = \exp\left(\frac{e_0(\Delta\phi_s - \Delta\phi_{s,0})}{kT}\right) = \exp\left(-\frac{e_0\,\eta}{kT}\right) \qquad (61)$$

and

$$\frac{p_s}{p_{s,0}} = \exp\left(-\frac{e_0(\Delta\phi_s - \Delta\phi_{s,0})}{kT}\right) = \exp\left(\frac{e_0\,\eta}{kT}\right) \qquad (62)$$

where $\eta = U - U_0$ is the overvoltage applied to the electrode, in its usual definition.

The combination of Eqs. (59), (61) and (62) results in a most simple type of current voltage curve, which, in the absence of concentration polarization, i.e. with

$$\frac{c_{R,s}}{c_{R,0}} = \frac{c_{Ox,s}}{c_{Ox,0}} = 1 \ ,$$

reads

$$j_C = j_{C,0} \left(1 - \exp \left(- \frac{e_0 \eta}{kT} \right) \right) \qquad (63a)$$

and

$$j_V = j_{V,0} \left(\exp \left(\frac{e_0 \eta}{kT} \right) - 1 \right) . \qquad (63b)$$

The characteristic feature of such a current voltage curve is that in the conduction band only the cathodic process is influenced by the applied voltage whereas in the valence band only the anodic process depends on the voltage. This difference gives the basis for a distinction between these two processes, as we shall see later in connection with some experimental examples.

Complications in the rate processes can arise by shifts in the Helmholtz layer potential drop with externally applied voltage. [Gerischer (1961)]. For semiconductors with a wide band gap, surface states as additional donor and acceptor energy levels in the forbidden range of the band gap should contribute essentially to the electron transfer processes. The energy conditions for such mechanisms of electron transfer are represented in Fig. 15.

B. Redox Reactions at Semiconductors

1. Techniques of investigations

The most interesting problem for redox reactions on semiconductor surfaces is to distinguish between electron transfer in the conduction band and in the valence band. This can be done by a few techniques which

will be discussed in some detail. A second step is the determination of exchange current rates, or rate constants, for the electron transfer processes in each separate band. The latter step is the more difficult because one runs into the same problems as with metal electrodes, namely the uncertainty of surface structure and of composition of the interfacial layer.

a. Current voltage curves at n- and p-type electrodes.

As long as electronic equilibrium remains established up to the surface of a semiconductor electrode, the surface concentration of electrons and holes, all other properties being equal, does not depend on the doping of the semiconductor if the electrode is on the same electrode potential. The reason is that the difference between the concentrations in the bulk is just compensated by the respective differences in $\Delta\phi_s$ at the same externally applied voltage, if the potential drop over the Helmholtz double layer is the same. Figure 16 shows schematically the course of band energies and concentrations for an n-type and a p-type electrode of the same material at the same electrode potential in contact with a metal on one side and with a redox electrolyte on the other, and for equal differences of the electron energy E_F between electrode and electrolyte.

From this figure, based on Eqs. (3) and (6), it can be seen that the rates of electron transfer should be equal and independent of the doping of a semiconductor, as already implicitly expressed in Eqs. (61), (62) and (63). But this also includes the assumption that electronic equilibrium can be maintained in the space-charge layer in spite of the current necessary for the electrode reaction in the surface.

There is one situation in the space charge layer, however, in which this obviously cannot be verified. This is the case of an inversion layer with consumption of the minority carriers of the bulk in the electrode reaction on the surface. The inversion layer represents a p-n junction which would be biased, in this case, in the reverse direction, and through which, therefore, only a limited current can pass, the so-called saturation current. This is controlled by diffusion and generation of minority carriers over the depth of the mean diffusion length, ℓ, e.g., for electrons as minorities,

$$j_{sat} = e_0 \cdot D_n \cdot \frac{n_0}{\ell_n} = e_0 \, n_0 \sqrt{\frac{D_n}{\tau_n}} \qquad (64)$$

where ℓ_n is the diffusion length (Eq. 43) and τ_n is the lifetime of electrons as in Eq. (39). D_n is the diffusion coefficient.

This saturation current can be increased considerably by surface generation, but, so long as surface generation does not become extremely fast, the consumption of minority carriers in a redox reaction is indicated by the appearance of a saturation current at high enough polarization for the particular material.

Equation (59) shows that an electron transfer in the conduction band would be indicated by a saturation current for the cathodic process on p-type samples and an electron transfer in the valence band by a saturation current for the anodic reaction on n-type crystals. Typical current voltage curves for all possible processes at n- and p-type specimens are drawn in Fig. 17, without taking into account concentration polarization, which in any case limits the current at high rates. Calculations of

the whole current voltage curves with control by minority carrier transport have been carried out by Vdovin et al. (1959).

Electronic saturation currents and mass-transfer-limited current can easily be distinguished by the presence or absence of a photoeffect, [Dewald (1960)], since only electronically controlled currents increase immediately under illumination. In this way, the comparison between n-type and p-type behavior will give in many systems direct information on the role of the energy bands in electron transfer.

b. Transistorlike devices

An ingenious method has been worked out by Brattain and Garrett (1955) using a coupled p-n junction as an indicator for the electronic processes in the electrode surface. Such a device is shown schematically in Fig. 18. One side of a thin slice of a semiconductor, either n- or p-type, serves as electrode. On the other side, a contact with a piece of opposite conductivity type is made in such a way that a p-n junction is formed, which covers the whole area used as electrode side. Around this slice an ohmic contact connects the interior of the slice with two separate external circuits. If the thickness of the slice is on the order of the diffusion length of the minority carriers in the slice, the p-n junction at the back can be used to measure the minority carrier currents which are injected or extracted in the electrode reaction at the front side.

Figure 18 shows how this device works for an n-type electrode as a detector for hole currents. If voltage is applied in the reverse direction of the p-n junction at the back, this junction acts as a collector for the hole injection current on the front. The losses by recombination

during the diffusion through the slice can be measured and when these losses are taken into account the result gives quantitative information on the injected currents. The same information can also be obtained, but with less accuracy, from voltage measurements at the p-n junction on the back side in open circuit.

The analogous device with a p-type slice acts as an indicator for electron injection and extraction. The function of these devices is the same as that of a transistor. The electrode side is the emitter, the ohmic contact is the base, and the p-n junction in the back is the collector.

A similar arrangement has been used by Pleskov (1961) with two electrolytic contacts on both sides of the slice. This works in the same way if an electrode process is found for the back side which is limited by the transport of minority carriers to the surface. Such reactions are the anodic dissolution for n-type germanium slices [Bohnenkamp and Engell (1957)] and the reduction of H_2O_2 for p-type slices [Mindt (1966)].

c. Other methods

A very simple indication can be used for the injection of holes by exploiting the fact that the anodic dissolution of all semiconductors consumes holes. This process is discussed in the next chapter and we use it here as a fact. If the anodic dissolution is controlled by hole transport to the surface, a saturation current is observed at n-type specimens. If a redox systems is added which is reduced under this condition by electrons of the valence band, holes are injected which allow the rate of dissolution to increase [Gerischer and Beck (1957)]. If the redox

system is oxidized by holes, the dissolution rate is reduced by this competing process. Processes in the conduction band interfere with simultaneous processes in the valence band only by recombination which is a minor effect and can be estimated.

The partial reactions can be determined by measuring the chemical changes in the system . Direct information on the mechanism of a redox reaction can be obtained by correlating these partial-current voltage curves with the net current voltage curve. Figure 19 shows an example for such a type of analysis.

The photo response can also be used for a quick qualitative analysis of the type of redox process going on. The current is changed under illumination only when the minority carriers take part in the redox reaction. Quantitative results can be obtained in the range of saturation currents from the current increase under illumination as has been already mentioned in Section IIIB.1a.

2. Selected experimental results

a. Mechanism of redox reactions

Germanium and gallium arsenide electrodes have been most intensively studied as electrodes for redox reactions. An example of the information as obtained from the difference in the behavior of p- and n-type specimens is given in Fig. 20 for the hydrogen evolution reaction in GaAs.

The current limitation at the p-type specimen and the photoeffect at this sample indicate clearly that the hydrogen ion reduction occurs by electron transfer from the conduction band. Similar behavior has been found in Ge electrodes, but the saturation current is much less

pronounced there and is clearly seen only in transient current voltage behavior, because surface states are formed in the cathodic range which act as highly active generation centers for electrons. The saturation current therefore vanishes after short times, [Brattain and Garrett (1955), Gerischer (1960)]. This could be caused also by deposition of impurities from the solution, which act as generation centers [Harvey (1968)].

No electronic limitation in the cathodic current for the reduction of Fe^{+3} ions is found at p-type Ge or GaAs electrodes, [Beck and Gerischer (1959), Pleskov (1961), Gerischer and Mattes (1966)]. The limiting current for this reaction is controlled by mass transfer in solution, indicating that the electron transfer is fast and not rate-determining. The same conclusion for the mechanism of the Fe^{+3}/Fe^{+2} redox reaction is obtained from an application of the transition technique. An example is shown in Fig. 21. This technique has been used extensively by Pleskov (1961) for studying redox reactions on germanium.

As explained in the preceding section, the anodic saturation current in presence of an oxidant can be used for the analysis of redox processes directly. Figure 22 shows current voltage curves for an n-type GaAs electrode without and in the presence of Fe^{+3} ions. The partial currents obtained from analysis of the net chemical changes are included also. One can see that the rate of dissolution increases linearly with the rate of reduction, completely compensating the cathodic process in the range of current saturation, which shows clearly that holes are injected in the redox reaction. For germanium electrodes there is even an overcompensation in the anodic range caused by the fact that the anodic oxidation there goes on partially via injection of electrons.

The results obtained for redox reactions in germanium are summarized in Table I, which gives direct evidence that the theoretical assumptions discussed in the first section describe the situation very well. Redox systems with a positive standard potential exchange holes, those with a negative standard potential electron.

There seem to be some exceptions to this rule [Pleskov (1961)], e.g. the process $J_3^- + 2e^- \rightarrow 3J^-$, which has a standard potential similar to that of the Fe^{+3}/Fe^{+2} redox system. From a naive approach, one would therefore expect that the iodine reduction should occur via the valence band too. But obviously the net reaction as given above does not represent the real charge-transfer step. It could be shown that the electron is picked up in the reaction $J_2 + e^- \rightarrow J_2^-$, with chemical reactions in series to obtain the overall reaction [Gerischer and Mattes (1967)]. For this charge-transfer step, the standard potential is in a range where the surface charge would be negative, which lets this process fit into the theory too. Other apparent exceptions, like the H_2O_2 reduction, could be explained in another way by a catalyzing surface reaction [Gerischer and Mindt (1966)]. There seem to be no contradictions, from present experimental evidence against the theoretical principles on which predictions of the expected type of electron transfer at semiconductors are based.

Table I. Redox systems on germanium

Redox system	Electrolyte	Standard potential	Mechanism
MnO_2/MnO_4^-	1N H_2SO_4	+ 1.62	valence band
Ce^{+3}/Ce^{+4}	1N H_2SO_4	1.39	valence band
$C_6H_4(OH)_2/C_6H_4O_2$	1N H_2SO_4	0.90	valence band
Fe^{+2}/Fe^{+3}	1N $HClO_4$	0.64	valence band
J_3^-/J^-	1N $HClO_4$		conduction band
$Fe(CN)_6^{+3/+4}$	0.01 N H_2SO_4	0.52	valence band
H_2O_2/O_2	1N H_2SO_4		conduction band
H^+/H_2	1N H_2SO_4	0	conduction band
V^{+2}/V^{+3}	0.1 N H_2SO_4	- 0.35	conduction band
$C_2O_4^{--}/CO_2$	0.1N HCl	- 0.50	conduction band

In semiconductors with a wide band gap, redox reactions of the minorities can be found only under illumination. A good example is zinc oxide, in which holes generated by light absorption can oxidize very stable molecules such as alcohols and carbonic acids [Markham and Upret (1965), Morrison and Freund (1967), (1968)]. Similar processes have been observed on CdS electrodes under illumination and anodic polarization [Haberkorn (1967)]. It is interesting to note that the primary reaction products of these processes are often further oxidized by electron injection into the conduction band, which tells us that the radical intermediates in these oxidation reactions have a relatively low work function and highly reducing character.

b. Rate of redox reactions

Experimental experience has shown that the exchange currents at equilibrium for a particular redox system are in most cases smaller at a semiconductor than at a metal. This is in agreement with the predictions from theory because the main electron exchange at a metal electrode occurs on the energy levels around the Fermi energy of the metal, whereas in semiconductors these energy levels are excluded as long as the Fermi energy of the redox systems does not fall into the range of any band in the semiconductor. The number of corresponding energy levels is therefore smaller in a semiconductor electrode, which results in a reduced exchange current.

The quantitative analysis is often complicated by parallel reactions or by more or less regular variations in the surface properties of the semiconductor. Figure 23 gives an example of a current-voltage curve obtained at a Ge electrode for the oxidation of V^{+2} ions. [Mauerer (1965).]

Since the oxidation occurs by injection of electrons into the conduction band, the rate should be equal at n- and p-type electrodes and independent of the applied voltage. Though the first prediction is fulfilled in the range of comparability, the current increases slightly with electrode potential. This can be explained in this system by the assumption that the potential drop in the Helmholtz layer does change simultaneously with $\Delta\phi_s$, which has been confirmed by capacity measurements from which the potential drop in the space-charge layer could be derived. At higher voltages, the electron injection current becomes constant because there the p-n-inversion is reached and any further increase in the voltage does not change the potential drop in the Helmholtz double layer.

Better agreement with theory, without the need of adjustment for kinetical complications, was found for redox reactions on semiconductors with a large band gap. Figure 24 gives an example in the reduction of Fe^{+3} ions in CdS, which is controlled by the electron concentration in the surface and should therefore have a slope of $\frac{d(-U)}{d\ \log(-j)} = \frac{kT}{e_0} \approx 60$ mV at room temperature [Tyagai (1965), Roth (1966)]. The measured slope is very close to this value. In other cases, the slope has been found higher than theory predicts, [Dewald (1960a), (1960b), Lohmann (1966)], which seems to be caused by variations in the Helmholtz double layer.

Quantitative data of this kind are scarce at present and more effort is needed in this field.

C. Charge Injection into Insulators

1. Carrier injection and current voltage curves

The use of insulators as electrodes seems rather paradoxical, since their high resistance allows only extremely small currents, and high voltages are needed as driving forces. But the resistance can decrease

by a large extent if insulators are brought into contact with suitable charge-injecting media. It has been found by Kallman and Pope (1960) that electrolytes which contain redox couples are often excellent charge injectors, which has subsequently been studied in more detail by Mehl (1965 and 1967). From a theoretical point of view, such contacts between insulators and electrolytes are of special interest. Therefore, their properties are discussed in this section.

The distinction between a semiconductor and an insulator is purely pragmatical and arbitrary. The electronic states in the insulator can also be described by the band model. Only, the band gap is higher than for most semiconductors and the absence of suitable dopants prevents conductivity. Under illumination of light of high enough energy, insulators become conducting by excitation of electrons. Electronic charge carriers produced in such a way, if they reach a surface that is in contact with an electrolyte, can react with any electron acceptor or donor in very much the same way as discussed in the preceding section for electrons and holes in semiconductors. The same principles can be applied, as shown by Mehl (1965), to explain the influence of the standard potential of a redox couple on the preferential type of electron-transfer reaction. Oxidizing redox couples react with electrons in the valence band, i.e., in bonding orbitals, and reducing systems can exchange electrons with the conduction band, i.e., with electrons in antibonding orbitals.

This means that oxidized species with high enough oxidation power can inject holes into insulators, and reducing species with high enough reduction power can inject electrons. A big difference in redox potential

corresponding to the band gap in the insulator should be found between systems which allow electron transfer with the valence band or with the conduction band according to the general principles outlined in section III.A1 (Fig. 12).

The high resistance of the insulator generally prevents the detection of this process as long as the electrical fields are not high enough to transfer the injected carriers from the surface to the bulk. If such carriers move into the interior, the conductivity in this range increases and therefore a plot of the current increase is steeper than a linear relation with the applied voltage. This is a characteristic difference between an insulator and a normal semiconductor electrode; the bulk of a semiconductor outside the space-charge layer remains electroneutral, whereas in an insulator the space charge extends over the whole crystal and only the uncompensated excess carriers of the space charge itself transport the current.

The relation between this current and the voltage applied over the insulator crystal of thickness d is given by Child's law, for the case that all injected carriers remain mobile and are not trapped at localized energy states in the crystal. Child's law can be derived from the following considerations for a crystal into which one type of carrier is injected.

In the stationary state, the current density in the crystal must be the same at all cross sections through the crystal, which we shall assume as being a slice of thickness d with parallel faces. The distance from the injecting surface will be denoted by x. The current density is

given by

$$j = u \cdot \rho(x) \cdot F(x) = \text{const.} \tag{65}$$

where u = mobility of the injected carrier, and F = field strength. The connection between electrostatic potential ϕ and charge density ρ is given by Poisson's law, Eq. (8). With the boundary condition that the field vanishes at the injective surface, one gets after first integration of Poisson's equation, and with use of Eq. (65),

$$\frac{dF}{dx} = -\frac{1}{\epsilon\,\epsilon_0}\,\rho(x) = +\frac{j}{u \cdot \epsilon \cdot \epsilon_0} \cdot \frac{1}{F(x)} \,. \tag{66}$$

This equation can be integrated again, with the result

$$F(x)^2 = \frac{2j}{u \cdot \epsilon \cdot \epsilon_0} \,. \tag{67}$$

The voltage drop over the crystal can be derived from integration of F(x):

$$\Delta\phi = \int_0^d F(x)\,dx = \frac{2}{3}\,\sqrt{2j/u\epsilon\epsilon_0}\cdot d^{3/2} \,, \tag{68}$$

from which we obtain a relationship between current density and applied voltage, U = $\Delta\phi$

$$j = \frac{9}{8}\,\frac{u\epsilon\epsilon_0}{d^3}\,U^2 \tag{69}$$

which is Child's law.

The difference in voltage dependence, from the law for space charge limited currents in vacuum, results from the different conductance mechanisms in a solid and in a vacuum.

If localized energy states for electrons are present within the band gap, the current voltage curves become much more complex. Mobile

carriers can be captured in such traps, increasing the space charge in this way without changing the conductivity. If this ratio between mobile and trapped carriers remains constant, the only change in Eq. (69) is a decrease of the effective mobility per charge carrier. But the traps normally have quite a distribution over a broad range of energies, with the results that the probability of liberating a trapped charge carrier is much higher for shallow than for deep traps. The trapped space charge which compensates to a large extent the externally applied voltage reduces the current considerably. This can only be overcome by a high enough increase of the external field strength which finally will cause an emptying of traps by internal field emission into the bands. For an exponential distribution of traps in energy, this leads to current voltage relations with a higher power than 2 for the voltage, as an approximation over some limited ranges, as expressed by Rose (1955), Lampert (1956), (1964), Mark and Helfrich (1962).

$$j \sim \frac{U^{n+1}}{d^{2n+1}} \quad , \quad n > 1 \tag{70}$$

At high enough field strengths, the traps tend to be depleted by field emission into the continuous energy bands. If no charges remain trapped at very high fields, one reaches the situation of Child's law again as a limiting case.

Obviously the current cannot exceed the rate of injection. Therefore, the current voltage curves must finally become controlled by this step, which will not be influenced by the applied field as long as the charge density in the space charge layer does not reach extremely high values. This results in a limiting current which can begin at any part

of the current voltage curve, and gives direct information on the rate of the injection process. These features of current voltage curves for insulator crystals with charge injection from contacts are schematically shown in Fig. 25.

2. Experimental techniques and selected results

The major experimental difference for studying the electrochemistry of insulators is the necessity of applying high electrical fields to the electrode. To handle this problem without unnecessarily high voltages the electrode should be made as thin as possible. There is usually no difficulty in mobile charge carriers' leaving an insulator at contacts with metals or with electrolytes. The side where carriers are injected can therefore be studied directly with the current behavior as related to the voltage drop over the crystal. The most direct and easiest way of determining the type of charge carrier which can be injected is to use an injecting contact on one side and a noninjecting on the other side of the insulator. Current will then flow in one direction only, indicating the sign of charge of the injected carrier. Electrolyte solutions which are free of redox components make convenient noninjecting contacts; it is difficult to make a good contact by metals. A cell of this type, with two electrolyte contacts for a thin insulator crystal, is shown in Fig. 26. [Mulder (1965), Gerischer et al. (1967)]

Since currents are usually small, the auxiliary electrodes give no special problems. If necessary, reference electrodes in the electrolyte can be used for determining the voltage drop over the crystal. Shielding and isolation from parasitic currents become a serious problem in all such measurements. Further, the slow response of the voltage

measurements at low voltages due to the high inner resistance must be taken into account if one tries to study the equilibrium situation for charge injection at the interface.

For simultaneous control of transport processes in the electrolyte, an insulator electrode mounted on a rotating disk has been used by Lohmann and Mehl (1967) for such cases where charge injection is a fast process. Typical current voltage curves for the injection of holes into a perylene crystal are shown in Fig. 27. In this system, a limiting current is reached already in the range where the trap distribution controls the current-voltage curve, which increases with a power of n in Eq. (70) between 5 and 6.

An example for electron injection is described by Mehl and Buchner (1965). In accordance with the theoretical principles outlined in the preceding sections, a very negative redox potential is necessary to allow electron injection into organic crystals of this type, in which the energy of the conduction band lies rather high. Therefore, non-aqueous solvents had to be used to obtain suitable systems for electron injection. The absence of a limiting current in these results indicates that the injection rate is high.

If the insulator is brought into contact with two different solutions, one of which is able to inject holes and the other electrons, double injection can be observed [Mehl (1966)]. This is an especially interesting case because the conductivity type is now different at both contacts of the crystal. In the interior where the carriers of opposite sign meet recombination occurs which is related, to

some extent, to the emission of light. The light intensity for such a double injection experiment in anthracene, in correlation with the current density, is plotted in Fig. 28 according to experiments by Mehl (1966). The highest intensity of light emission is reached when one of the injection processes becomes saturated; for the case represented in Fig. 28 this is the hole injection. Further increase of the current does not increase the concentration of holes in the crystal, but only the concentration of electrons, which should result in giving a constant light intensity. In the experiments shown in Fig. 28, however, the amount of light even decreases at higher current densities, because of some additional radiationless surface-recombination processes, which cannot be discussed in detail here.

D. Light-Induced Electron Transfer

In the foregoing sections we have discussed some processes in which the absorption of light in the semiconductor enhances possible electron transfer reactions by creating additional charge carriers. We shall discuss in the following such processes that are possible only under illumination and do not take place in the dark. Two different possibilities can be distinguished, depending on whether light is absorbed in the electrode and the reaction is due to the excitation of electrons in the semiconductor or whether it is the reactant that absorbs the light and reacts in an excited state.

1. Excitation of the electrode as a primary step

If the light is absorbed by the electrode, we can find either the generation of electron-hole pairs, as already discussed, or of excited

energy states of the crystal, the so-called "excitons," where the electrons remain in strong coupling with the positive charge. The reactions of free carriers with electron acceptors or donors have already been discussed in enough detail that little has to be added here, since it makes no difference whether electrons or holes are already present in the dark or only produced by the illumination. The latter situation is often found for semiconductors with a wide band gap and a very deep lying energy of the valence band. Such crystals are n-type, either by a natural electron donor excess or by doping, but cannot be made p-type, and the generation of holes by illumination is the only way for studying their reactions. The same is true for electrons and holes in insulators. To study the reactions of those carriers generated by light it is necessary to apply an electric field in sich a way that recombination is prevented. For an n-type semiconductor, this condition is fulfilled in the depletion layer when all the light is absorbed in the depleted range. Under the influence of the electric field, all electron-hole pairs are separated then, the holes moving to the surface, where no electrons are present with which they could recombine. This process is shown in Fig. 29 in terms of the band model. [Gerischer (1966).]

Holes which accumulate in the surface in this way can cause oxidation processes which are otherwise very unlikely. As already mentioned in Section IIIB.2a, at a surface of a ZnO or CdS electrode, when illuminated by suitable light and anodically polarized, many organic molecules are oxidized to radicals, in reactions such as [Morrison and Freund (1967), (1968), Markham and Upret (1965), Haberkorn (1967)]

$$R{\cdot}H_2 + h^+ \rightarrow \cdot\ RH + H^+ \cdot\ solv \qquad (71)$$

In p-type semiconductors with a wide band gap, the equivalent reduction reactions by electrons should occur at cathodic polarization and illumination.

Besides such a direct charge transfer, an indirect type of charge injection has been observed after excitation of a crystal by light of a wavelength that does not generate free carriers. The excitons that are generated can diffuse to the surface and can react there with electron acceptors or donors in either of the two following ways: [Kallmann and Pope (1960), Mulder (1967), Mulder and de Jonge (1963)]

$$\text{excit.} + A \rightarrow A^- + h^+ \qquad (72)$$

$$\text{excit.} + D \rightarrow D^+ + e^- \qquad (73)$$

The conditions for such surface processes are not yet fully understood. The process must obey the conditions of energy conservation and the Franck-Condon restriction for the charge transfer step. The latter results, as we have seen in section II.A, in the necessity to have electron energy levels on equal height available for the transition from one quantum state to the other.

We assume that the excitation energy is transferred primarily from the crystal to the acceptor or donor and subsequently the excited acceptor or donor molecule injects the charge carrier into the semiconductor, being reduced or oxidized in this excited state.

The mechanism would be then very similar to this which will be discussed in the next section and the mechanism should be formulated instead with Eqs. (72) and (73) by

$$\text{excit.} + A \rightarrow A^* \rightarrow A^- + h^+ \qquad (72a)$$

$$\text{excit.} + D \rightarrow D^* \rightarrow D^+ + e^- \qquad (73a)$$

The necessary conditions for the electron energy levels in the acceptor and donor molecules are shown in Fig. 30. For process (72) to occur, the ground level S must be in the range of the valence band. For process (73), the excited level S^* must be in the range of the conduction band. In both cases, the difference between S and S^* must correspond to the exciton energy.

An example of a charge-transfer process, induced by generation of excitons in a crystal, is given in Fig. 31.

2. Excitation of the electron donor or acceptor as a primary step

Spectral sensitization of photosensitive materials has been discussed frequently under the aspect of electron injection or extraction by the excited dye molecules [Dörr and Scheibe (1961), Nelson (1967)]. The same process has been found at semiconductor or insulator electrodes, [Gerischer et al. (1967), Gerischer and Tributsch (1968)], and can be understood in ways fully analogous to the previously discussed transfer processes.

A simple picture of the possible mechanism is represented in Fig. 32. The excited molecules, X, usually a dye because it needs a high absorption coefficient to get a big effect, can act either as a donor or as an acceptor of electrons in the electrode. After light absorption, $X + h\nu \rightarrow X^*$, either of the following steps can occur:

$$X^* \rightarrow X^+ + e^- \qquad (74)$$

or

$$X^* \rightarrow X^- + h^+ \qquad (75)$$

Which of the two actually occurs depends on the correlation of the excited and the ground states of the dye to the band edges. Figure 32 shows the two different conditions; for the process of Eq. (74), the electronic

level of the excited molecule must be above the conduction band edge, and for process (75), the ground level, which becomes emptied by excitation, must be below the valence band edge.

To make these processes most effective and to exclude the reverse reactions, the electrode has to be polarized anodically (positively charged) for the process of Eq. (74) and cathodically for that of Eq. (75).

Presence of impurity states or trap levels between the band gap usually makes the situation more complex. Transfer of the excitation energy to the crystal, with the generation of mobile charge carriers as a result, is possible, and seems to play some role in those cases which are of practical interest for photography. In the few hitherto studied cases of sensitized electrode reactions, however, the dyes are either oxidized or reduced, which proves that they exchange electrons with the electrodes either in the excited state directly or with the impurity states secondarily. The spectral efficiency of sensitized charge injection, the so-called action spectrum, is identical with the absorption spectrum of the adsorbed dye molecules, indicating that there is only weak interaction of their electronic system with the electrode surface.

The following figures give examples for such processes. Figure 33 shows current voltage curves for ZnO electrodes under anodic polarization without and in the presence of a sensitizing dye, at various concetrations of the dye [Gerischer and Tributsch (1968)]. As one sees, at high enough anodic voltage -- with formation of a depletion layer, compare Fig. 29 -- a saturation current is reached which is proportional to the light intensity. The action spectrum is given in Fig. 34, with the normal absorption spectrum for comparison. All long-known photographic phenomena of

sensitization could be observed in such sensitized electrode reactions, too, e.g. the effect of supersensitization, for which an example is given in Fig. 35. The action spectrum is not changed by the presence of the supersensitizer in this case indicating that the main interaction between supersensitizer and sensitizer occurs after excitation of the dye molecule [Gerischer and Tributsch (1968)].

Whereas the direction of the current emphasizes electron injection by excited dye molecules in ZnO electrodes, an effect of opposite direction has been found at organic insulator electrodes such as anthracene and perylene [Gerischer et al. (1967)]. Figure 36 gives the injection current for a perylene crystal in contact with rhodamine B. The current voltage curve obtained is typical for space-charge-limited currents up to the voltage at which saturation is reached, which depends on light intensity in these systems. In these crystals, holes are injected and the dye is reduced. The action spectrum is seen in Fig. 37.

Because the dyes are oxidized or reduced in these processes they can sensitize only one if they are not regenerated by another redox reaction. In presence of a suitable reductant, or oxidant, respectively, a dye molecule can act repeatedly as a sensitizer until an irreversible change occurs by chemical side reactions.

IV. ELECTROLYTIC PROCESSES WITH CHEMICAL CHANGE OF THE SEMICONDUCTOR

All elements that are the constituents of semiconductor crystals are rather reactive chemically. In the semiconductor crystal, however, the atoms are to a great extent stabilized against attack from outside by their strong interaction -- i.e., by chemical bonds -- with their nearest neighbors in the crystal. These bonds have mainly a covalent character, with some degree of polarity in the compound semiconductors. Any chemical attack that would result in forming new and stronger chemical bonds to other reactants has first to break these bonds in the crystal, and this creates a high energy barrier for such reactions. This is why electrons and holes play such a decisive role in decomposition reactions of semiconducting crystals. They represent electronic defects where the bond network of the crystal is weakened and the attack can be initiated. Since the concentration of the electronic carriers can be easily varied in the surface of a semiconductor electrode over orders of magnitude, and the progress of oxidation or reduction can be followed with greatest sensitivity by the current of an electrochemical cell, the mechanism of such bond breaking can be studied in detail by electrochemical techniques, as is discussed in this chapter.

A. Oxidation Processes

1. Theoretical considerations

In an electrochemical oxidation, the electrons of the surface atoms which are in bonding energy states are removed from these states and finally transferred to the external voltage source, which supplies the driving force for this process. The transport of the charge through the

interior of the semiconductor will occur, in accordance with the conductivity type, preferentially in either the conduction or the valance band. In the surface reaction itself, however, electronic equilibrium cannot be expected, since this is an irreversible process and since the oxidation reactions in the surface are exclusively restricted to alternative paths which involve either holes or electrons per step. Full equilibrium distribution of the carriers is established at some distance from the surface. We discuss here first the oxidation of a chemical bond between two surface atoms that might be located in the attackable site (kink site) of a crystal surface. Because two electrons have to be removed from one covalent bond, two steps are involved in the reaction in any case. These, together with the two electronic alternatives, give us four reactions to discuss [Gerischer (1968)]:

$$A - A + X^- \xrightarrow{v_1} A - X + A^\bullet + e^- , \qquad (76)$$

$$A - A + X^- + h^+ \xrightarrow{v_2} A - X + A^\bullet , \qquad (77)$$

$$A^\bullet + X^- \xrightarrow{v_3} A - X + e^- , \qquad (78)$$

$$A^\bullet + X^- + h^+ \xrightarrow{v_4} A - X \qquad (79)$$

The assumption that the bond is broken in two steps leads to the postulation of a radical intermediate, $A^\bullet$, with one unpaired electron. The new bond is formed with a nucleophilic ligand, X^-, to which, for simplicity, a negative charge has been attributed to compensate for the positve charge of the oxidized surface atoms. This ligand could also be a neutral molecule and the resulting product would then be an ion in the electrolyte, or may later undergo some chemical change.

The kinetics of these steps are described by relationships as given in the following equations,

$$v_1 \propto \nu_1 \cdot c_{X^-} \cdot N_S \cdot N_C \exp\left(-\frac{E_1^*}{kT}\right), \tag{76a}$$

$$v_2 \propto \nu_2 \cdot c_{X^-} \cdot N_S \cdot p_s \cdot \exp\left(-\frac{E_2^*}{kT}\right), \tag{77a}$$

$$v_3 \propto \nu_3 \cdot c_{X^-} \cdot N_R \cdot N_C \cdot \exp\left(-\frac{E_3^*}{kT}\right) \tag{78a}$$

$$v_4 \propto \nu_4 \cdot c_{X^-} \cdot N_R \cdot p_s \cdot \exp\left(-\frac{E_4^*}{kT}\right). \tag{79a}$$

In these equations the frequency factors are denoted by ν_i and the activavation energies by E_i^*; N_S is the number of kink sites, N_R the concentration of radicals in the surface.

The competing processes are reactions (76) and (77) on the one hand and (78) and (79) on the other. Since the frequency factors are similar, the two last factors in the rate equations (76a-79a) decide which process is faster and therefore determine the reaction path.

We obtain some estimate of these relations from Fig. 38 in which an energy profile is plotted against a reaction coordinate representing the reaction path for both steps. The energy difference for the initial states of reactions (76) and (77) is equal to the band gap, because the presence of a hole in a semiconductor means that one electron has been excited from a bonding state in the valence band to an antibonding state in the conduction band. The transition states for both reactions are closer to the final state of these first steps, and therefore it is to be assumed that the difference in the activation energies $E_1^* - E_2^*$ will be close to E_{gap},

$$E_1^* - E_2^* = \gamma_1 E_{gap};\ 0.5 < \gamma_1 < 1\ . \tag{80}$$

Comparing now the rates of the parallel paths (76) and (77), we obtain

$$\frac{v_2}{v_1} \approx \frac{p_s}{N_C} \cdot \exp\left(\gamma_1 \cdot \frac{E_{gap}}{kT}\right)\ , \tag{81}$$

where p_S is related to the difference in energy between the Fermi level in the surface, ${}_sE_F$, and the top of the valence band by the relation

$$p_s = N_V \cdot \exp\left(-\frac{{}_sE_F - E_V}{kT}\right)\ . \tag{82}$$

We therefore get from (81) and (82),

$$\frac{v_2}{v_1} \approx \frac{N_V}{N_C} \cdot \exp\left(\frac{\gamma_1 \cdot E_{gap} - ({}_sE_F - E_V)}{kT}\right). \tag{83}$$

The effective densities of states in the valence and in the conduction band are normally in the same order of magnitude. The exponential term is therefore decisive. This term tells us that with $\gamma_1 > 1/2$, the second path is much more likely if the surface becomes p-type, which means if ${}_sE_F - E_V < 1/2\ (E_{gap} + kT\ \ell n\ \frac{N_V}{N_C})$. Since the activation energy is usually high for the bond breaking reaction, one should expect that in all systems it will need p-type surfaces until this oxidation reaches measurable rates. The predominance of path (77), i.e., the reaction with holes is more pronounced as the band gap is higher, because the activation energy must increase with the band gap according to the conditions plotted in Fig. 38.

For the second step, the situation is somewhat different. The comparison between the rates of steps (78) and (79) can be made in fully analogous ways. But the difference in activation energies is now correlated with the energy difference between the energy term E_R of the unpaired electron in the intermediate reaction state, the radical surface state, and the energy at the bottom of the conduction band, because oxidation of this radical surface state means, in terms of energy, transfer of the unpaired electron to the conduction band:

$$E_3^* - E_4^* = \gamma_2 \cdot (E_C - E_R) \quad . \tag{84}$$

The relation between the rates of those second steps is therefore

$$\begin{aligned} \frac{v_4}{v_3} &\approx \frac{p_s}{N_c} \exp\left(\gamma_2 \frac{E_C - E_R}{kT}\right) \\ &= \frac{N_V}{N_C} \exp\left[\frac{\gamma_2(E_C - E_R) - ({}_sE_F - E_V)}{kT}\right] \quad , \end{aligned} \tag{85}$$

where γ_2 again is between 0.5 and 1. But Eq. (85) shows that this relation now depends strongly on the position of E_R. If E_R is close to the valence band edge, we have the same situation as for the first reaction step. If it is closer to the middle of the gap, a higher probability will be found for an excitation of the unpaired electron into the conduction band and the second step involves an injection of electrons instead of hole consumption. This injection of electrons in the second step will become more and more unlikely as the band gap increases, because this means an increase of the activation barriers for both steps. The reaction will then go only under such conditions that ${}_sE_F$ is close to E_V and far below the middle of the gap. So, for semiconductors with a high band gap,

one should expect a completely hole-consuming process.

For compound semiconductors, where the bond has some degree of polarity, one can predict that the more electropositive component will form the new bond to the ligand in the first reaction step, and the more electronegative component will remain in the radical state. Besides further oxidation of this radical atom, if possible at all, an association type of reaction between adjacent surface radicals must then be taken into account as an additional reaction possibility as shown in the following series of reactions:

$$\overset{(\delta+)}{A} \text{---} \overset{(\delta-)}{B} + X^- \xrightarrow{v_1'} A - X + B^{\bullet} + e^- \quad , \tag{86}$$

$$\overset{(\delta+)}{A} \text{---} \overset{(\delta-)}{B} + X^- + h^+ \xrightarrow{v_2'} A\text{-}X + B^{\bullet} \quad , \tag{87}$$

$$B^{\bullet} + X^- \xrightarrow{v_3'} B\text{-}X + e^- \quad , \tag{88}$$

$$B^{\bullet} + X^- + h^+ \xrightarrow{v_4'} B\text{-}X \quad , \tag{89}$$

$$B^{\bullet} + B^{\bullet} \xrightarrow{v_5'} B\text{-}B \quad . \tag{90}$$

A comparison between the competing reactions (86) and (87), or (88) and (89), can be made in the same way as before for the fully covalent bond type. From such comparison, it can be derived that a contribution of electron injection by reaction (88) should become more and more unlikely with increasing polarity of the bond. The reason is that the bonding energy states in a polar bond are more similar to the atomic energy states of the more electronegative component than to those of the electropositive ones. Since the electron orbital of the unpaired electron at component B is like an atomic orbital and has less interaction with the crystal

than equivalent ones in intact bonds, this radical energy level, E_B, must be close to E_V in a polar crystal. This means that the relation equivalent to Eq. (85) becomes very similar to that in Eq. (83), where we could with great certainty exclude the electron injection for semiconductors with a wider band gap.

If the electronegative component of the semiconductor is already so negative in the electronegativity scale that it is unlikely to find a more electronegative partner for further oxidation, the association or recombination type of reaction is the most likely -- or the only possible one-- for this series of reactions.

In a real semiconductor, an atom or molecule in a kink site has always more than one chemical bond to the crystal. But, usually, breaking of the first bond is the slowest step; the other ones follow relatively fast in consecutive reaction steps which all contain the two stages as discussed before but with lower activation barriers. What can be seen in experiments will be the highest barrier and the net contribution of holes and electrons in all bond-breaking steps necessary to remove one kink site atom or molecule from the crystal. In spite of this complication the experiments seem to give, in most cases, rather clear information on the type of preferential reactions, which will be shown in the next section.

2. Selected examples

That holes are needed for the anodic oxidation of semiconductor electrodes can be seen immediately from the different behavior of p-type and n-type crystals [Brattain and Garrett (1955)]. Figure 39 gives an example for germanium, showing that a saturation current is found in n-type specimens which decreases with rising electron conductivity and increases

under illumination. Obviously, hole transport to the surface, by diffusion and generation, controls this saturation current range, as discussed previously for hole-transfer reactions in Eqs. (50)and (64), indicating that holes are consumed in the rate-determining step.

More detailed analysis of the electronic processes by various techniques have shown [Brattain and Garrett (1955), Turner (1956), Beck and Gerischer (1959), Boddy (1964)] that electrons are injected at Ge electrodes simultaneously, and the net reaction can be described by

$$Ge + mh^{+} \longrightarrow Ge^{+4} + (4-m)\, e^{-} \quad . \qquad (91)$$

The contribution of holes, characterized by the stoichiometric number m, was found between 2 and 4, and depends on the concentration of holes in the surface [Gerischer and Beck (1960b)]. The kink site on a Ge crystal surface has two intact bonds to the crystal. The lower limit of m is 2, which means that the bond breaking needs one hole in the first stage for either bond. The second stage follows a statistical correlation between hole consumption and electron injection which favors hole consumption if holes are easily enough available [Gerischer and Beck (1960b)].

The current voltage curve, in a semilogarithmic plot, has a slope of $\frac{dU}{d \log j}$ between 70 and 80 mV in alkaline solutions and up to 120 mV in acidic solutions, instead of the theoretical slope of 60 mV for a rate-determining step with consumption of one hole [Beck and Gerischer (1959a)]. As proven by Brattain and Boddy (1965), this higher slope is caused by a change in the potential drop over the Helmholtz double layer, and if one plots the current in the logarithmic scale against the independently measured $\Delta\phi_s$ values, one obtains indeed the theoretical slope of 60 mV

per decade of the current. In highly concentrated HF solution, Mehl and Lohmann (1967) have observed the theoretical slope of about 60 mV/decade. Summarizing the various experiments: The mechanism of the anodic oxidation of germanium in alkaline solution can be described by the steps given in Fig. 40.

For silicon, with which the experiments must be carried out in HF solutions to avoid the formation of current-blocking oxide layers, it was found that the primary oxidation leads to Si^{+2}, with consumption of two holes, and the formation of Si^{+4} is completed in consecutive chemical reactions with water as oxidant [Flynn (1958), Turner (1958)]. This indicates either an association reaction of the radical surface states or, what seems more likely, a fast chemical attack by the electrolyte on the intermediates. Under high voltages, a direct oxidation to the tetravalent state has been observed [Memming and Schwandt (1966)]. Gallium arsenide is oxidized with consumption of six holes to Ga^{+3} and As^{+3} [Gerischer (1965)]. Only a very small contribution of electrons has been found (less than 0.1%) [Gerischer and Mattes, unpublished].

In ZnO crystals the energy terms of the valence band are at such low levels that thermal generation of holes does not occur at normal temperatures. The specimens are usually n-type because of an excess of Zn atoms. When ZnO crystals of this type are used as electrodes, a negligible current flows under anodic polarization. The remaining tiny current is caused by chemical dissolution of the crystal, and indicates the oxidation of excess Zn atoms which become exposed to the electrolyte during the progress of dissolution. Under illumination with light of 3700Å or smaller wave lengths, however, a current is found which is

proportional to the light intensity and causes decomposition of the ZnO crystal [Williams (1960), Gerischer (1966), Lohmann (1966), Hauffe (1967)]. Such current voltage curves are shown in Fig. 41.

The decomposition reaction under illumination can be described by

$$ZnO + 4\,h\nu \rightarrow ZnO + 4h^{+} + 4e^{-} \quad ,$$
$$2ZnO + 4h^{+} \rightarrow 2Zn^{+2} + O_2 \quad . \qquad (92)$$

The situation found in the anodically polarized ZnO surface under illumination has already been shown in Fig. 29. At high enough voltage, the depletion layer in which we have the high electric field that separates electrons and holes has extended far enough into the crystal to obtain 100% efficiency for the charge separation. This situation is indicated by the saturation current in Fig. 41, where all holes produced by light absorption react according to Eq. (92) without loss by recombination. This reaction is an example for the mechanism of bond breaking in a polar crystal where the association reaction of Eq. (90) is the second step because the electronegative component cannot be oxidized further.

CdS crystals have been found quite similar in behavior, with a decomposition reaction forming Cd^{+2} and elemental sulfur under illumination [Williams (1960), Haberkorn (1967)]. Another interesting case is the behavior of p-type CuO, which decomposes in acid solutions under anodic polarization into Cu^{+2} and O_2 [Bickl (1966)]. Since this oxide can be made p-type by doping, the anodic decomposition in a reaction analogous to Eq. (92) needs no illumination, and the electric field is already sufficient to let the concentration of holes increase enough for breaking the bonds in the crystal surface with sufficient rate.

B. Reduction Processes

1. Kinetics

The presence of an electron in an antibonding orbital at surface atoms means bond weakening as well as the absence of an electron in a bonding orbital. This type of electronic defect, however, is attacked by electrophilic reagents if a new bond can be formed by a rearrangement of the electrons in the bonding orbitals. Again, the other partner of the attached bond remains in a radical state as intermediate and can react further with the electrophilic reagent or recombine. We discuss this process for a semiconductor with a polar bond, because this is the more general case and one of practical importance. The following reaction steps are to be expected [Gerischer and Mindt (1968)]:

$$\overset{(\delta+)}{A}\!\!-\!\!\overset{(\delta-)}{B} + e^- + Y^+ \xrightarrow{\nu_1} A^\bullet + B\text{-}Y\,, \tag{93}$$

$$\overset{(\delta+)}{A}\!\!-\!\!\overset{(\delta-)}{B} + Y^+ \xrightarrow{\nu_2} A^\bullet + B\text{-}Y + h^+\,, \tag{94}$$

$$A^\bullet + e^- + Y^+ \xrightarrow{\nu_3} A\text{-}Y\,, \tag{95}$$

$$A^\bullet + Y^+ \xrightarrow{\nu_4} A\text{-}Y + h^+ \tag{96}$$

$$A^\bullet + A^\bullet \xrightarrow{\nu_5} A\text{-}A\,. \tag{97}$$

The kinetics can be expressed by

$$v_1 \propto \nu_1 \cdot c_{Y^+} \cdot N_S \cdot n_s \cdot \exp\left(-\frac{E_1^*}{kT}\right), \tag{93a}$$

$$v_2 \propto \nu_2 \cdot c_{Y^+} \cdot N_S \cdot N_V \cdot \exp\left(-\frac{E_2^*}{kT}\right), \tag{94a}$$

$$v_3 \propto \nu_3 \cdot c_{Y^+} \cdot N_R \cdot n_s \cdot \exp\left(-\frac{E_3^*}{kT}\right), \tag{95a}$$

$$v_4 \propto \nu_4 \cdot c_{Y^+} \cdot N_R \cdot N_V \cdot \exp\left(-\frac{E_4^*}{kT}\right), \tag{96a}$$

$$v_5 \propto \nu_5 \cdot N_R^2 \cdot \exp\left(-\frac{E_5^*}{kT}\right) . \tag{97a}$$

An argument similar to that given for the anodic processes, Eqs. (76-79), leads to the result that the difference of activation energies between steps (93) and (94) are correlated to the band gap by the relation

$$E_2^* - E_1^* \approx \gamma_1 \cdot E_{gap} ,$$

with $\gamma_1 > \frac{1}{2}$. That means that in the first competing parallel reaction step, the relationship should be

$$\frac{v_1}{v_2} \approx \frac{N_C}{N_V} \cdot \exp\left(\frac{sE_F - E_C + \gamma_1 E_{gap}}{kT}\right) . \tag{98}$$

For the second competing steps, the difference in activation energy will be correlated to the energy levels $E_{A\cdot}$ of the unpaired electron in the radical A· and the energy at the top of the valence band. In a polar bond, the anti-bonding orbitals are constituted mainly by the atomic orbitals of the more electropositive component. The radical A· represents, therefore a surface state, the energy level of which is close to the bottom of the conduction band. This has the consequence that process (96) becomes very unlikely for semiconductors with a wide band gap, since this reaction includes thermal excitation of an electron from the valence band, whereas the competing step (95) is favored by the high electron concentration necessary to start the preceding step

(93), which has a higher activation barrier anyway.

From this discussion we would expect that the reduction of semiconductors with a wide band gap would proceed 100% via electrons of the conduction band, and a saturation current should be found for p-type specimens. Unfortunately, however, generation-recombination centers developed during the reduction process seem to play a much more important role here than for oxidation reactions, and this can mask the electronic effects discussed above to a great extent.

2. Examples

Experimentally, one has to face the problem that the products of the reductive decomposition of a semiconductor, in contrast to the anodic decomposition, usually stick on the surface and change its properties radically. Furthermore, electrophilic reagents are much less common in electrochemical processes than nucleophilic ones. The predominant electrophilic reagent in aqueous electrolytes is the proton, but only a few of the hydrides formed in the surface reaction are soluble or volatile.

Therefore, the reduction process of the semiconductors germanium and gallium arsenide stops after hydrogenation of the surface atoms, and no further decomposition by formation of volatile hydrides could be detected [Mindt (1966)].

That the hydrogenation of a germanium surface occurs by participation of electrons could be shown by studying transient current voltage behavior of thin slices, where the transistor technique described in Section IIIB.1 could be applied. Figure 42 shows a transient current voltage curve with linear change of voltage over time, for p-type and n-type Ge slices

[Gerischer et al. (1966)]. Simultaneously, the electron or the hole current on the back side of the slice is registered. The collector currents for electrons on the back side (p-type slice) indicate clearly that electrons are consumed during reduction and injected during oxidation. On the other hand, the hole current (n-type specimen) shows that, during reduction, holes are injected and are extracted during oxidation. From this and other evidence it was concluded that the hydrogenation and reoxidation of a germanium surface follows a mixed type of reaction mechanism, as described by

$$Ge \text{ —— } OH + H^+ + e^- \rightleftharpoons Ge^* + H_2O \quad , \tag{99}$$

$$Ge^* + H^+ \rightleftharpoons Ge\text{—}H + h^+ \quad . \tag{100}$$

In the direction of reduction, the first step involving electron consumption is rate-determining; in the reverse direction, the second step involving hole consumption. Therefore, for the reduction step, a current saturation has been observed in p-type samples, and for the oxidation, in n-type samples.

The reduction of II-VI-compound semiconductors with a high polarity of the bonds -- as in ZnO, CdS, or other oxides and sulfides -- has not yet been studied under these circumstances. The reason is that a new phase, the metal deposit, is formed by reduction, which not only acts as generation-recombination source of high efficiency but also represents a new interface that has a very complex and unknown geometrical structure and poorly defined physical and chemical properties. But there is no doubt that the initial formation of metal nuclei is catalyzed by electrons

in the conduction band, and follows such kinetics as outlined in this section. An example of the mechanism is given in Fig. 43 for the reduction of a ZnO crystal.

C. Decomposition Without External Current

In the presence of oxidizing reagents, a semiconductor is attacked, like most metals. If this happens in an electrolytic conductive environment, the probability is very high that this attack proceeds according to an electrochemical mechanism; that means an anodic and a cathodic process go on at equal rates on the surface, in this way compensating the net electrical current to zero. The theory of such independent, superimposed partial currents, which are coupled only by the electrical field in the surface, has been worked out by C. Wagner (1938). But the application of this treatment without modification to semiconductors leads to some unexpected difficulties, which are caused by the differentiation of the partial currents into electron and hole currents. This causes a new type of coupling, discussed in the following section.

Besides this electrochemical type of attack, a direct chemical oxidation has been observed [Gerischer and Mindt (1968)]: in which the rate does not depend on the charge in the surface. This attack is found only for oxidants which can form two new chemical bonds simultaneously with the two partners of a chemical bond on the surface. The most important of such reagents are Cl_2, Br_2, I_2, and H_2O_2. The mechanism of this direct attack is represented by Fig. 44.

1. Theory of electrochemical corrosion for semiconductors

The general condition for a steady state in corrosion is the balance of anodic and cathodic currents: $j^+ = j^-$. In metals, the partial currents depend not only on the composition of the surface and of the electrolyte adjacent to the surface, but also on the electrical field strength in the interface. This electrical field influences these two processes oppositely and the electrode potential adjusts itself to fulfill this balancing condition.

As we have seen in previous sections, the field strength varies little at a semiconductor surface. The governing factors for the rate of charge transfer reactions are the concentrations of electrons and holes in the surface. But only an anodic reaction in the valence band and a cathodic reaction in the conduction band is influenced by any change of hole or of electron concentration, while the reverse processes go on at practically constant rate. The balancing condition for the net current does not necessarily mean the balancing of the partial currents in each of the bands. It only means

$$j_C^+ + j_V^+ = j_C^- + j_V^- \quad . \tag{101}$$

The net currents in each of the energy bands must not be zero, but will have opposite sign:

$$j_C^+ - j_C^- = j_C = -j_V = j_V^- - j_V^+ \quad , \tag{102}$$

where j_C is the electron injection current and $-j_V$ is the hole injection current, which must be equal under corrosion conditions. We see from Eq. (102) that corrosion can lead to simultaneous injection of electrons

and holes. Though formally j_C could be negative, and corrosion would then mean electron-hole pair extraction, this seems rather unlikely. The reason is that the cathodic process is usually overwhelmingly a hole-injection reaction, because oxidants which can pick up electrons only from the conduction band are not able to oxidize the semiconductor crystal. But electron-hole pair injection is a rather common possibility in the steady state for the corrosion of semiconductors.

In this case, the situation is very similar to that under illumination and electron-hole pair injection causes a change in the distribution of carriers in the space-charge layer, as was discussed for capacity in Section IIB.3. A detectable effect can be expected only if the space-charge layer is very sensitive to any change in the equilibrium distribution, that is, for a depletion or an inversion layer. As we have seen, the anodic oxidation of semiconductors consumes holes and occurs only if the surface is p-type. Therefore, this electron-hole-pair injection can be noticed only in n-type specimens, and especially when an inversion layer is formed underneath the surface.

The resulting effect is a deviation of corrosion potential in the negative direction from that value which one would expect from simple superposition of anodic and cathodic current voltage curves. This can be treated [Gerischer and Beck (1960a)] like the origin of a photovoltage in a p-n junction, which reduces the potential drop over this junction according to the well known relationship [Ryvkin (1965), Bube (1960)]

$$\Delta u = \frac{kT}{e_0} \cdot \ln \left(1 + \frac{j_C}{j_{sat}}\right) , \qquad (103)$$

where j_{sat} represents the saturation current of the minority carrier (holes in this case) to the surface. Since the change of the measured electrode potential is opposite in sign to that of $\Delta\phi_S$, such a deviation in corrosion potential must have the negative sign for an n-type specimen.

2. Examples

The dissolution rate of germanium in various oxidizing electrolytes is controlled by the transport of the oxidant. In such a case, the corrosion potential, according to the superposition principle, should follow the anodic current voltage curve as measured in the absence of the oxidant. This has been confirmed for p-type specimens but is not correct for n-type ones, as expected from the preceding section [Gerischer and Beck (1960a)]. Figure 45 shows the relationship between corrosion rate and corrosion potential for p- and n-type germanium samples. The deviation between p- and n-type samples increases with the corrosion rate and with the concentration of electrons in the bulk. The reason for both effects is expressed by Eq. (103). Increasing corrosion rate increases j_C, because the anodic process in germanium involves a large amount of electron injection, as we have seen in Section IVD.2. Higher n-type conductivity normally reduces the saturation current and therefore increases Δu at the same corrosion rate.

These effects become the more pronounced the higher the band gap is. This can be seen in Fig. 46 for the corrosion of GaAs, where the electron injection could hardly be detected in another way than by studying the corrosion potential. The high sensitivity is reached in this case because of the small value of j_{sat}.

A helpful means for corrosion studies in semiconductors is illumination, which increases the difference between n- and p-type samples at the same corrosion rate because of an additional photovoltage to that given in Eq. (103). If one knows or can measure the electron-hole pair generation rate by light of suitable intensity, this additional photovoltage can give quantitative information on the unknown injection rate by corrosion. To account for the effect of illumination in Eq. (103), j_C in the numerator of the last term has to be replaced by $(j_C + j_{illum})$, where j_{illum} is the illumination effect in terms of an equivalent injection current.

The corrosion behavior of semiconductors with a wide band gap is generally controlled by chemical reactions which are not in the scope of this chapter. Under illumination, however, the decomposition processes by reactions of holes play a rather important role. For example, ZnO corrodes under illumination by anodic decomposition into Zn ions and O_2. Simultaneously, H^+ or H_2O from the electrolyte is reduced, or if enough oxygen is present, the cathodic process is the reduction of oxygen [Lohmann (1967)]. That the anodic decomposition is the primary step can be concluded here from the fact that the steady-state potential shifts to the cathodic direction under illumination, because of the loss of positive charge in the anodic process, until the cathodic processes can compensate any further shift of the voltage.

There are many more important problems in the corrosion and etching of semiconductors, e.g., the question of how faces with opposite polarity behave at crystals with a polar axis [Gatos and Lavine (1960a), Gatos and Lavine (1960b), Lavine et al. (1961), Heiland et al. (1963),

Mariano and Haneman (1963)]. But these problems are not mainly controlled by the semiconductor properties of the crystals on which emphasis was placed in this chapter, and are not discussed further here.

Acknowledgements: This work was supported in part by the United States Atomic Energy Commission through the Inorganic Materials Research Division of the Lawrence Radiation Laboratory, University of California, Berkeley, California.

REFERENCES

Beck, F., and Gerischer, H. (1959a). Z. Elektrochem. 63, 500.

Beck, F., and Gerischer, H. (1959b). Z. Elektrochem. 63, 943-950.

Bickl, H. (1966). Thesis, Techn. Hochschule, München.

Boddy, P. J. (1964). J. Electrochem. Soc. 111, 1136-47.

Boddy, P. J. (1965). J. Electroanalyt. Chem. 10, 199.

Boddy, P. J., and Brattain, W. H. (1963a). J. Electrochem. Soc. 110,570.

Boddy, P. J., and Brattain, W. H. (1963b). Ann. N. Y. Acad. Sci. 101,683.

Boddy, P. J., and Sundburg, W. J. (1963). J. Electrochem. Soc. 110, 1170.

Bohnenkamp, K., and Engell, H. J. (1957). Z. Elektrochem. 61, 1184.

Brattain, W. H., and Bardeen, J. (1953). Bell System Tech. J. 32, 1.

Brattain, W. H., and Garrett, C. G. B. (1955). Bell System Tech. J. 34, 129.

Brattain, W. H., and Boddy, P. J. (1962). J. Electrochem. Soc. 109, 574.

Bube, R. H. (1960). "Photoconductivity of Solids." Wiley, New York.

Dewald, J. F. (1959). In "Semiconductors" (N. B. Hanney, ed.), ACS Monograph 140, p. 727. Reinhold Publishing Company, New York.

Dewald, J. F. (1960a). Bell System Tech. J. 39, 615

Dewald, J. F. (1960b). In "The Surface Chemistry of Metals and Semiconductors," (H. C. Gatos, ed.), p. 205. Wiley, New York.

Dogonadze, R. R., and Chizmadzhev, Yu. A. (1962). Dokl. Akad. Nauk. USSR 144, 1077; 145, 848 (1962), Engl. Trans. p. 563.

Dogonadze, R. R., and Chizmadzhev, Yu. A. (1963). Dokl. Akad. Nauk. USSR 150, 333; Engl. Trans. p. 402.

Dörr, F., and Scheibe, G. (1961). Z. Wiss. Photographie 55, 133.

Flynn, J. B. (1958). J. Electrochem. Soc. 105, 715.

Frankl, D. R. (1967). "Electrical Properties of Semiconductor Surfaces," Pergamon Press, Oxford.

Garrett, C. G. B., and Brattain, W. H. (1955). Phys. Rev. 99, 376.

Gatos, H. C., and Lavine, M. C. (1960a). J. Electrochem. Soc. 107, 427.

Gatos, H. C., and Lavine, M. C. (1960b). J. Phys. Chem. Solids 14, 169.

Gerischer, H. (1960a). Anal. Real. Soc. Espan. Fis. Quin. B56, 535.

Gerischer, H. (1960b). Z. Phys. Chem. (Frankfurt) 26, 223-247.

Gerischer, H. (1960c). Z. Phys. Chem. (Frankfurt) 26, 325-338.

Gerischer, H. (1961a). Z. Phys. Chem. (Frankfurt) 27, 48-79.

Gerischer, H. (1961b). In "Advances in Electrochemistry and Electrochemical Engineering" (P. Delahay and C. W. Tobias, eds.), Vol. I, p. 139. Interscience, New York.

Gerischer, H. (1965). Physik. Chem. 69, 578-583.

Gerischer, H. (1966). J. Electrochem. Soc. 113, 1174-1181.

Gerischer, H., and Beck, F. (1957). Z. Physik. Chem. N.F. 13, 389-395.

Gerischer, H., and Beck, F. (1960a). Z. Physik. Chem. (Frankfurt) 23, 113-132.

Gerischer, H., and Beck, F. (1960b). Z. Physik. Chem. (Frankfurt) 24, 378-389.

Gerischer, H., and Mattes, I. (1966). Z. Physik. Chem. (Frankfurt) 49, 112.

Gerischer, H. and Mindt, W. (1966). Surface Science 4, 440.

Gerischer, H., and Mattes, I. (1967). Z. Physik. Chem. (Frankfurt) 52, 60-72.

Gerischer, H., and Mindt, W. (1968). Electrochim. Acta. (in press.)

Gerischer, H., and Tributsch, H. (1968). Ber Bunsenges. Physik. Chem. 72, 437.

Gerischer, H., Hofmann-Perez, M., and Mindt, W. (1965). Ber. Bunsenges. Physik. Chem. 69, 130-138.

Gerischer, H., Mauerer, A., and Mindt, W. (1966). Surface Sci. 4, 431-439.

Gerischer, H., Michel-Beyerle, E. M., and Rebentrost, F. (1968). Conference on Spectral Photosensitization, Bressanone, 1967, (in press.)

Gobrecht, H., and Meinhardt, O. (1963). Ber. Bunsenges. Physik. Chem. 67, 151.

Gobrecht, H., and Meinhardt, O. (1964). Phys. Letters, 11, 103.

Gobrecht, H., Meinhardt, O., and Lerche, M. (1963). Ber. Bunsenges. Physik. Chem. 67, 486-493.

Gobrecht, H., Schaldach, M., Hein, F., Blaser, R., and Wagemann, H. G. (1966). Ber. Bunsenges. Physik. Chem. 70, 946.

Green, M. (1959a). In "Modern Aspects of Electrochemistry" (J. O'M. Bockris, ed.), Vol. II, p. 343. Butterworth, London.

Green, M. (1959b). J. Chem. Phys. 31, 200.

Haberkorn, R. (1967). Thesis, Techn. Hochschule München.

Hanney, N. B. (1959). "Semiconductors." Reinhold, New York.

Harten, H. U. (1964). In "Festkörperprobleme III" (F. Sauter, ed.) p. 81. Vieweg Publishers, Braunschweig.

Harvey, W. W. (1968). Electrochim. Acta. (in press.)

Harvey, W. W., Sheff, S., and Gatos, H. C. (1960). J. Electrochem. Soc. 107, 560.

Hauffe, K. (1967). Ber. Bunsenges. Physik. Chem. 71, 690.

Hofmann-Perez, M., and Gerischer, H. (1961). Z. Elektrochem. 65, 771.

Holmes, P. J. (1961). "The Electrochemistry of Semiconductors." Academic Press, New York.

Hush, N. S. (1958). J. Phys. Chem. 28, 962.

Hush, N. S. (1961). Trans. Faraday Soc. 57, 557.

Kallman, H., and Pope, M. (1960). J. Chem. Phys. 32, 300.

Kingston, R. H. and Neustadter, S. F. (1955). J. Appl. Phys. 26, 718.

Lampert, M. A. (1956). Phys. Rev. 103, 1648.

Lampert, M. A. (1964). Rept. Progr. Phys. 27, 329.

Lavine, M. C., Gatos, H. C., and Flynn, M. C. (1961). J. Electrochem. Soc. 108, 974.

Lazorenko-Manevich, R. M. (1962). Z. Fiz. Khim. SSSR 36, 2066.

Levich, V. G. (1962). In "Advances in Electrochemistry and Electrochemical Engineering" (P. Delahay and C. W. Tobias, eds.), Vol. IV, p. 249. Interscience Publishers, New York.

Lohmann, F. (1966a). Ber Bunsenges. Physik. Chem. 70, 87-92.

Lohmann, F. (1966b). Ber Bunsenges. Physik. Chem. 70, 428-434.

Lohmann, F, and Mehl, W. (1967). Ber Bunsenges. Physik. Chem. 71, 493-503.

Many, A., Goldstein, Y., and Grover, N. B. (1965). "Semiconductor Surfaces." North Holland Publishing Company, Amsterdam.

Marcus, R. A. (1956). J. Chem. Phys. 24, 966.

Marcus, R. A. (1959). Canad. J. Chem. 37, 138.

Marcus, R. A. (1964). Ann. Rev. Phys. Chem. 15, 155.

Marcus, R. A. (1968). Electrochim. Acta. (in press).

Mariano, A. N., and Haneman, R. E. (1963). J. Appl. Phys. 34, 384.

Markham, M. C., and Upret, M. C. (1965). J. Catalysis. 4, 229.

Mark, P., and Helfrich, W. (1962). J. Appl. Phys. 33, 205.

Mauerer, M. (1965). Master's Thesis, Techn. Hochschule, München.

McDonald, J. R. (1962). Solid-State Electronics 5, 11.

Mehl, W. (1965). Ber. Bunsenges. Physik. Chem. 69, 583-589.

Mehl, W. (1966). In "Proceedings of International Symposium on Luminescence," Munich, 1965 (N. Riehl and H. Kallmann, eds.)

Mehl, W. and Buchner, W. (1965). Z. Physik. Chem. (Frankfurt) 47, 76.

Mehl, W., and Hale, J. M. (1967). In "Advances in Electrochemistry and Electrochemical Engineering (P. Delahay and C. W. Tobias, eds.), Vol. VI, Interscience Publishers, New York.

Mehl, W., and Lohmann, F. (1967). Ber. Bunsenges. Physik. Chem. 71, 1055-1060.

Memming, R. (1963). Phys. Letters 4, 89.

Memming, R., and Schwandt, G. (1966). Surface Science 4, 109.

Memming, R., and Schwandt, G. (1967). Angew. Chemie 79, 833-876.

Mindt, W. (1966). Thesis, Technische Hochschule, München.

Morrison, S. R., and Freund, T. (1967). J. Chem. Phys. 47, 1543.

Mott, N. F. (1939). Proc. Roy. Soc. (London) A171, 27.

Mulder, B. J. (1965). Recueil Trav. Chim. 84, 713-728.

Mulder, B. J. (1967). Ph.D. Thesis, Tech. Hagenschool, Eindhoven.

Mulder, B. J., and de Jonge, J. (1963). Proc. Koninkl. Ned. Akad. Wetenschap. B66, 303.

Myamlin, V. A., and Pleskov, Yu. V. (1965). "Electrochemistry of Semiconductors" Nauka, Moscow. Engl. Trans., 1967, Plenum Press, New York.

Nelson, R. C. (1967). J. Phys. Chem. 71, 2517.

Pleskov, Yu. V. (1959). Dokl. Akad. Nauk SSSR 126, 111.

Pleskov, Yu. V. (1961). J. Physik. Chem. SSSR 35, 2540-2546.

Pleskov, Yu. V. (1961). J. Physik. Chem. SSSR 35, 2576-2581.

Pleskov, Yu. V. and Tyagai, V. A. (1961). Dokl. Akad. Nauk. SSSR 141, 1135-1138.

Randles, J. E. B. (1952). Trans. Faraday Soc. 48, 828.

Rebentrost, F. (1968). Thesis, Techn. Hochschule, München.

Rose, A. (1955). Phys. Rev. 97, 1538.

Roth, C. (1966). Thesis, Techn. Hochschule, München.

Ryvkin, S. M. (1965). "Photoelektrische Erscheinungen in Halbleitern" Akademie-Verlag, Berlin.

Seiwatz, R., and Green, M. (1958). J. Appl. Phys. 29, 1034.

Schottky, W. (1939). Z. Phys. 113, 367; 118, 539 (1942).

Shockley, W. (1963). "Electrons and Holes in Semiconductors." Van Nostrand, New York.

Spenke, E. (1965). "Elektronische Halbleiter," Springer-Verlag, Berlin.

Tauc, J. (1962). "Photo and Thermoelectric Effects in Semiconductors," Pergamon Press, Oxford.

Turner, D. R. (1956). J. Electrochem. Soc. 103, 252.

Turner, D. R. (1958). J. Electrochem. Soc. 105, 402.

Tyagai, V. A. (1963). Izvest. Akad. Nauk. SSSR Ser. Khim. 1556.

Tyagai, V. A. (1965). Elektrokhimiya, 1, 377-387.

Vdovin, Yu. A., Levich, V. G., and Myamlin, V. A. (1959). Dokl. Akad. Nauk SSSR 124, 350.

Williams, R. (1960). J. Chem. Phys. 32, 1505-1514.

Wagner, C., and Traud, W. (1938). Z. Elektrochem. 44, 391.

Legends for Figures

Fig. 1. Electrostatic potential ϕ at metal-electrolyte and semiconductor-electrolyte interfaces.

Fig. 2. Charge distribution at semiconductor-electrolyte interface.

Fig. 3. Space-charge differential capacity for intrinsic and n-type semiconductor versus potential drop between surface and bulk.

Fig. 4. Carrier distribution and band bending for n-type semiconductor:

(a) accumulation layer,

(b) depletion layer,

(c) inversion layer.

Fig. 5. Additional differential capacity versus potential difference between surface and bulk for two separate surface states.

Fig. 6. Equivalent circuit for net semiconductor-electrolyte interfacial capacity.

Fig. 7. Depth of light penetration, $1/\kappa$, depth of space charge layer, L, and mean diffusion length, ℓ, at semiconductor surface.

Fig. 8. Differential capacity of an intrinsic germanium electrode in contact with aqueous electrolyte at pH 5.7 (from Gerischer et al. 1965).

Fig. 9. Depletion layer at CdS electrode in contact with electrolyte at pH 13. Mott-Schottky plot for determining the flat band potential (from Haberkorn, 1967).

Fig. 10. Instantaneous photovoltaic response versus electrode potential for a germanium electrode in aqueous electrolyte at pH 7.4 (after Boddy and Brattain 1963).

Fig. 11. Flat band potential of intrinsic germanium electrode versus pH (from Hofmann-Pérez and Gerischer 1961).

Fig. 12. Energy correlations for electron transfer processes at semiconductor-electrolyte interface.

Fig. 13. Free enthalpy cycle for electron transfer from and towards a redox couple in solution under consideration of the Franck-Condon principle.

Fig. 14. Distribution functions of energy states for electrons, D_θ, and holes, $D_\oplus$, as well as for the reduced and oxidized components of two different redox systems, W_R and W_{Ox} versus energy (left and middle parts). On the right part, the resulting rate of electron transfer for the two redox couples according to Eq. (57).

Fig. 15. Electron transfer via surface states at cathodic (left side) or anodic polarization (right side).

Fig. 16. Course of energy bands (upper part) and electronic carrier concentrations (lower part) in n- and p-type semiconductor electrodes polarized to the same Fermi level by means of contact with a metal.

Fig. 17. Typical current voltage curves for the partial electron-transfer currents in the conduction band and in the valence band. (Concentration polarization in the electrolyte is neglected.)

Fig. 18. Transistor-like device for the detection of hole injection or extraction,

(a) schematic sketch of the circuit,

(b) current-voltage curves for collector-base circuit.

Fig. 19. Analysis of superimposed partial currents for determining hole injection at n-type semiconductors (after Gerischer and Beck 1957; Beck and Gerischer 1959).

Fig. 20. Current voltage curves for hydrogen evolution at Ga-As electrodes (from Gerischer and Mattes 1966).

Fig. 21. n-type Ge slice in transistor arrangement. Upper part: variation of indicator current, under reversal bias of p-n junction at back side, in dependence of polarization voltage for electrolysis. Lower part: current voltage curve for reduction of Fe^{+3} at front surface.

Fig. 22. Analysis of partial current voltage curves for GaAs electrode in presence of Fe^{+3} in the electrolyte (from Gerischer and Mattes 1966).

Fig. 23. Current voltage curve for oxidation of V^{2+} ions at n-Ge electrode, corrected for concentration polarization (after Mauerer 1964).

Fig. 24. Current voltage curve for reduction of Fe^{+3} at CdS electrode (after Roth 1966).

Fig. 25. Typical current voltage behavior of insulators.

Fig. 26. Cell arrangement for studying electrolytic processes at insulators (after Mulder 1965; Gerischer et al. 1968).

Fig. 27. Rate of hole injection into perylene crystals by $[Fe(CN)_6]^{-3}$ ions versus voltage applied to the crystal (15 μ thick) (after Rebentrost 1968).

Fig. 28. Intensity of emitted light (in arbitrary units) as function of the double injection current (after Mehl 1966).

Fig. 29 Separation of electron-hole pairs, generated by light absorption in the space-charge layer, under the influence of the electric field as indicated by the band bending.

Fig. 30. Energy correlations for charge injection by interaction of excitons with electron acceptors or donors. S = energy range for ground level; S^* = range for excited levels.

Fig. 31. Injection current into anthracene crystal by interaction of excitons with Tl^{+3} ions (10^{-2}M in 0.5M HCl); crystal illuminated with light of 403 mμ wavelength (from Mehl and Hale 1968).

Fig. 32. Energy correlations for electron or hole injection by excited molecules adsorbed on the surface.

Fig. 33. Sensitized photoinjection current at ZnO electrode versus electrode potential. Lowest curve without sensitizer. Solution: 1 N KCl; sensitizer: rhodamine B (from Gerischer and Tributsch 1968).

Fig. 34. Action spectrum of photosensitized electron injection into ZnO electrodes by rhodamine B; polarization, 0.5 volt (from Gerischer and Tributsch 1968).

Fig. 35. Supersensitization effect of added hydroquinone. ZnO electrode, anodically polarized into saturation region; sensitizer: Rosebengale 2.5×10^{-5} M (from Gerischer and Tributsch 1968).

Fig. 36. Photosensitized hole injection into perylene crystals from rhodamine B for various concentrations of the sensitizer (after Rebentrost 1968).

Fig. 37. Action spectrum for photosensitized charge injection at perylene by rhodamine B (after Rebentrost 1968).

Fig. 38. Energy profile for attack of covalent bonds in semiconductor crystal surface.

Fig. 39. Current voltage curves for anodic dissolution of p-type and n-type germanium (from Beck and Gerischer 1959).

Fig. 40. Mechanism of anodic dissolution of ⟨111⟩ face on germanium.

Fig. 41. Anodic decomposition of ZnO under illumination in terms of current voltage curves (from Gerischer 1966).

Fig. 42. Cyclic current voltage curves for transistor-like circuit,

(a) n-type slice, indicating hole currents,

(b) p-type slice, indicating electron currents,

Δj_{h^+} : variation of hole current

Δj_{e^-} : variation of electron current in indicator circuit

(from Gerischer et al. 1966).

Fig. 43. Mechanism of cathodic decomposition of ZnO by the action of electrons.

Fig. 44. Chemical oxidative attack on surface bonds.

Fig. 45. Corrosion potential versus corrosion rate for p- and n-type germanium (after Gerischer and Beck 1960).

Fig. 46. Corrosion potential versus rate of corrosion for p- and n-type GaAs 2N H_2SO_4, Ce^{+4} as oxidant.

List of Symbols

$^{\circ}A$	electron affinity
C	capacity
C_{ad}	capacity of adsorbed ions
C_D	net capacity of the double layer
C_H	capacity of Helmholtz double layer
C_{sc}	space charge capacity
C_{ss}	capacity of surface states
$_AC_{ss}$	capacity of acceptor surface states
$_DC_{ss}$	capacity of donor surface states
c	concentration
c_A	acceptor concentration
c_A^-	concentration of ionized acceptors
c_D	donor concentration
c_D^+	concentration of ionized donors
c_{Ox}	concentration of oxidized species
$c_{Ox,O}$	concentration of oxidized species in the interior of the electrolyte
$c_{Ox,s}$	concentration of oxidized species near the electrode surface
c_R	concentration of reduced species
$c_{R,O}$	concentration of reduced species in the interior of the electrolyte
$c_{R,s}$	concentration of reduced species near the electrode surface
c_{sol}	ion concentration in solution
$^{o}c_{sol}$	standard ion concentration in solution
D	diffusion coefficient of minority carriers.
$D_\ominus$	density of states for electrons
$D_\oplus$	density of states for holes

d	thickness of insulator slice
E	electron energy
E^*	activation energy (for electrochemical reactions)
E_A	acceptor energy level
${}_sE_A$	energy level of acceptor surface state
E_C	energy of conduction-band edge
E_D	donor energy level
${}_sE_D$	energy level of donor surface state
E_F	Fermi energy
${}_iE_F$	Fermi energy of intrinsic semiconductor
${}_OE_F$	Fermi energy in semiconductor bulk
${}_sE_F$	Fermi energy in semiconductor surface
${}^\circ E_{F,redox}$	Fermi energy of electron in redox system under standard conditions
E_{gap}	energy gap
${}^\circ E_{Ox}$	most probable energy level of the electron in the oxidized species
${}^\circ E_{Red}$	most probable energy level of the electron in the reduced species
E_R	electronic energy level of radical intermediate
E_V	energy of valence-band edge
e_O	absolute value of electron charge
F	electric field strength
f_i	activity coefficient
g	rate of thermal generation of electron-hole pairs
g_A	degeneracy of acceptor level
g_D	degeneracy of donor level
${}_sg_A$	degeneracy of acceptor surface state

$_{s}g_{D}$	degeneracy of donor surface state
$^{\circ}I$	ionization energy
I_{O}	light intensity
I_{s}	rate of surface recombination
i	$=\sqrt{-1}$
j	current density
j^{+}	anodic current density
j^{-}	cathodic current density
j_{C}	electron current density
$j_{C,O}$	electron exchange current density at equilibrium
j_{illum}	injection current density by illumination
j_{ind}	diode current density (indicating minority carrier injection)
j_{sat}	saturation current density of minority carrier diffusion
j_{V}	hole current density
$j_{V,O}$	hole exchange current density at equilibrium
k	Boltzmann constant
k_{C}^{+}	rate constant of anodic electron reaction
k_{C}^{-}	rate constant of cathodic electron reaction
k_{V}^{+}	rate constant of anodic hole reaction
k_{V}^{-}	rate constant of cathodic hole reaction
k_{ion}	rate constant for ionization
k_{neutr}	rate constant for neutralization
L	Debye length of intrinsic semiconductor
l	diffusion length of minority carriers
m	stoichiometric number, characterizing contribution of holes to germanium dissolution

N_A	concentration of acceptor surface states
N_{A^-}	concentration of ionized acceptor surface states
$_0N_{A^-}$	equilibrium concentration of ionized acceptor surface states
N_{ad}	surface concentration of adsorbed species
$^\circ N_{ad}$	surface concentration of adsorbed species for maximal coverage
N_C	effective density of states in the conduction band
N_D	concentration of donor surface states
N_{D^+}	concentration of ionized donor surface states
N_R	concentration of radicals in the surface
N_S	number of kink sites
N_V	effective density of states in the valence band
n	electron concentration
n^*	electron concentration under illumination
n_i	intrinsic carrier concentration
n_0	electron concentration in the bulk at equilibrium
n_s	electron concentration in the surface at equilibrium
n_s^*	electron concentration in the surface under illumination
$n_{s,0}$	value of n_s in equilibrium with a special redox system
p	hole concentration
p^*	hole concentration under illumination
p_0	hole concentration in the bulk at equilibrium
p_s	hole concentration in the surface at equilibrium
p_s^*	hole concentration in the surface under illumination
$p_{s,0}$	value of p_s in equilibrium with a special redox system
q	electric charge
q_{ad}	charge in adsorbed surface groups

q_{el} double layer charge in the electrolyte

q_{sc} space charge in the semiconductor

q_{ss} charge in surface states

R_{ext} ohmic resistance of semiconductor and electrolyte

R_{sc} ohmic resistance of the space charge layer

r rate of electron-hole recombination in the bulk

T absolute temperature

t time

U electrode potential

U_{cal} electrode potential vs. calomel electrode

U_{el} cell voltage

U_H electrode potential vs. hydrogen electrode

U_{ind} diode voltage

U_O electrode potential in equilibrium with a special redox system

$^{\circ}U_{redox}$ standard redox potential

U_{fb} electrode potential at flat band condition

u carrier mobility

v reaction rate

V_s $= e_O \Delta\Phi_s/kT$, potential drop in the space charge layer (dimensionless)

W_{Ox} distribution function for oxidized species

W_R distribution function for reduced species

x coordinate

x_i mole fraction

x_s coordinate at semiconductor surface

y $= \sqrt{p_O/n_O}$

Δj_{e^-} variation of electron current density in indicator circuit

Δj_{h^+} variation of hole current density in indicator circuit

Δn^* excess electron concentration under illumination

Δn_L^* excess electron concentration under illumination at $x = L$

Δp^* excess hole concentration under illumination

$\Delta\Phi$ $= \Phi_i - \Phi_{el}$, potential difference between interior of the semiconductor and the electrolyte

$\Delta\Phi_H$ $= \Phi_s - \Phi_{el}$, potential drop in the Helmholtz double layer

$\Delta\Phi_s$ $= \Phi_s - \Phi_i$, potential drop in the space charge layer

$\Delta\Phi_{s,0}$ value of $\Delta\Phi_s$ in equilibrium with a special redox system

δ_H thickness of Helmholtz double layer

ϵ dielectric constant of the semiconductor (dimensionless)

ϵ_H effective dielectric constant of the Helmholtz double layer (dimensionless)

ϵ_0 dielectric constant of vacuum (coulomb volt^{-1} cm^{-1})

η $= U - U_0$, overvoltage

κ light absorption coefficient

$\kappa(E)$ electron transfer probability

λ light wavelength

λ_{Ox} polarization energy for oxidized species

λ_R polarization energy for reduced species

$^\circ\mu_{ad}$ standard chemical potential at the electrode surface

$^\circ\mu_{sol}$ standard chemical potential in solution

ν frequency

ν_i frequency factor

ρ charge density

τ lifetime of minority carriers

τ_n	lifetime of electrons
τ_A	relaxation time for acceptor surface states
τ_D	relaxation time for donor surface states
Φ	electrostatic potential
Φ_{el}	electrostatic potential in the interior of the electrolyte
Φ_i	electrostatic potential in the interior of the semicondutor
Φ_s	electrostatic potential at the semiconductor surface
χ_{dipole}	contribution of oriented dipoles to electrostatic potential
ω	angular frequency

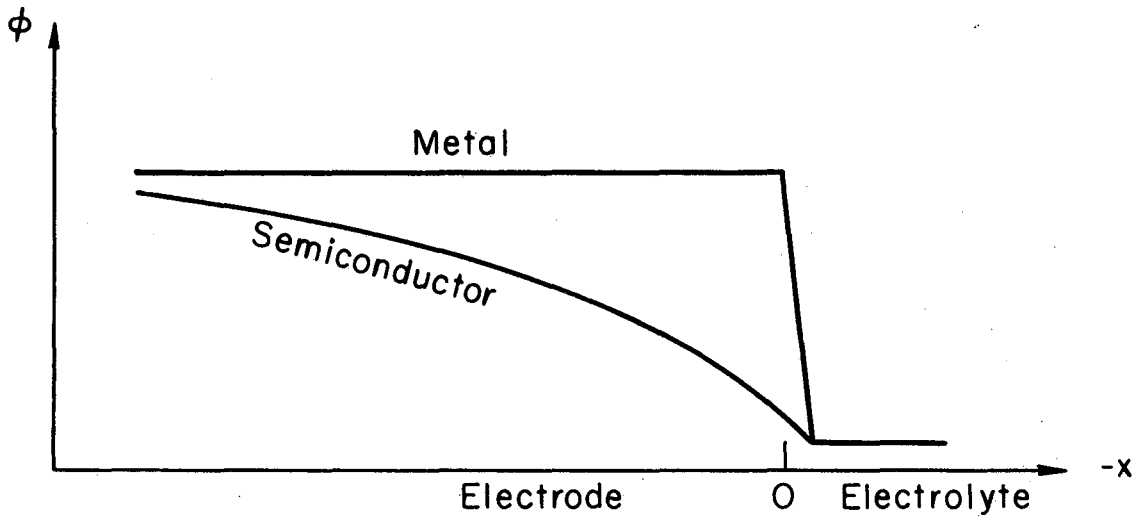

XBL689-6977

Fig. 1

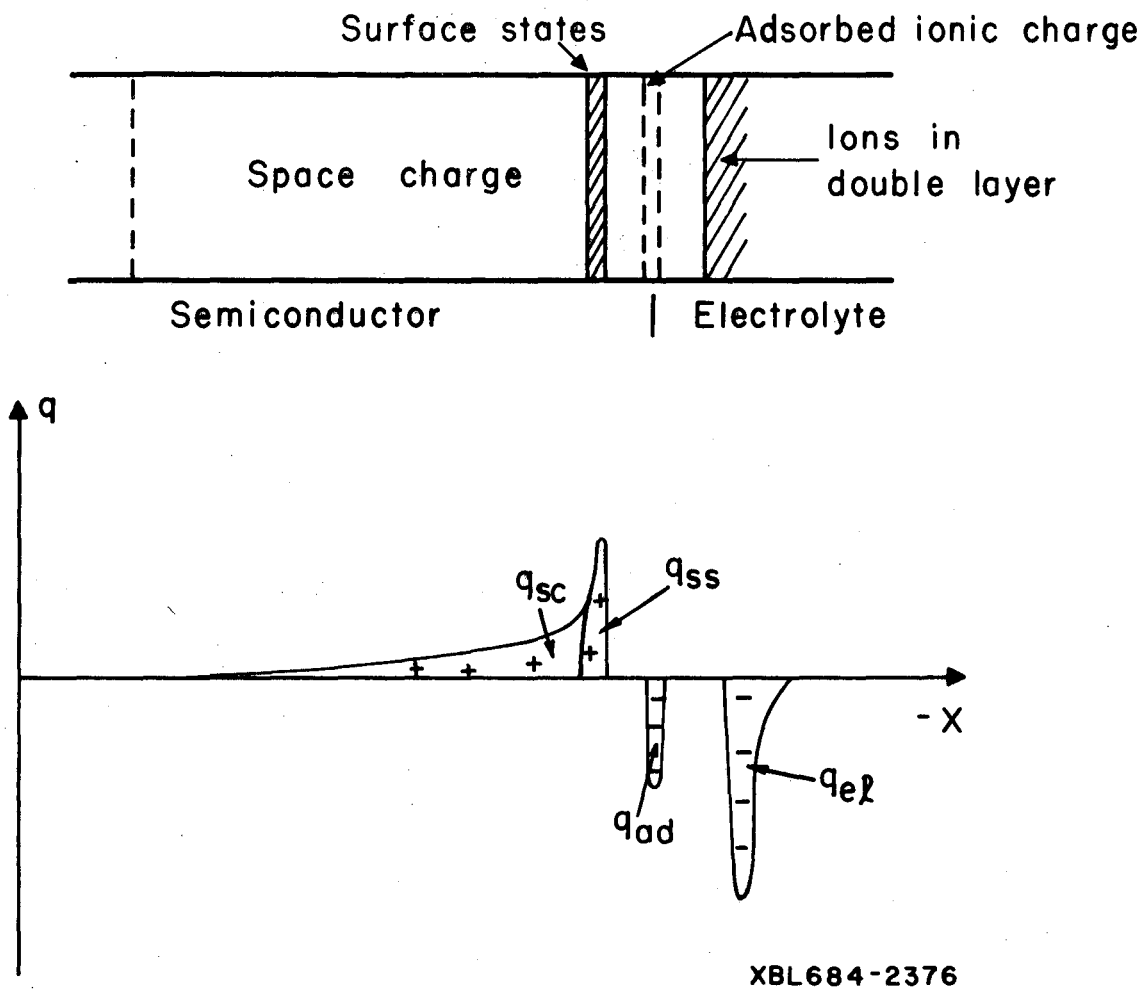
Surface states
Adsorbed ionic charge
Space charge
Ions in
double layer
Semiconductor
Electrolyte
q
q_{sc}
q_{ss}
q_{ad}
q_{el}
-X
XBL684-2376

Fig. 2

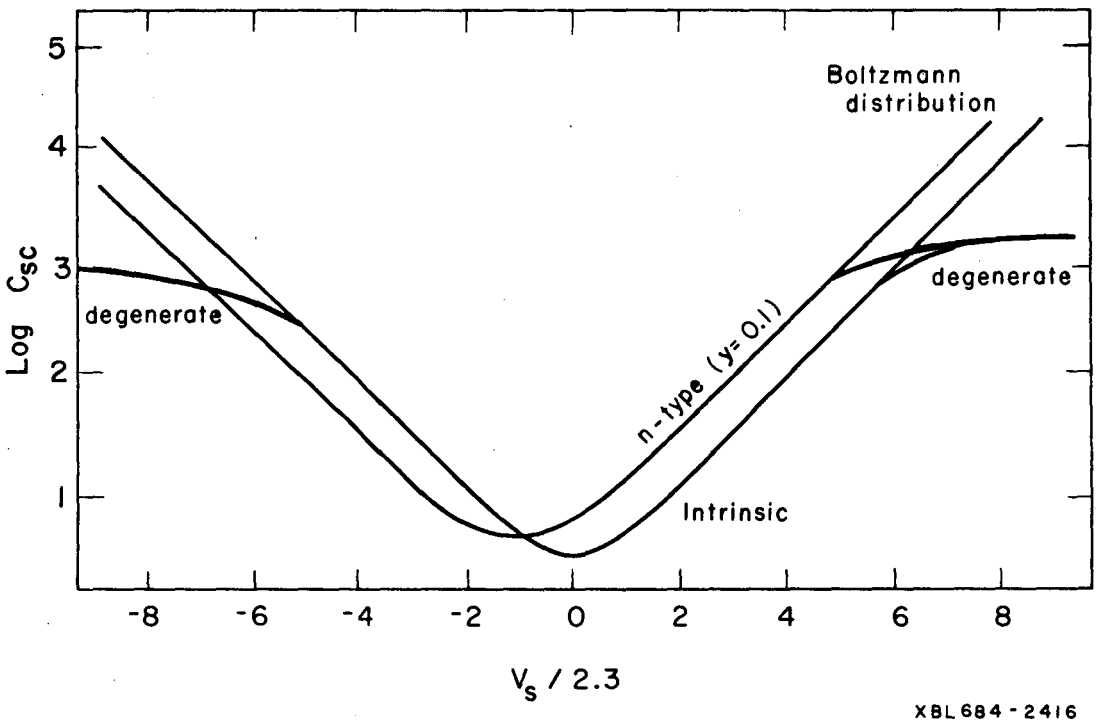
Log C_{sc}
5
4
3
2
1
-8
-6
-4
-2
0
2
4
6
8
V_s / 2.3
Boltzmann distribution
degenerate
degenerate
n-type (y=0.1)
Intrinsic
XBL684-2416

Fig. 3

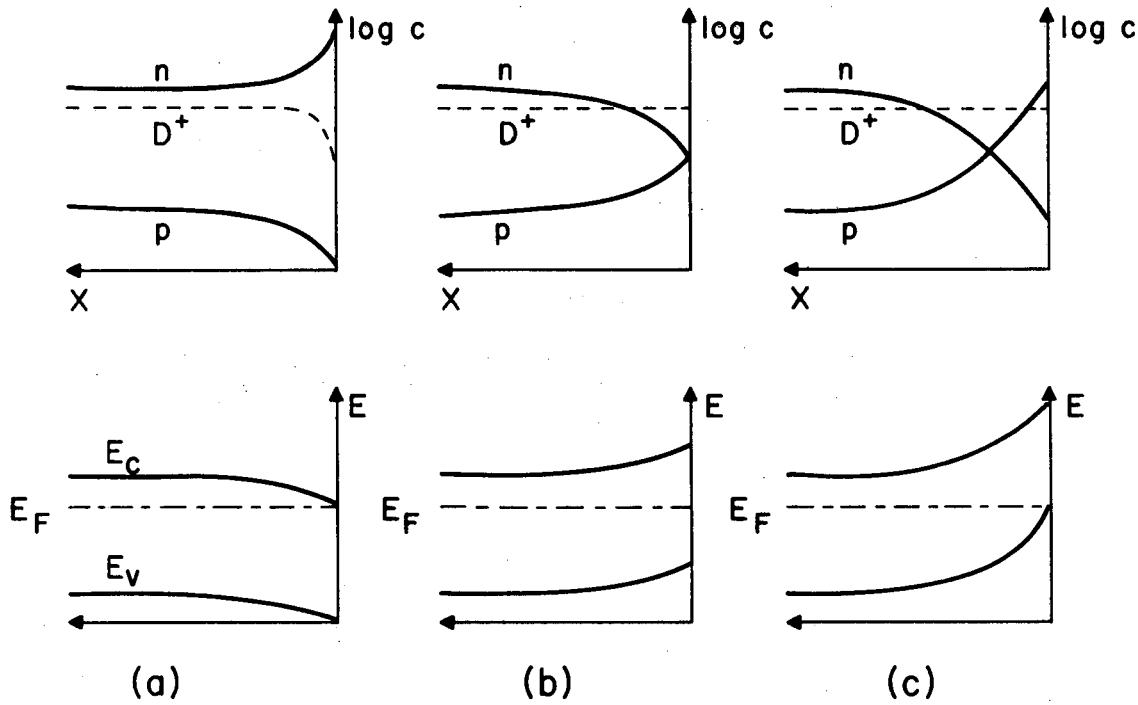
log c
n
D+
p
X
log c
n
D+
p
X
log c
n
D+
p
X
E
Ec
EF
Ev
E
EF
E
EF
(a)
(b)
(c)
XBL684-2378

Fig. 4

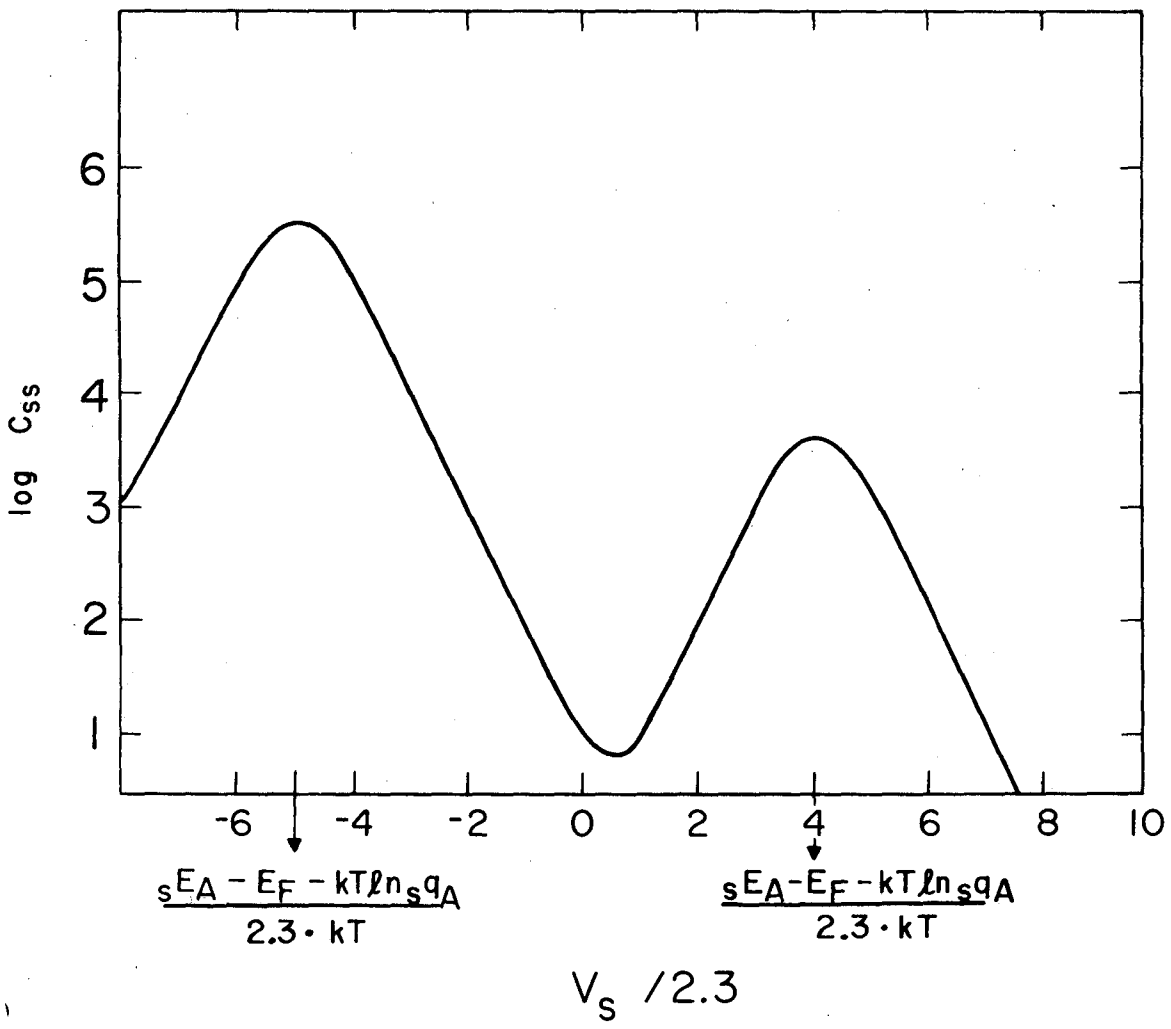

XBL684-2369

Fig. 5

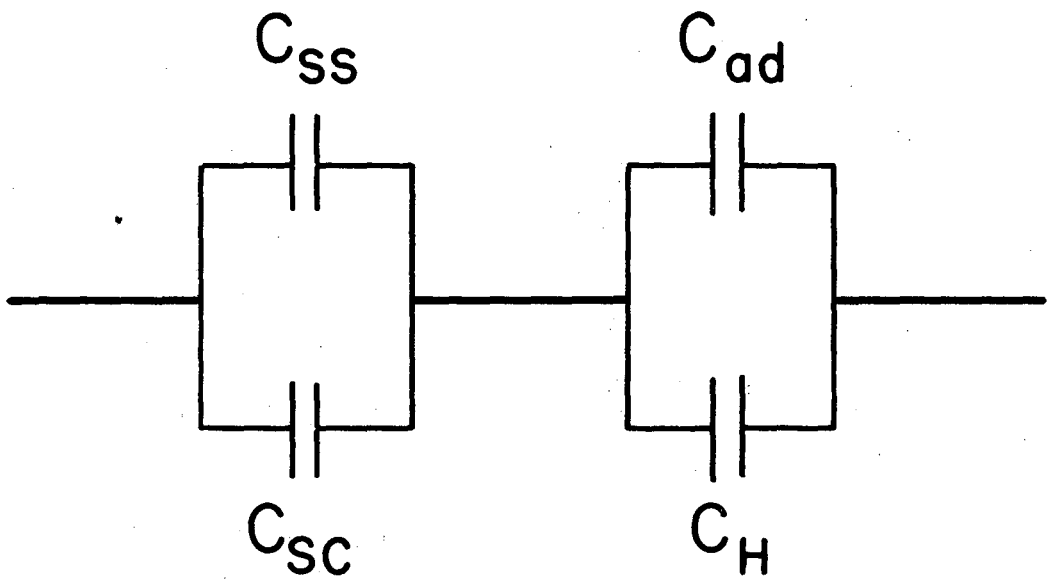

XBL684-2375

Fig. 6

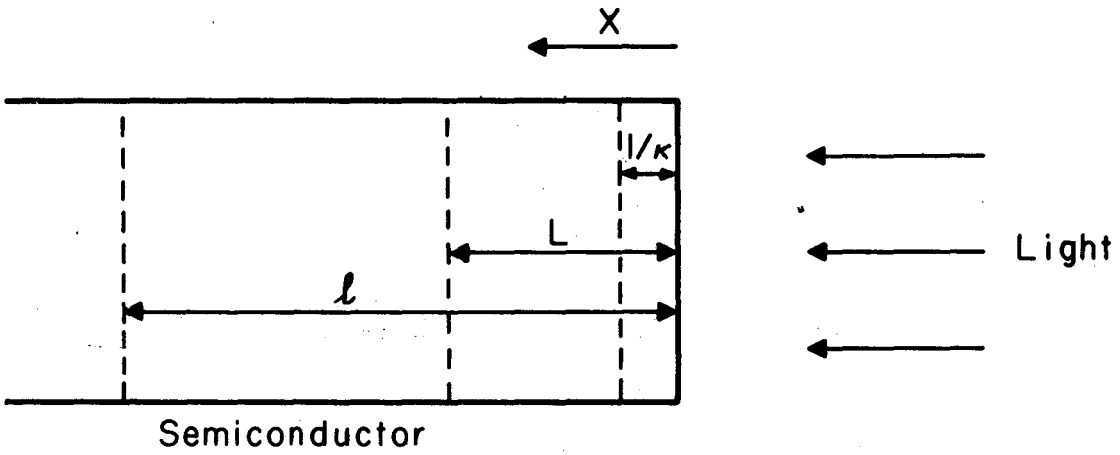

Fig. 7

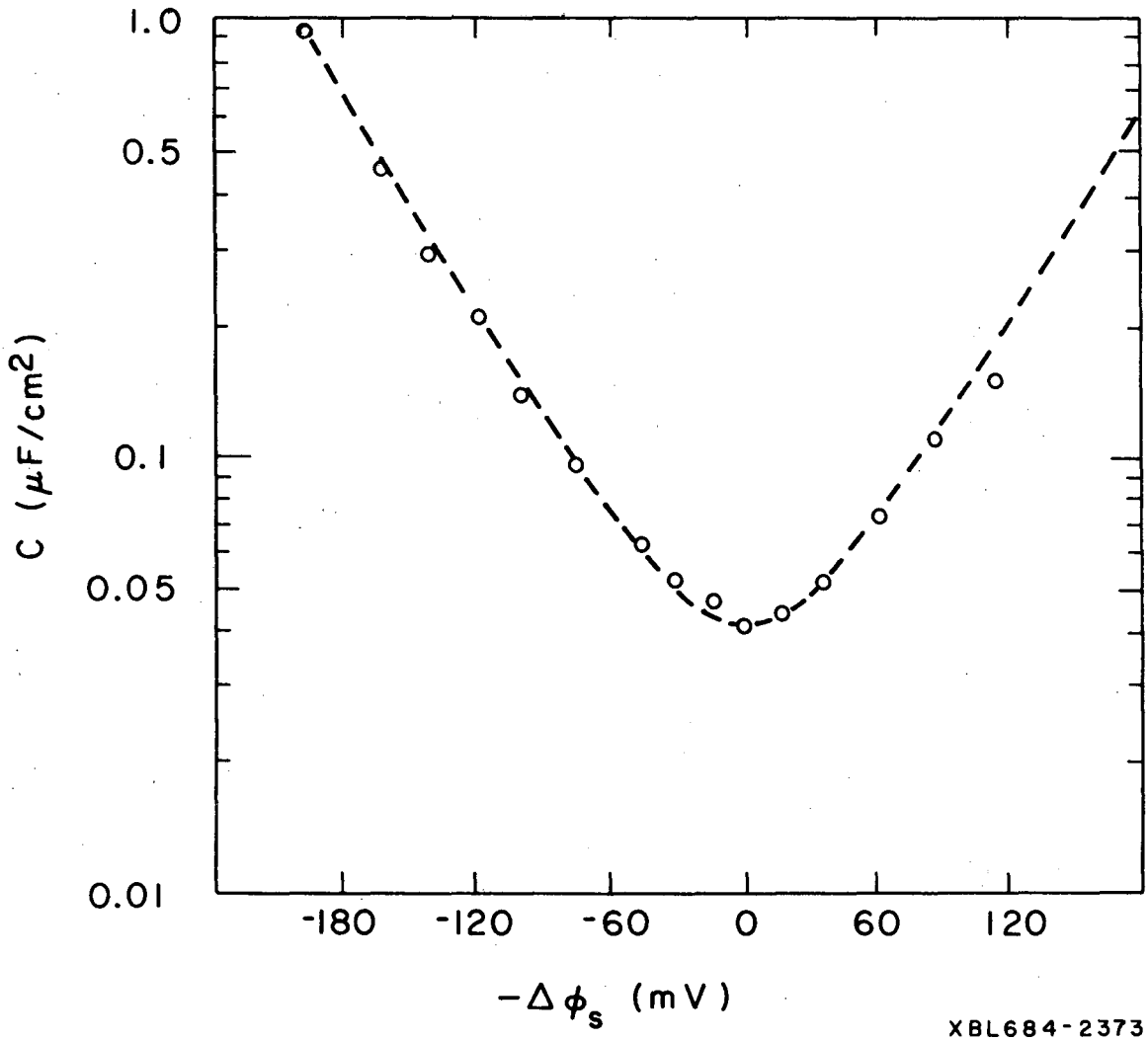

Fig. 8

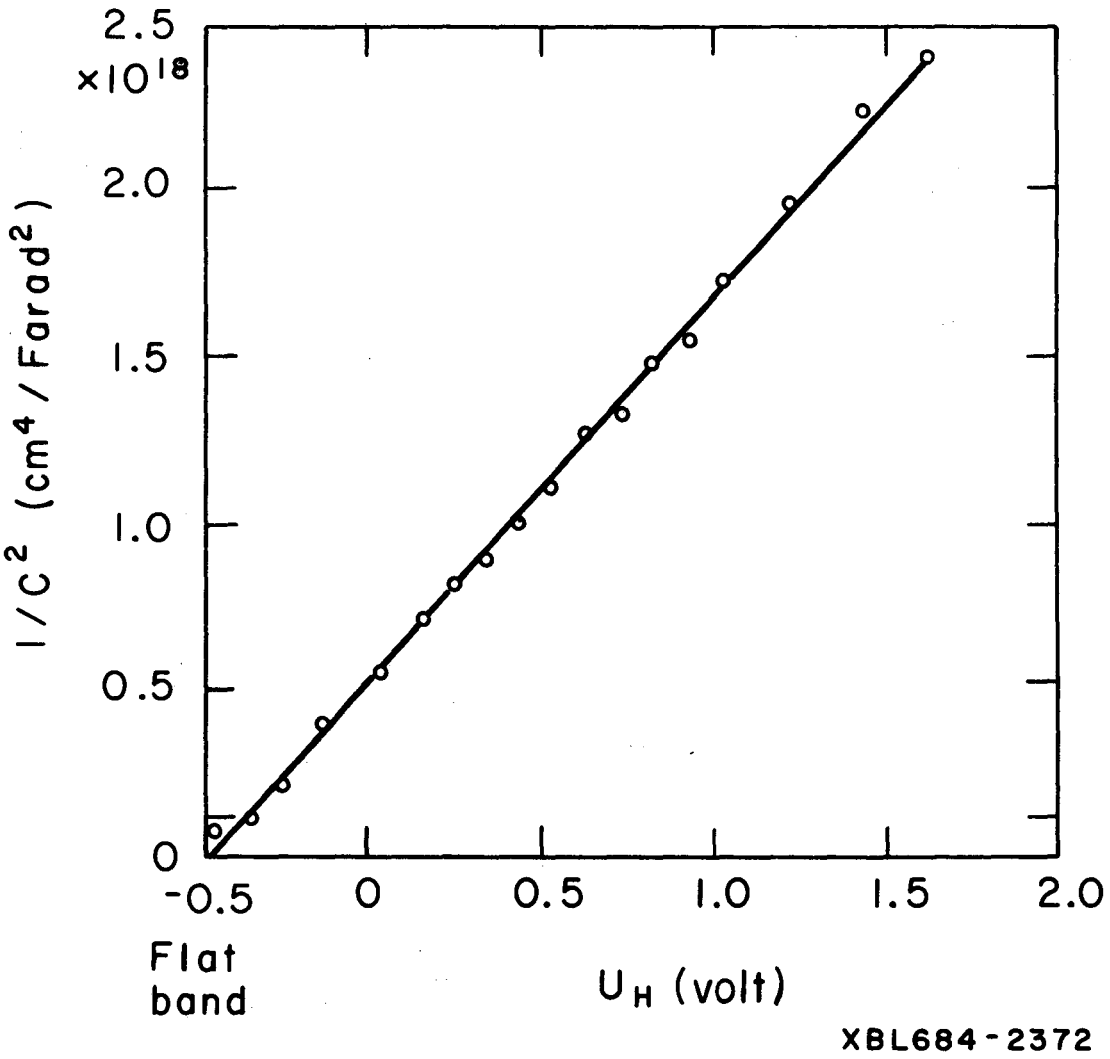
2.5
×10^18
2.0
1.5
1.0
0.5
0
1/C^2 (cm^4 / Farad^2)
-0.5
0
0.5
1.0
1.5
2.0
Flat
band
U_H (volt)
XBL684-2372

Fig. 9

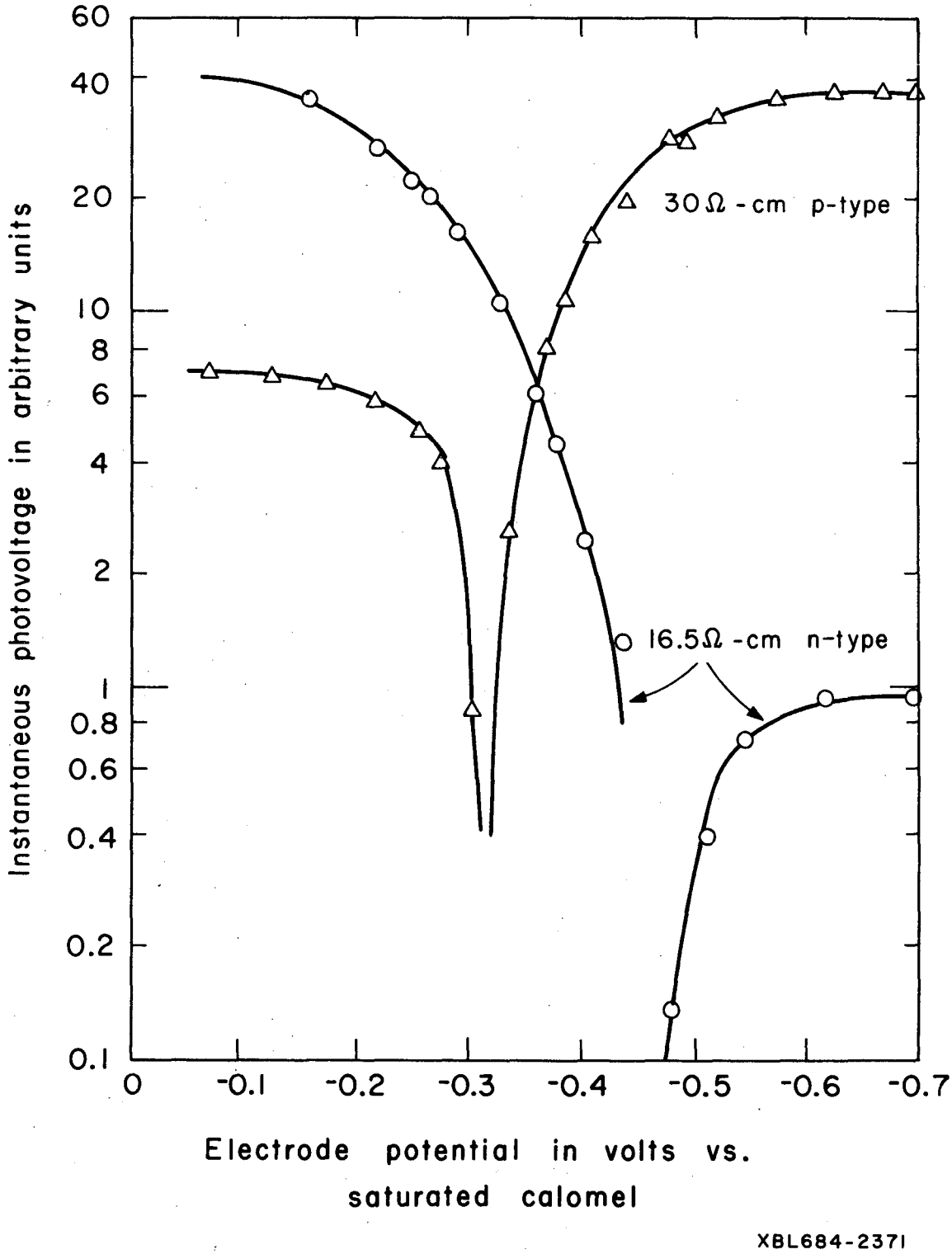
60
40
20
10
8
6
4
2
1
0.8
0.6
0.4
0.2
0.1
Instantaneous photovoltage in arbitrary units
30Ω-cm p-type
16.5Ω-cm n-type
0
-0.1
-0.2
-0.3
-0.4
-0.5
-0.6
-0.7
Electrode potential in volts vs.
saturated calomel
XBL684-2371

Fig. 10

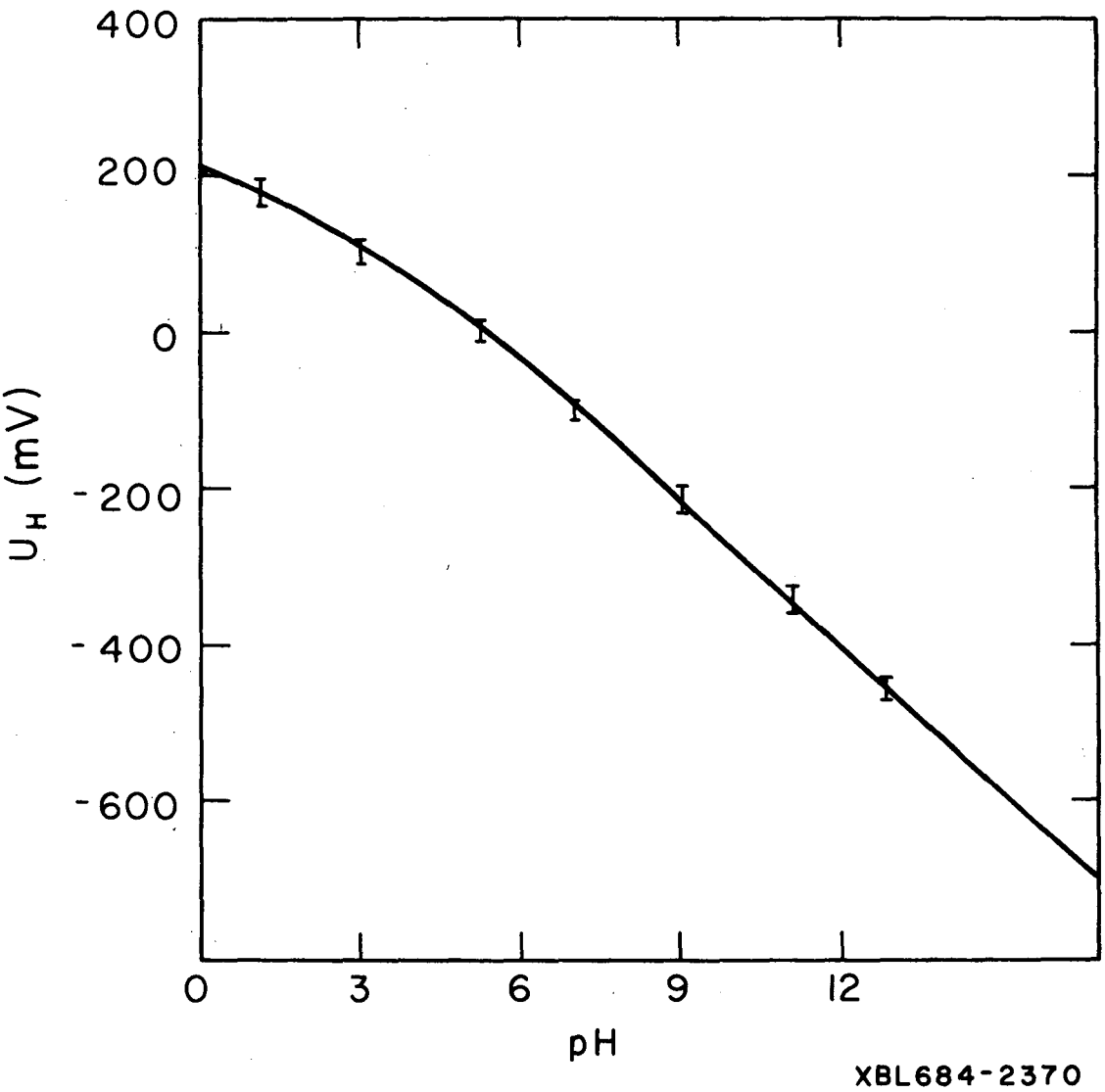

Fig. 11

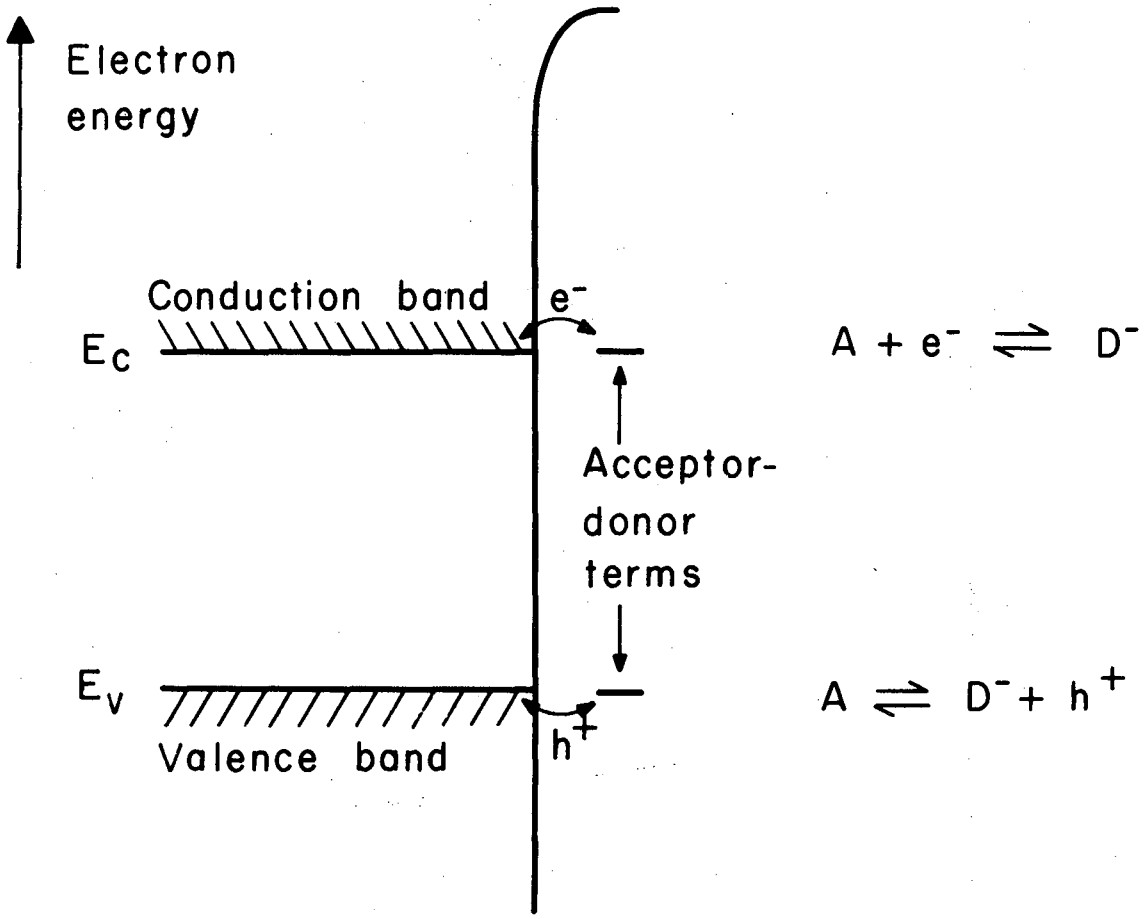

XBL683-2225

Fig. 12

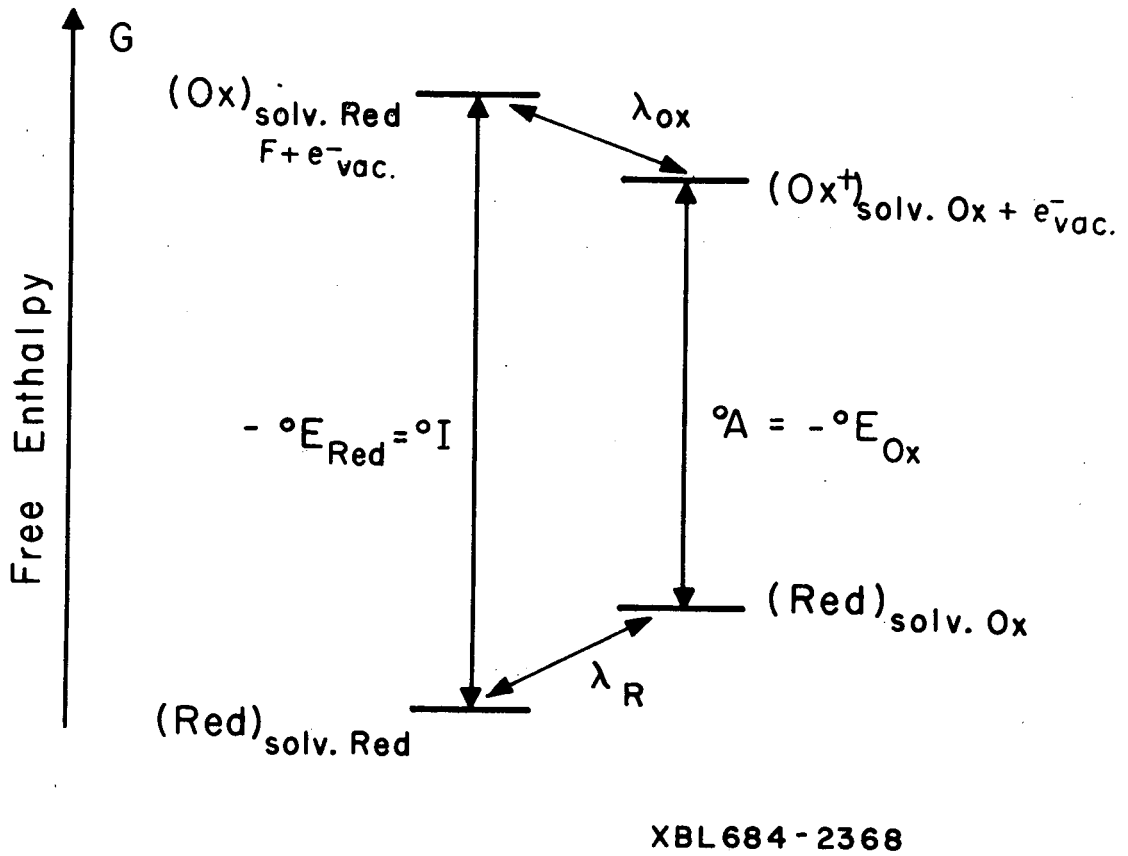
G
Free Enthalpy
(Ox)solv. Red
F+e⁻vac.
λox
(Ox⁺)solv. Ox + e⁻vac.
- °ERed = °I
°A = - °EOx
(Red)solv. Ox
λR
(Red)solv. Red
XBL684-2368

Fig. 13

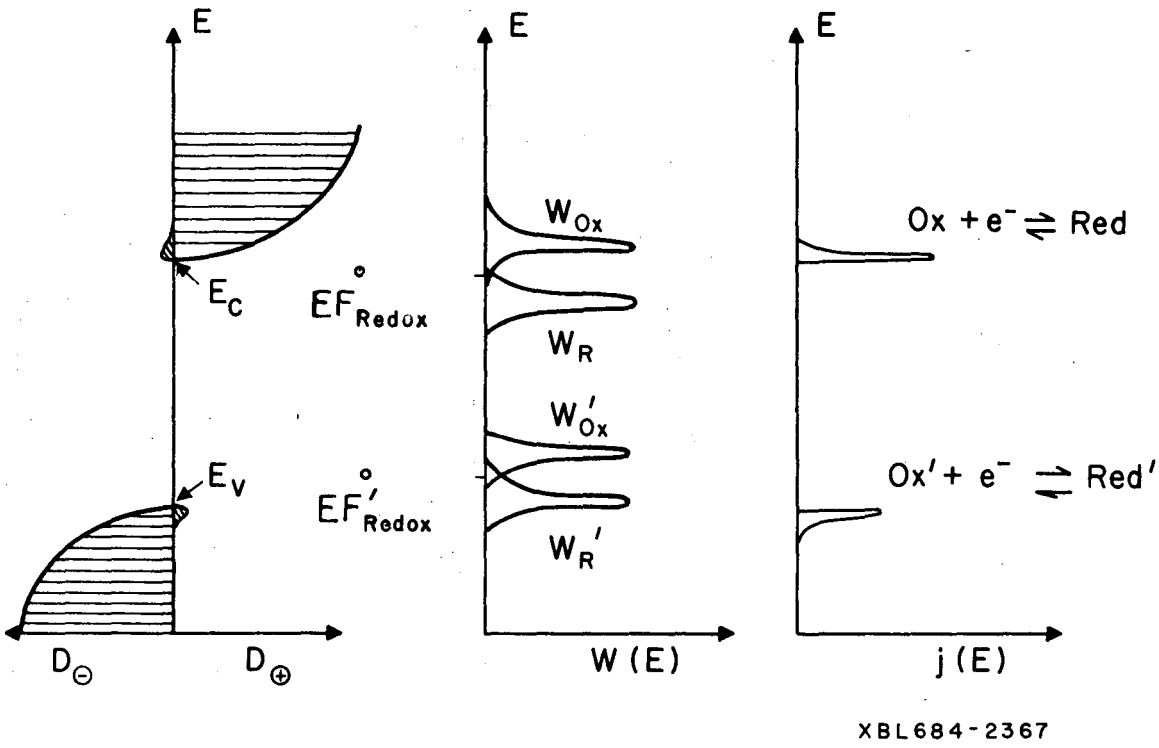
E
E
E
E_C
EF°_{Redox}
E_V
EF'°_{Redox}
$D_{\ominus}$
$D_{\oplus}$
W_{Ox}
W_R
W'_{Ox}
W'_R
W (E)
Ox + e⁻ ⇌ Red
Ox′ + e⁻ ⇌ Red′
j (E)
XBL684-2367

Fig. 14

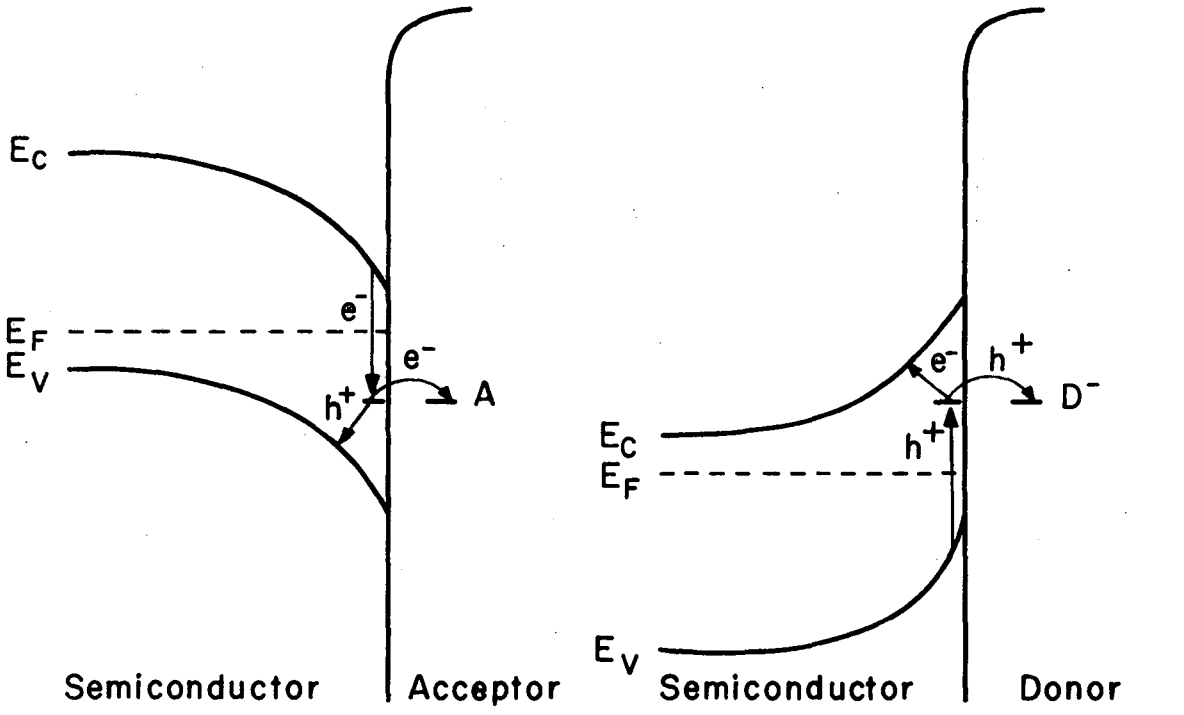

XBL681-2224

Fig. 15

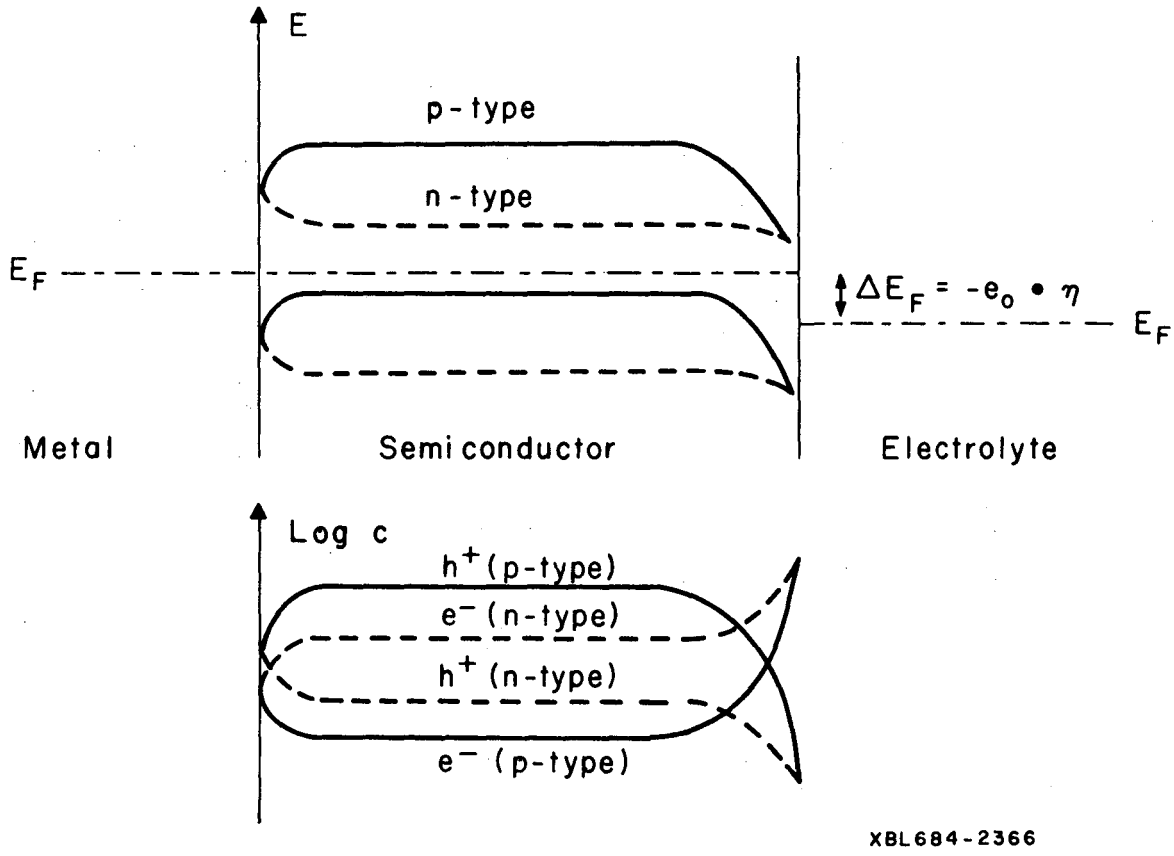
E
p-type
n-type
E_F
$\Delta E_F = -e_o \cdot \eta$
E_F
Metal
Semiconductor
Electrolyte
Log c
h^+ (p-type)
e^- (n-type)
h^+ (n-type)
e^- (p-type)
XBL684-2366

Fig. 16

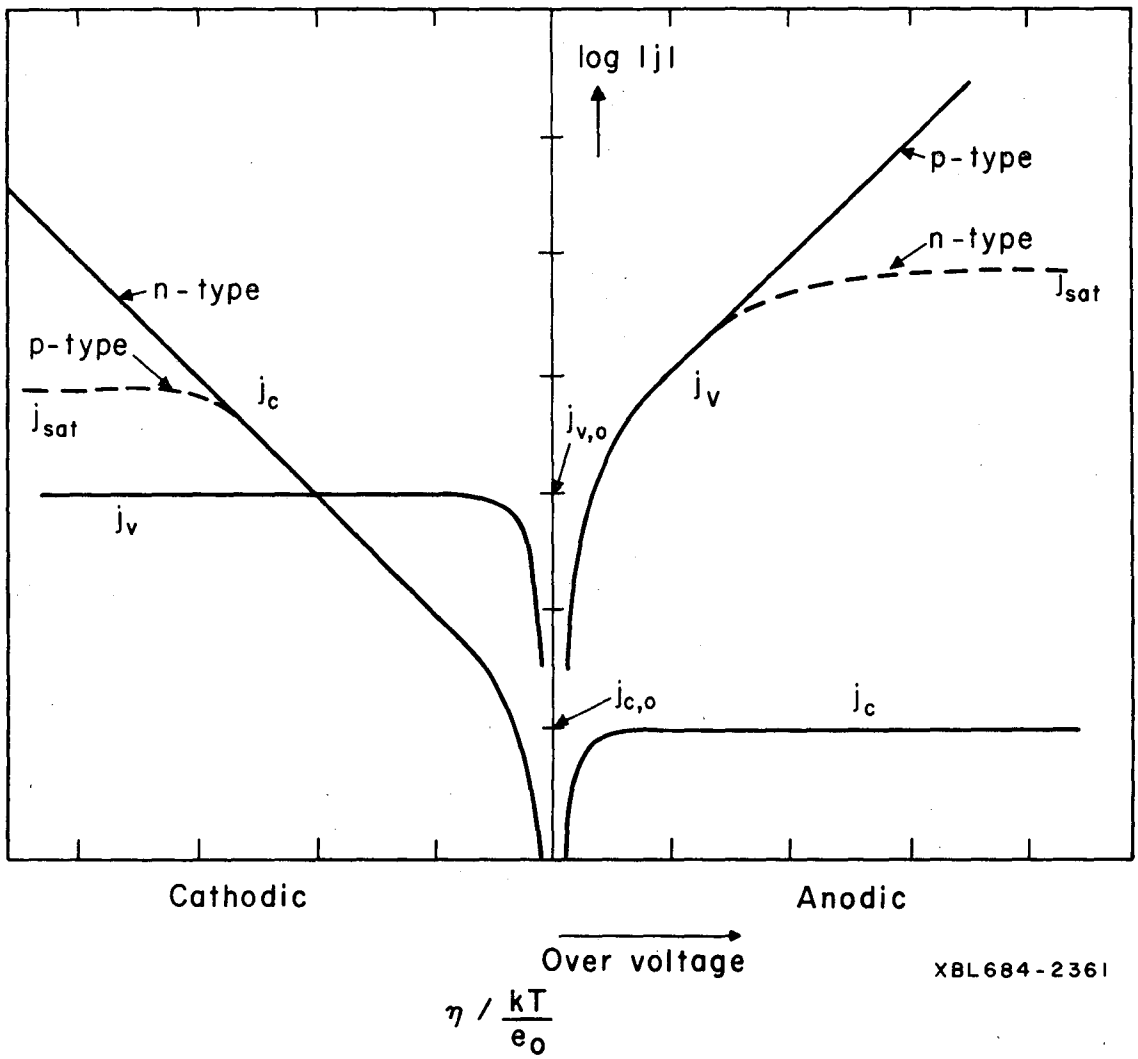
log |j|
p-type
n-type
j_{sat}
n-type
p-type
j_{sat}
j_c
$j_{v,o}$
j_v
j_v
$j_{c,o}$
j_c
Cathodic
Anodic
Over voltage
$\eta / \frac{kT}{e_o}$
XBL684-2361

Fig. 17

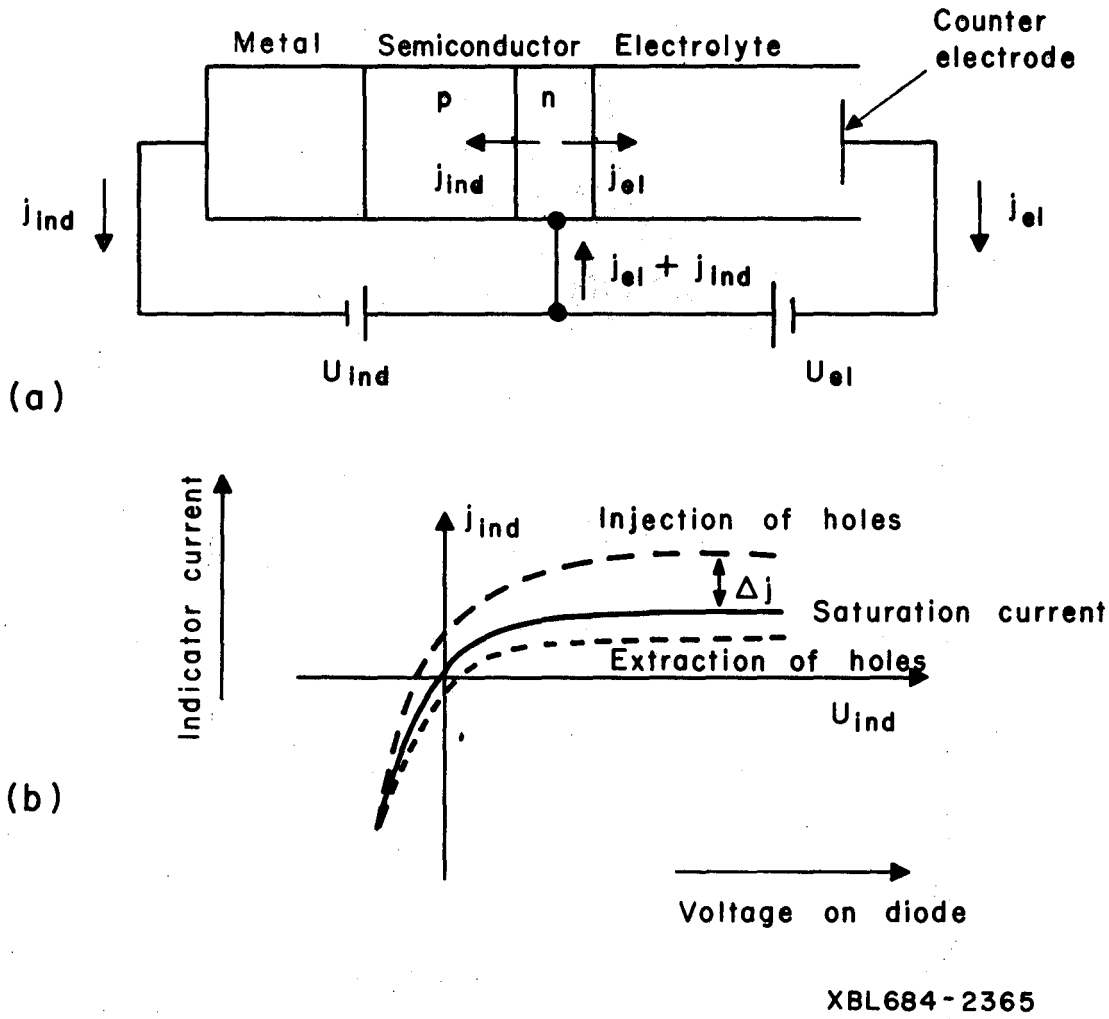
Metal
Semiconductor
Electrolyte
Counter electrode
p
n
j_{ind}
j_{el}
j_{ind}
j_{el}
$j_{el} + j_{ind}$
U_{ind}
U_{el}
(a)
Indicator current
j_{ind}
Injection of holes
Δj
Saturation current
Extraction of holes
U_{ind}
(b)
Voltage on diode
XBL684-2365

Fig. 18

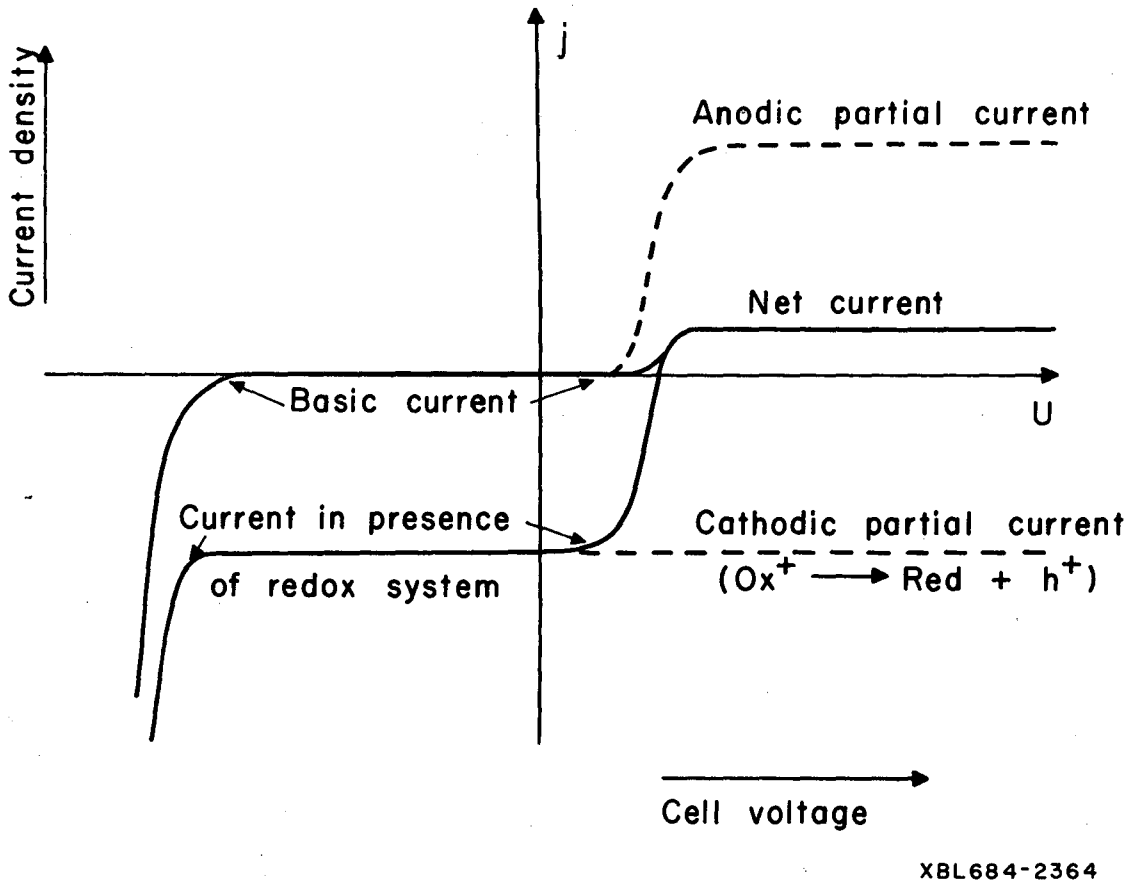
j
Current density
Anodic partial current
Net current
Basic current
U
Current in presence
of redox system
Cathodic partial current
(Ox+ → Red + h+)
Cell voltage
XBL684-2364

Fig. 19

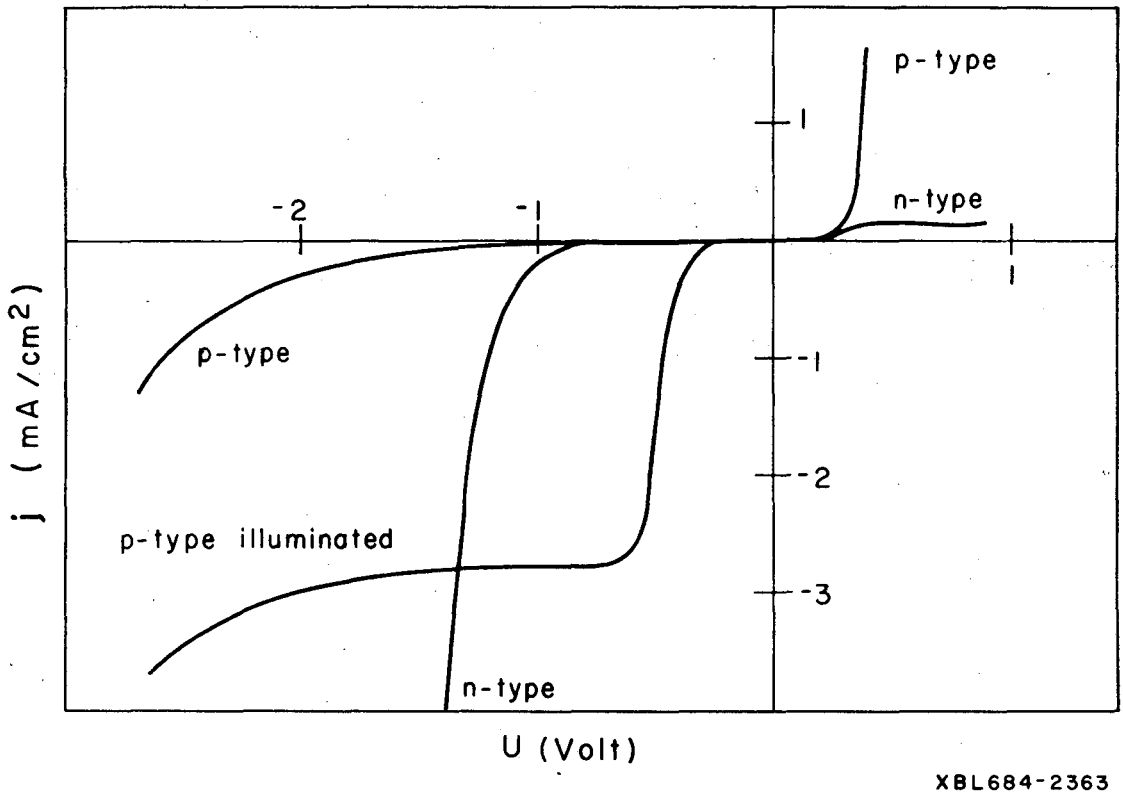
p-type
n-type
-2
-1
1
1
-1
-2
-3
p-type
p-type illuminated
n-type
j (mA/cm²)
U (Volt)
XBL684-2363

Fig. 20

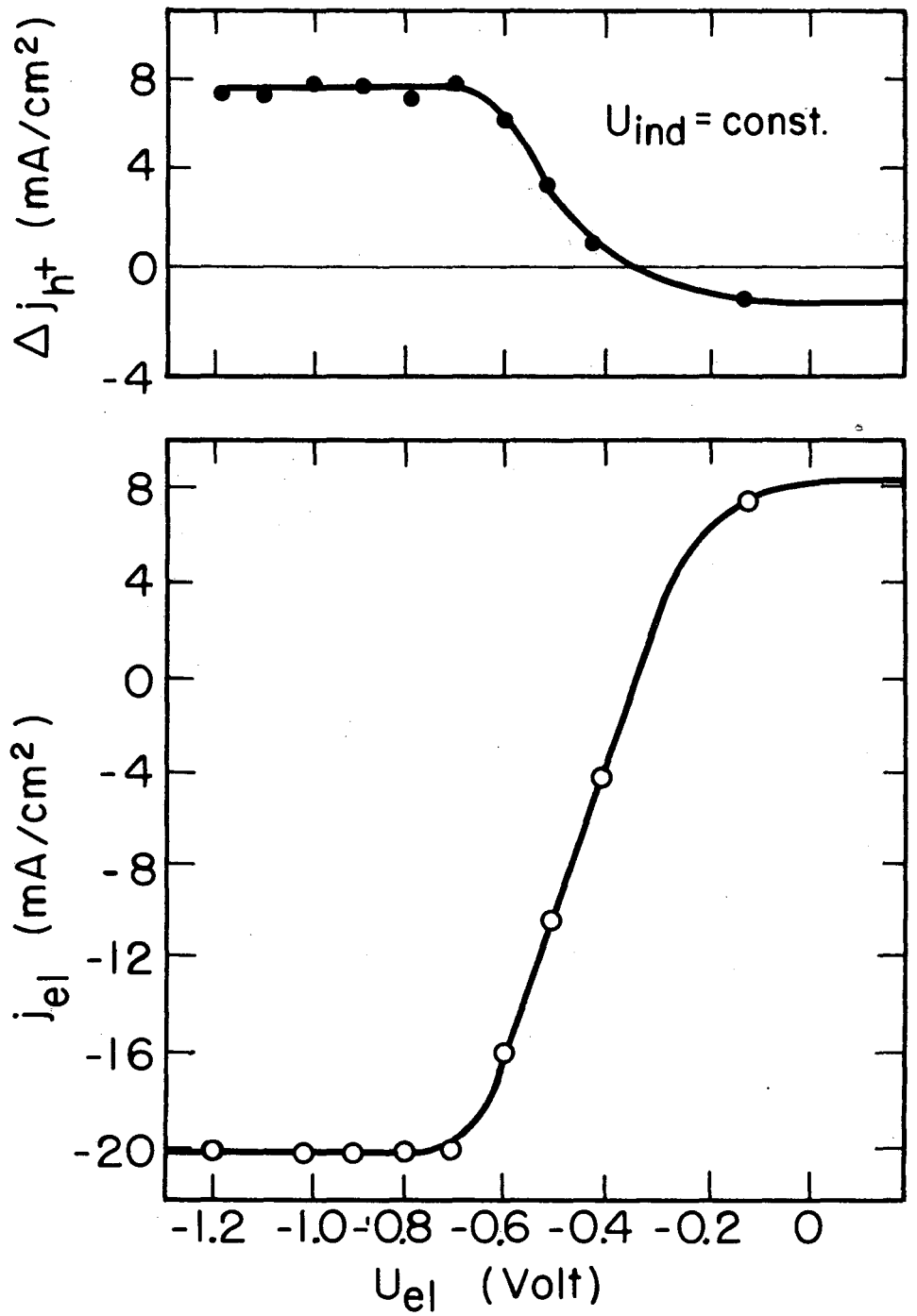

XBL689-6978

Fig 21

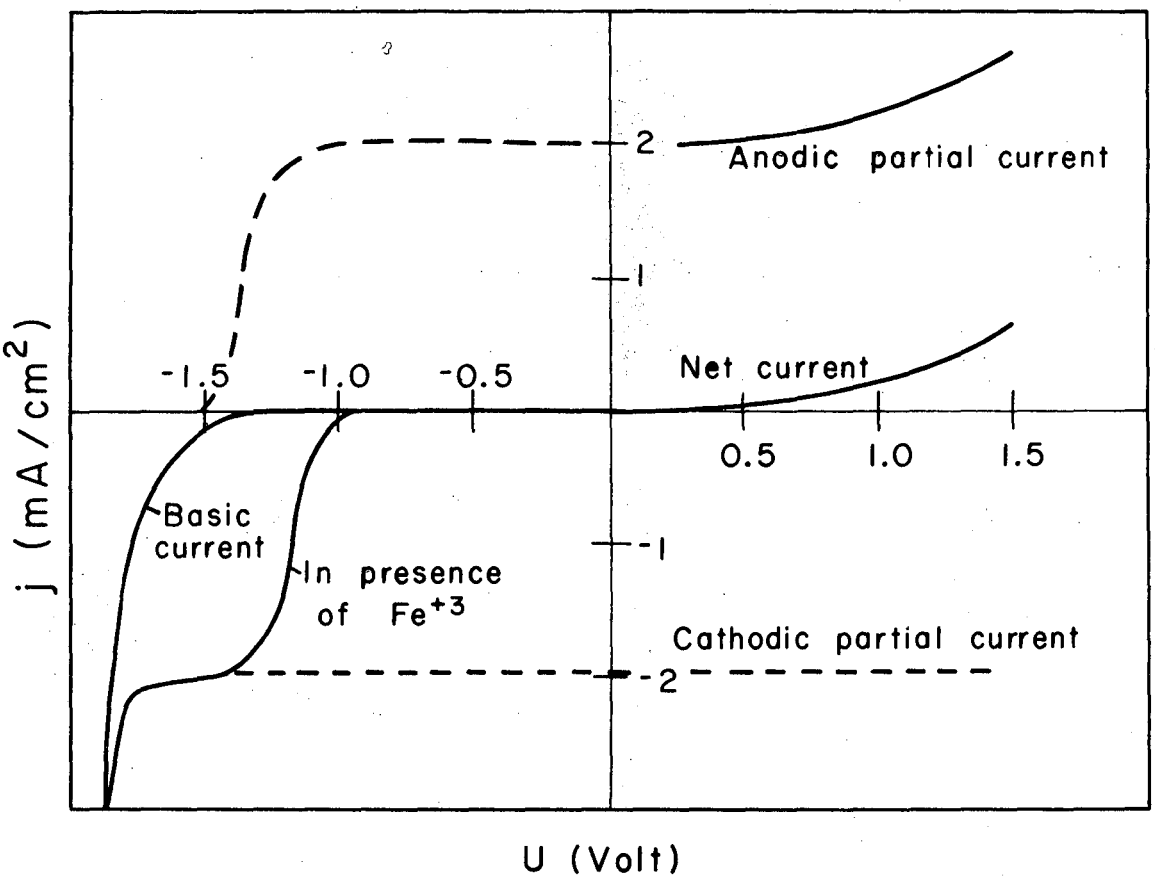
j (mA/cm²)
2
1
-1
-2
-1.5
-1.0
-0.5
0.5
1.0
1.5
Anodic partial current
Net current
Basic current
In presence of Fe+3
Cathodic partial current
U (Volt)
XBL684-2360

Fig. 22

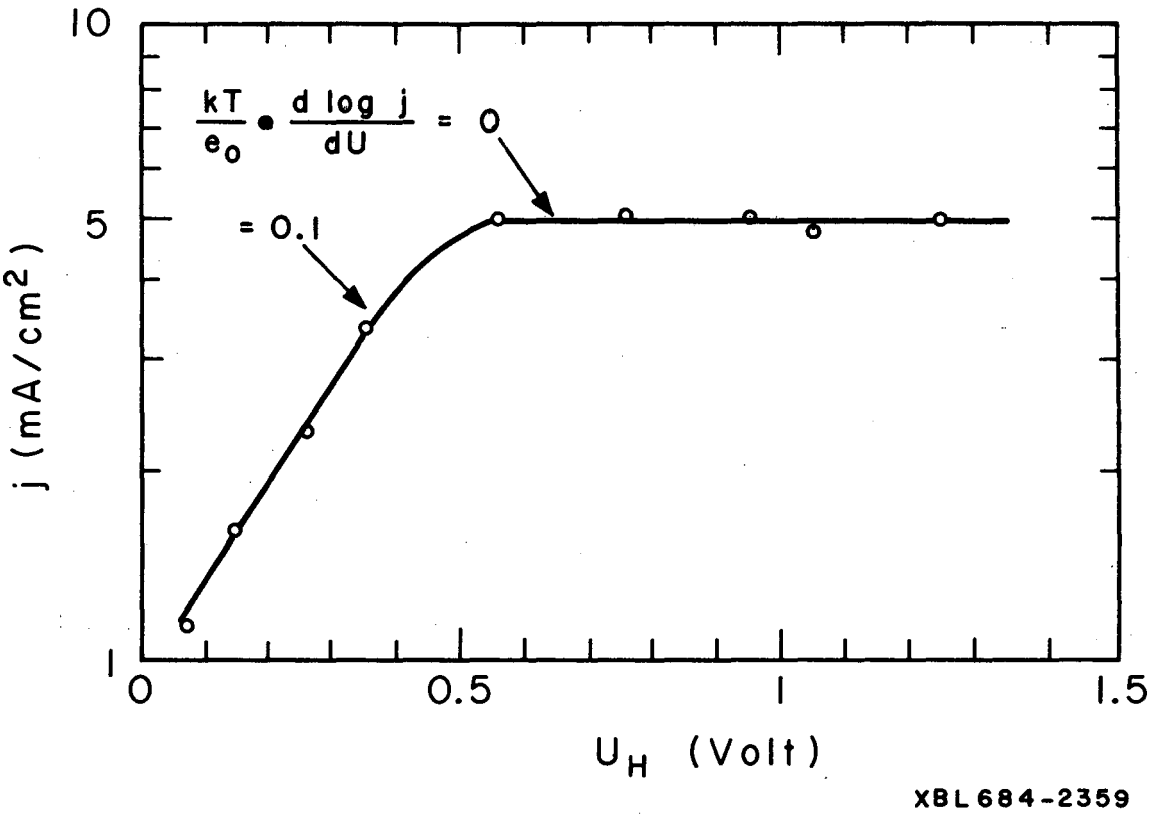
10
5
1
0
0.5
1
1.5
$\frac{kT}{e_o} \cdot \frac{d \log j}{dU} = 0$
= 0.1
j (mA/cm²)
U_H (Volt)
XBL684-2359

Fig. 23

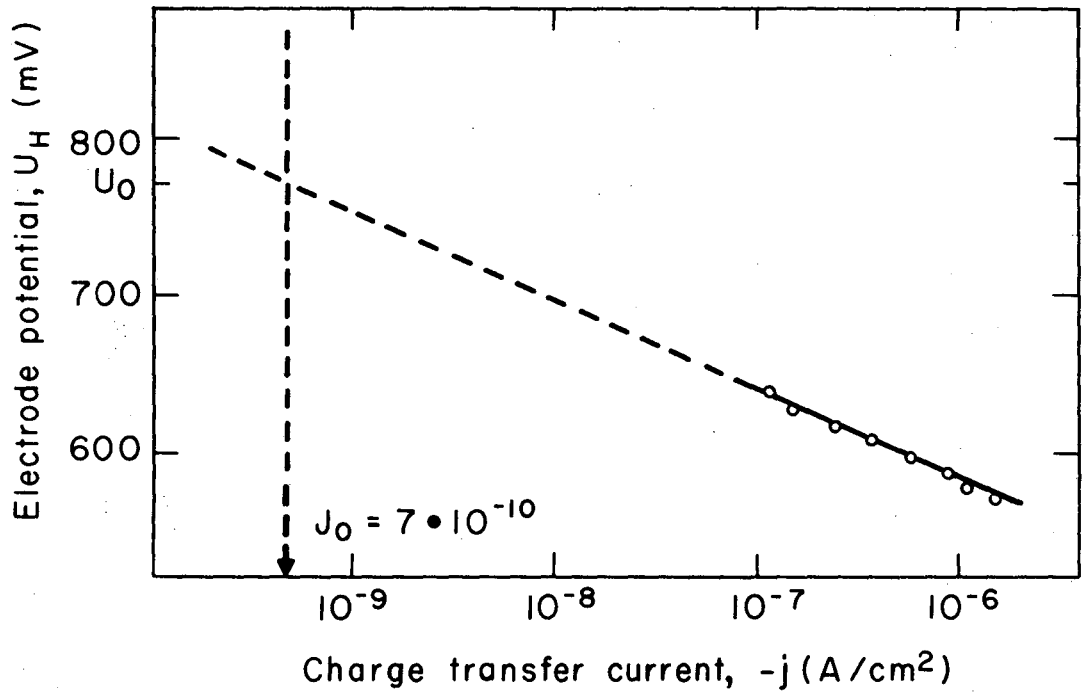
Electrode potential, U_H (mV)
800
U_0
700
600
$J_0 = 7 \cdot 10^{-10}$
10^{-9}
10^{-8}
10^{-7}
10^{-6}
Charge transfer current, -j (A/cm^2)
XBL684-2358

Fig. 24

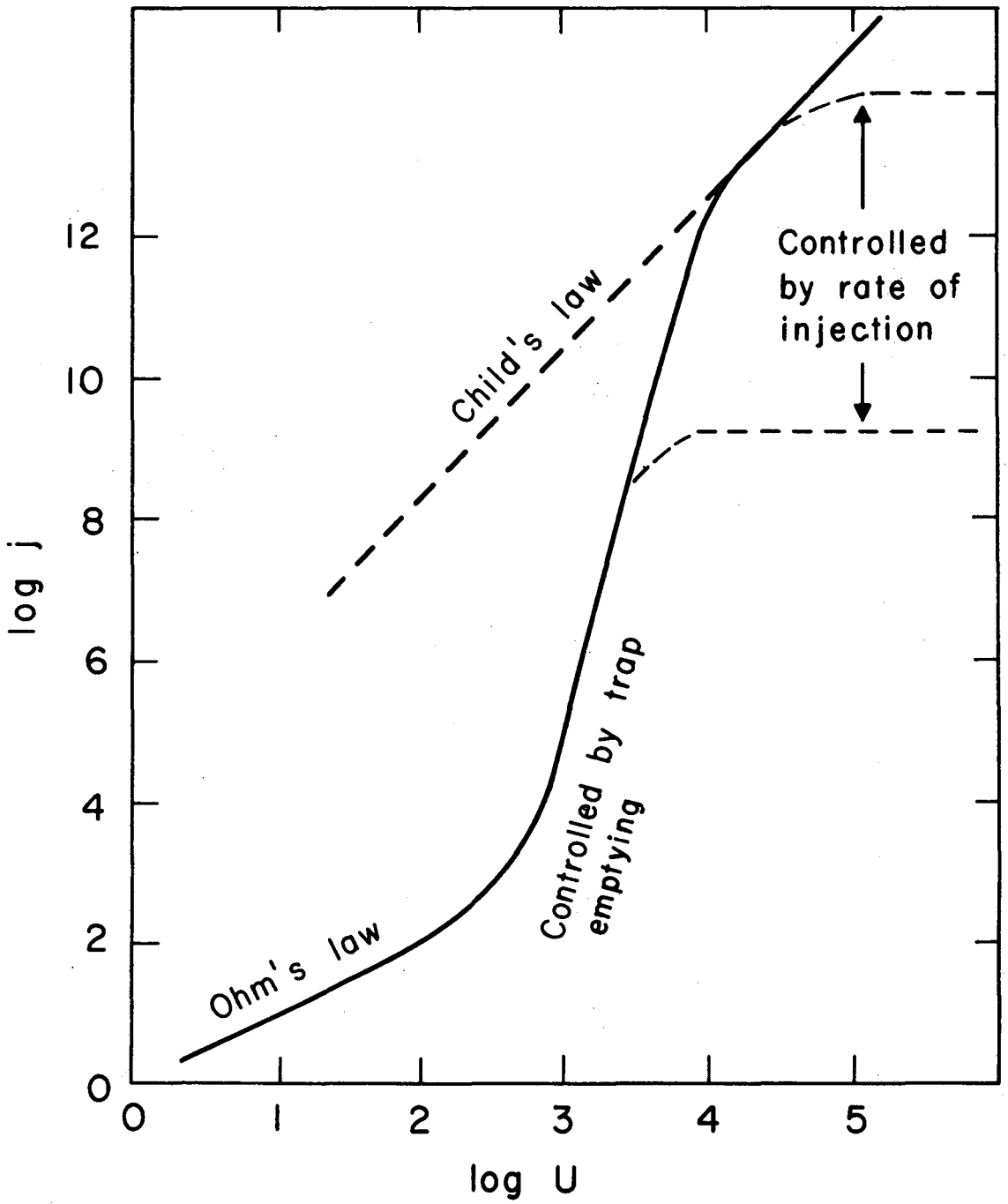
log j
log U
0
2
4
6
8
10
12
0
1
2
3
4
5
Child's law
Controlled by rate of injection
Controlled by trap emptying
Ohm's law
XBL684-2400

Fig. 25

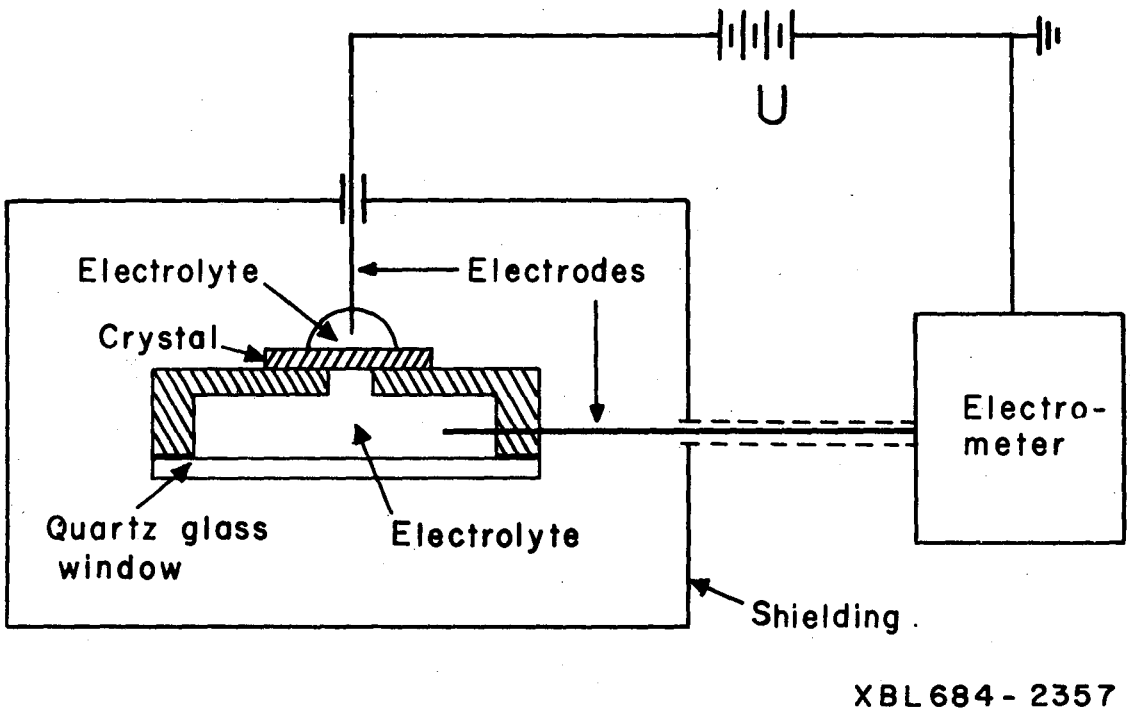
U
Electrolyte
Electrodes
Crystal
Electro-
meter
Quartz glass
window
Electrolyte
Shielding
XBL684-2357

Fig. 26

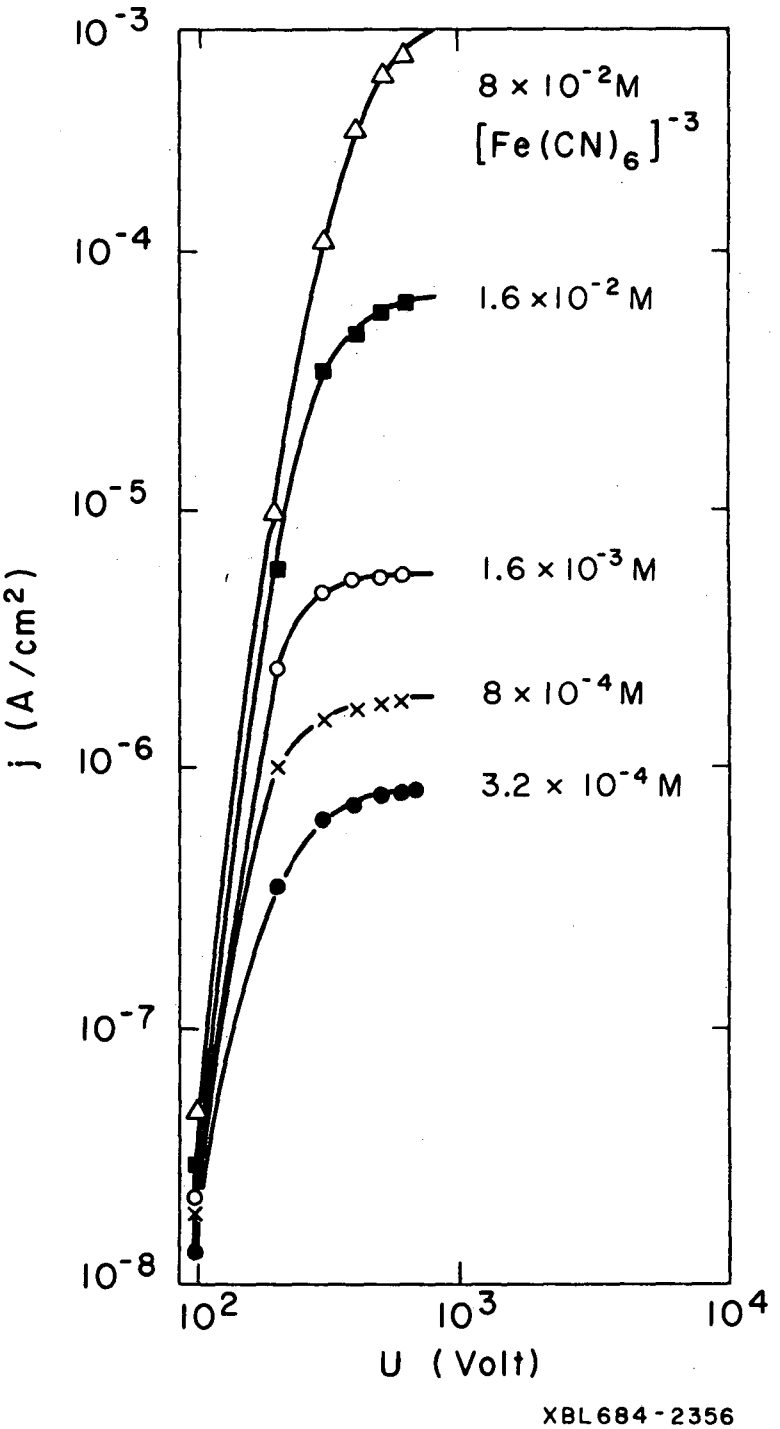
10^{-3}
10^{-4}
10^{-5}
10^{-6}
10^{-7}
10^{-8}
j (A/cm²)
8×10^{-2}M
$[Fe(CN)_6]^{-3}$
1.6×10^{-2} M
1.6×10^{-3} M
8×10^{-4} M
3.2×10^{-4} M
10^2
10^3
10^4
U (Volt)
XBL684-2356

Fig. 27

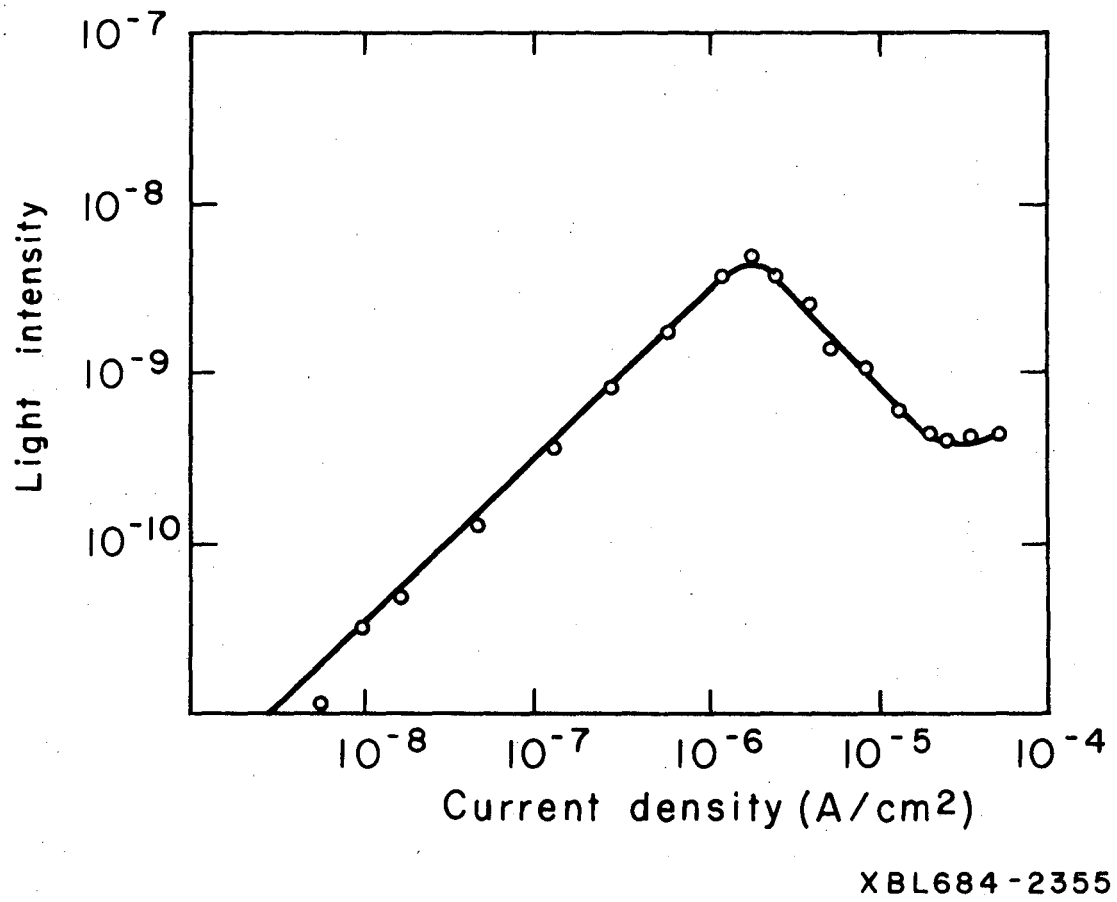
Light intensity
10-7
10-8
10-9
10-10
10-8
10-7
10-6
10-5
10-4
Current density (A/cm2)
XBL684-2355

Fig. 28

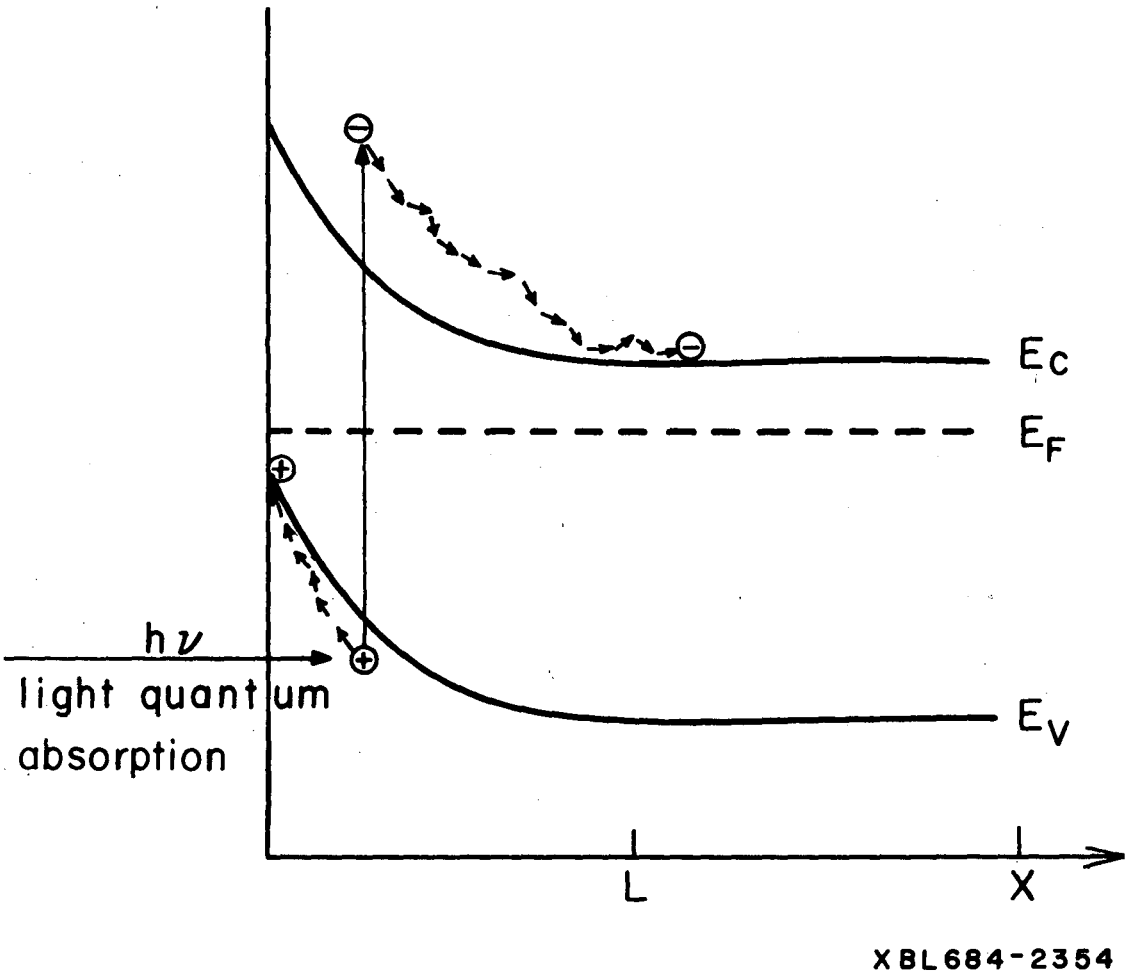

Fig. 29

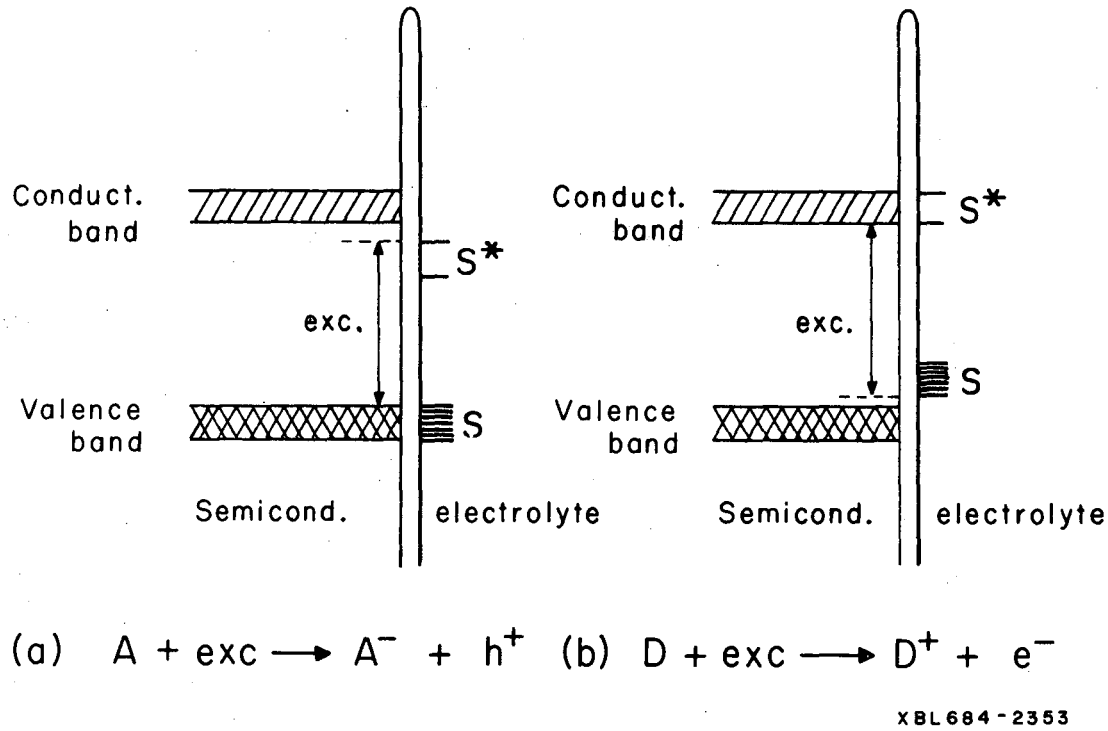
Conduct. band
S*
exc.
Valence band
S
Semicond.
electrolyte
Conduct. band
S*
exc.
S
Valence band
Semicond.
electrolyte
(a) A + exc ⟶ A⁻ + h⁺ (b) D + exc ⟶ D⁺ + e⁻
XBL684-2353

Fig. 30

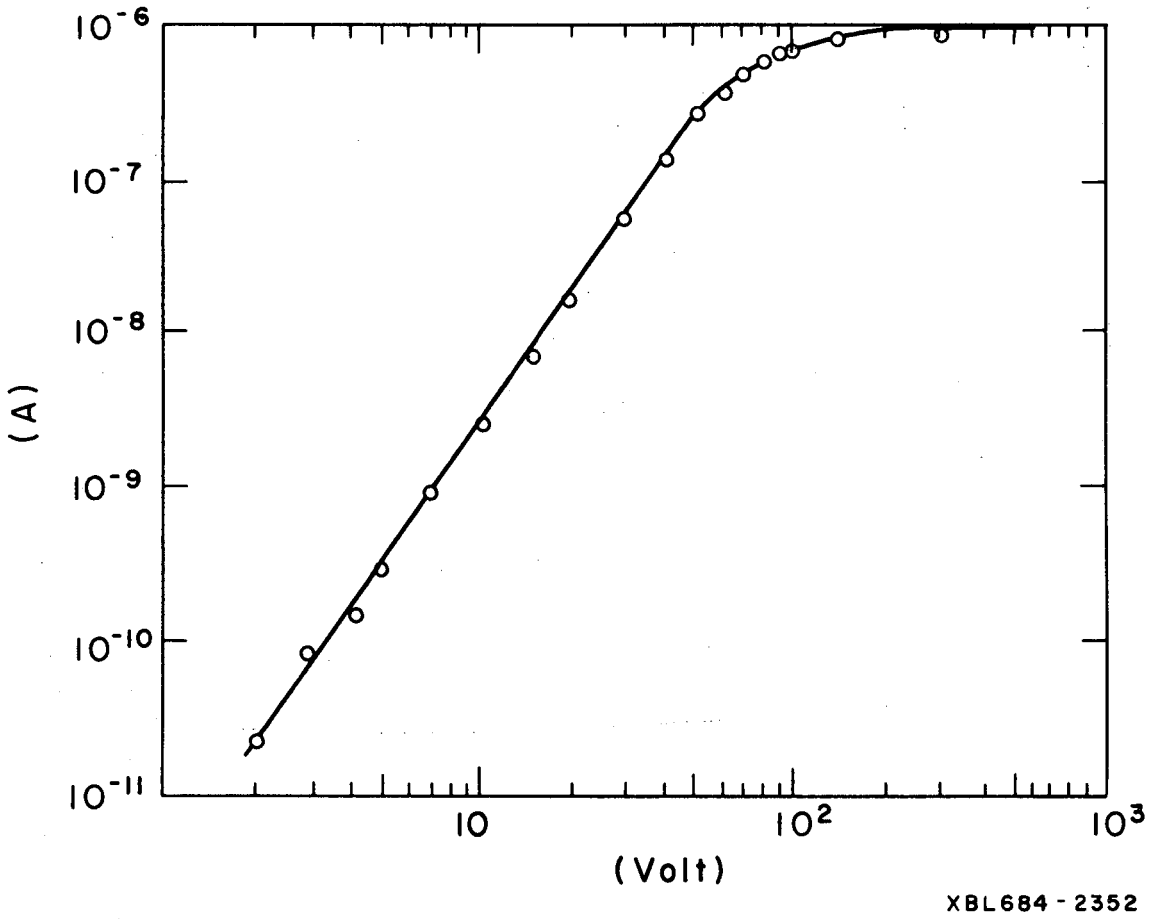

Fig. 31

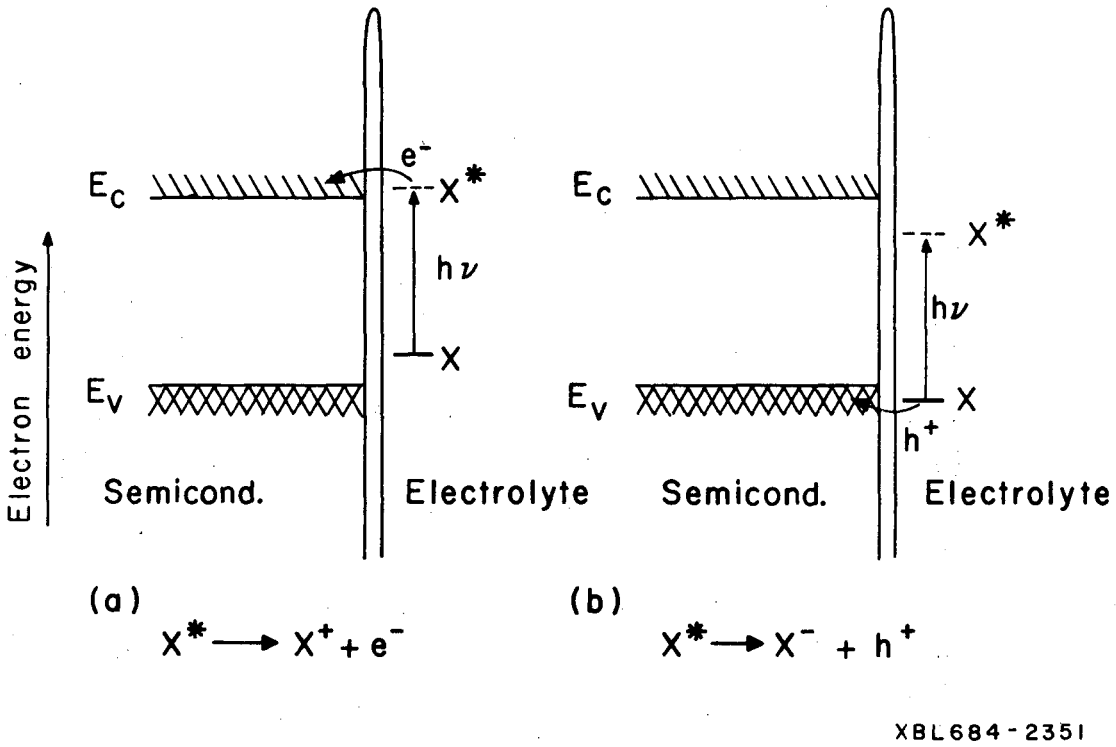

XBL684-2351

Fig. 32

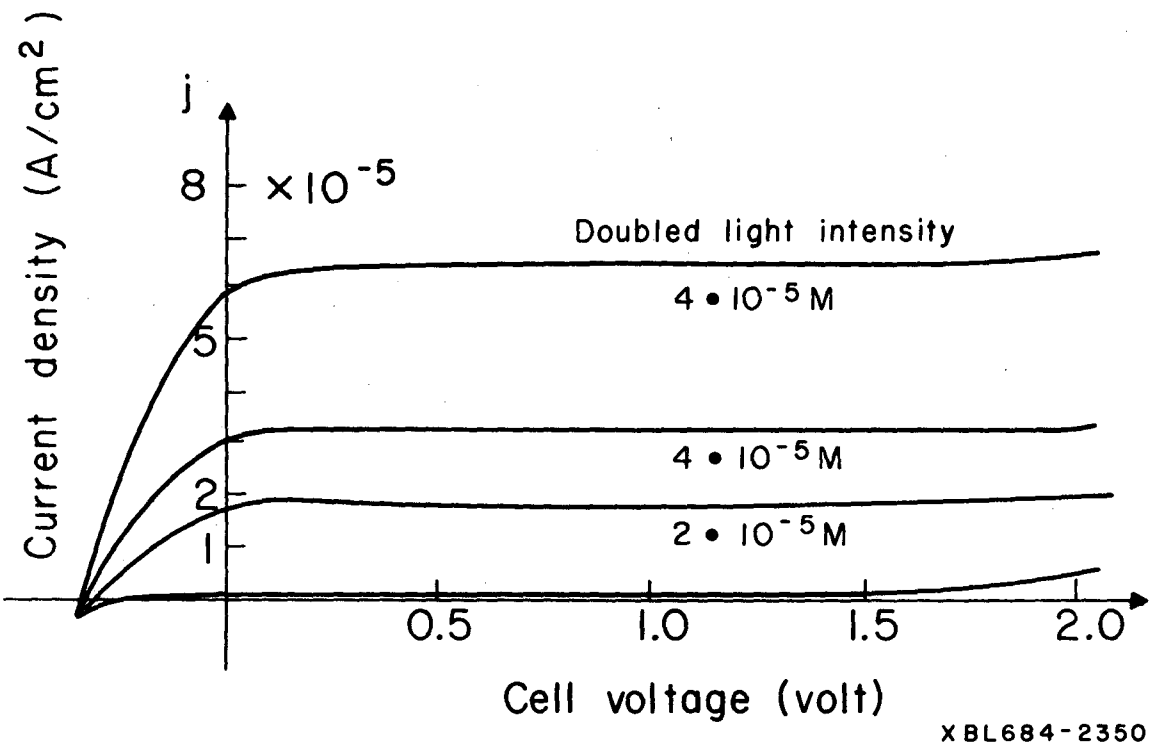
Current density (A/cm²)
j
8
×10⁻⁵
5
2
1
Doubled light intensity
4 • 10⁻⁵ M
4 • 10⁻⁵ M
2 • 10⁻⁵ M
0.5
1.0
1.5
2.0
Cell voltage (volt)
XBL684-2350

Fig. 33

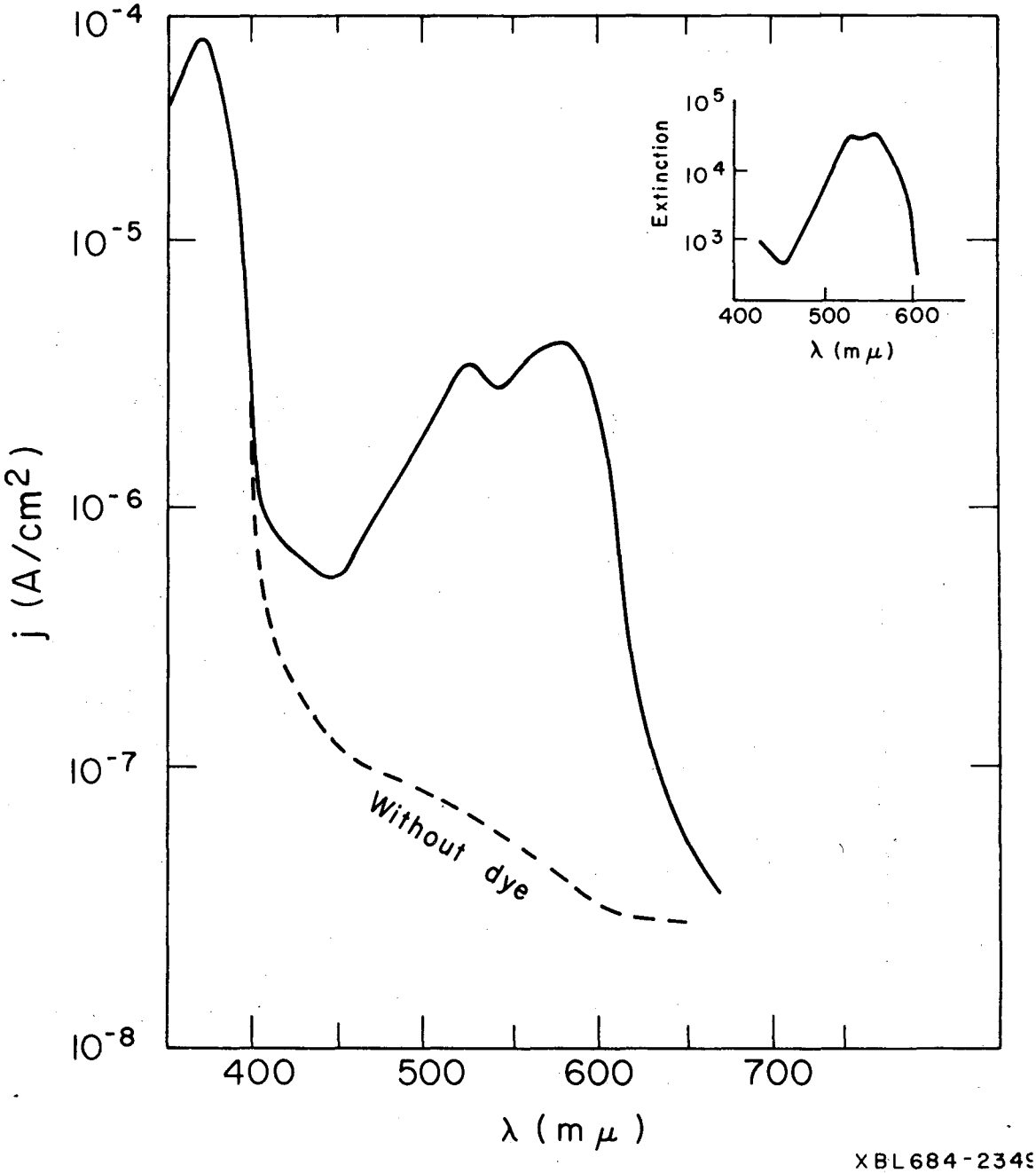
10^-4
10^-5
10^-6
10^-7
10^-8
j (A/cm^2)
400
500
600
700
λ (mμ)
Without dye
Extinction
10^5
10^4
10^3
400
500
600
λ (mμ)
XBL684-2349

Fig. 34

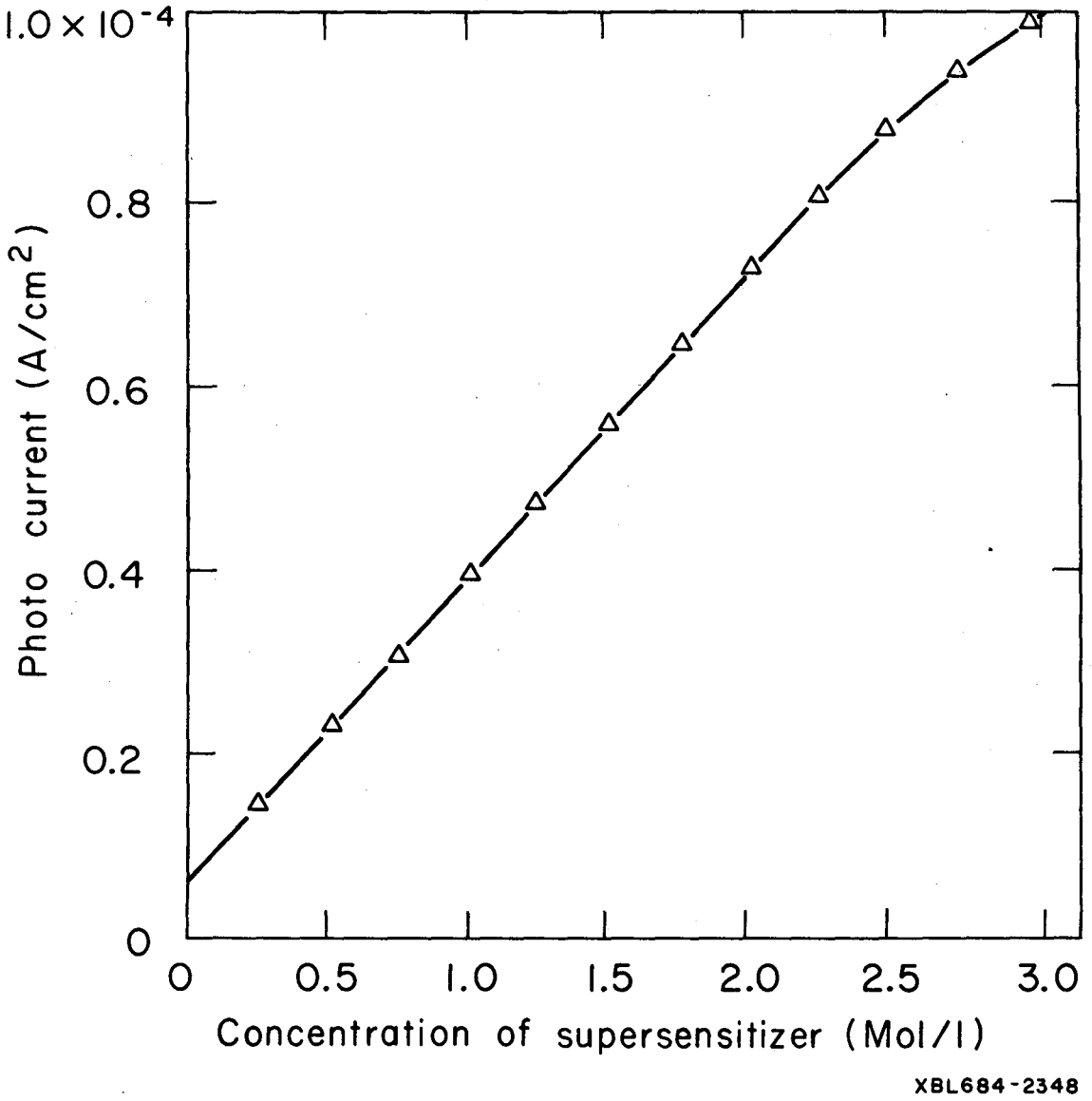
1.0 × 10⁻⁴
0.8
0.6
0.4
0.2
0
Photo current (A/cm²)
0
0.5
1.0
1.5
2.0
2.5
3.0
Concentration of supersensitizer (Mol/l)
XBL684-2348

Fig. 35

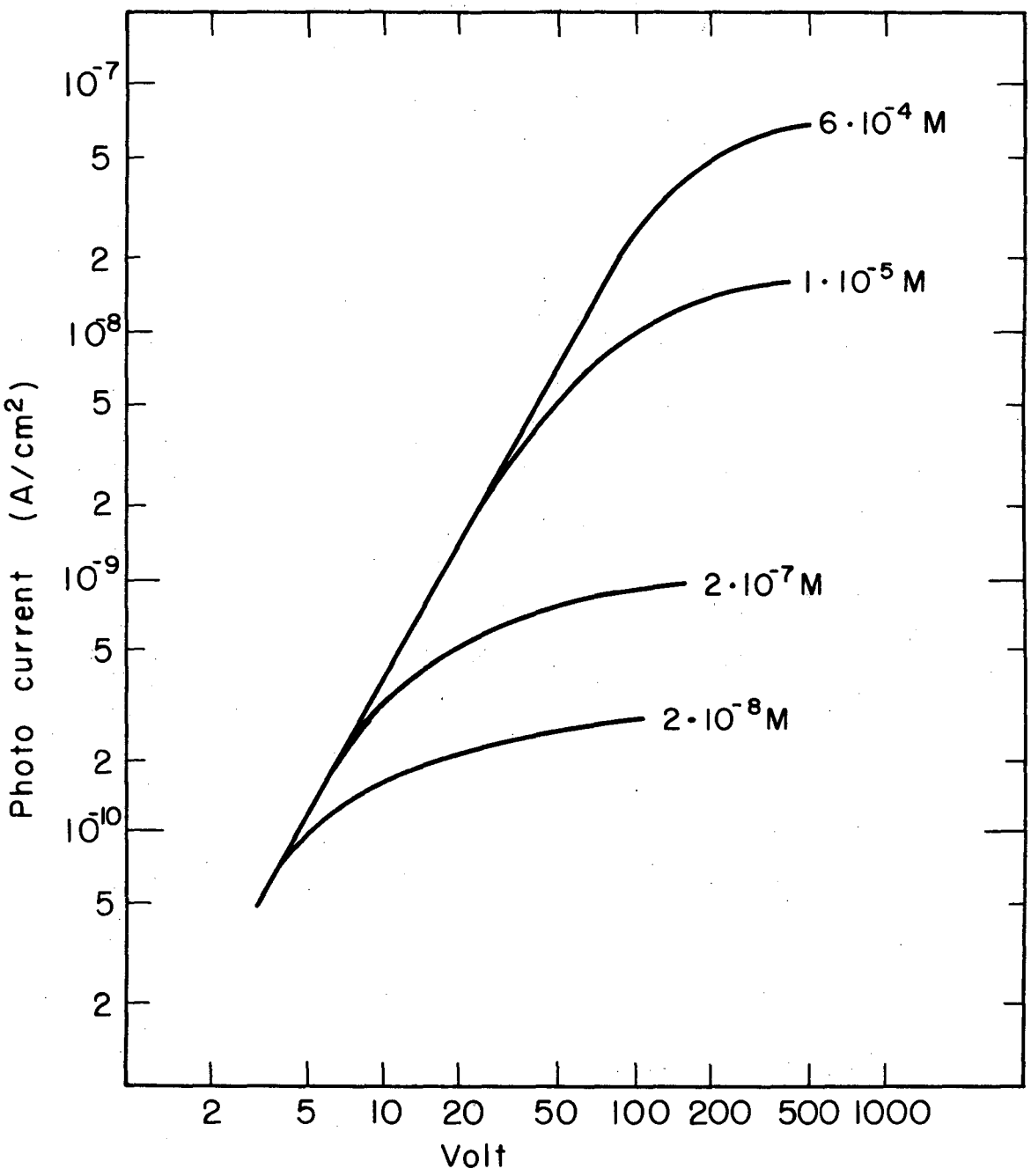

XBL689-6979

Fig. 36

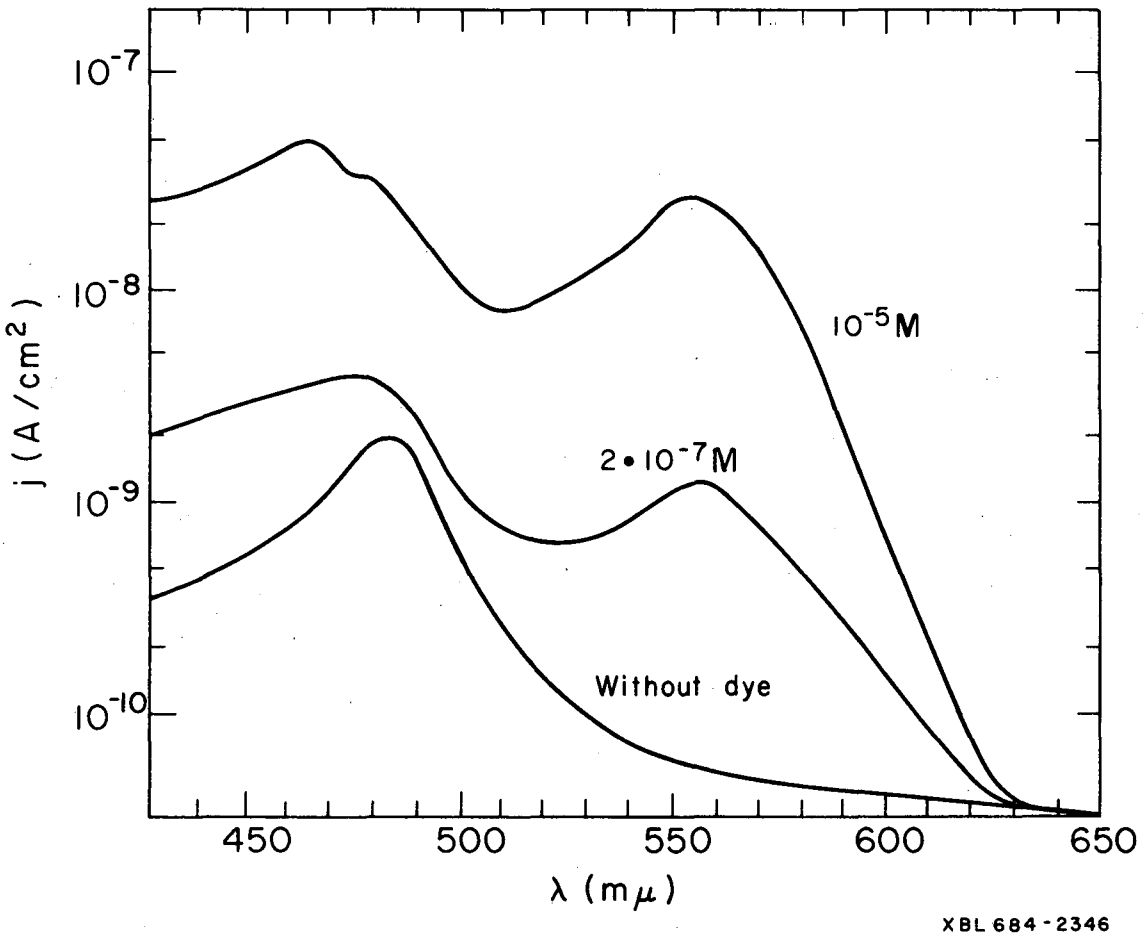
10^{-7}
10^{-8}
10^{-9}
10^{-10}
j (A/cm^2)
10^{-5}M
$2 \cdot 10^{-7}$M
Without dye
450
500
550
600
650
λ (mμ)
XBL 684-2346

Fig. 37

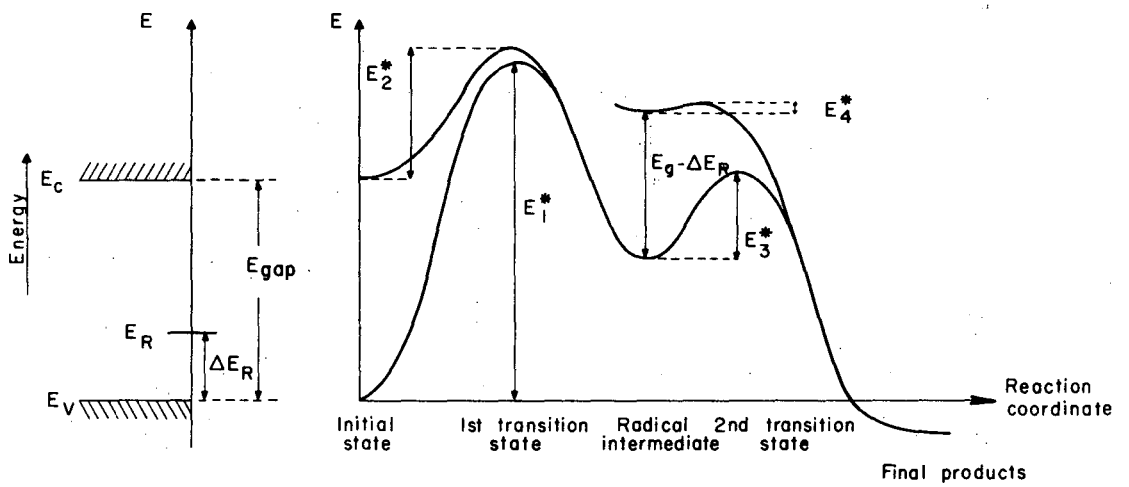
E
Energy
E_c
E_{gap}
E_R
ΔE_R
E_V
E
E_2^*
E_1^*
$E_g - \Delta E_R$
E_3^*
E_4^*
Initial state
1st transition state
Radical intermediate
2nd transition state
Final products
Reaction coordinate
XBL684-2345

Fig. 38

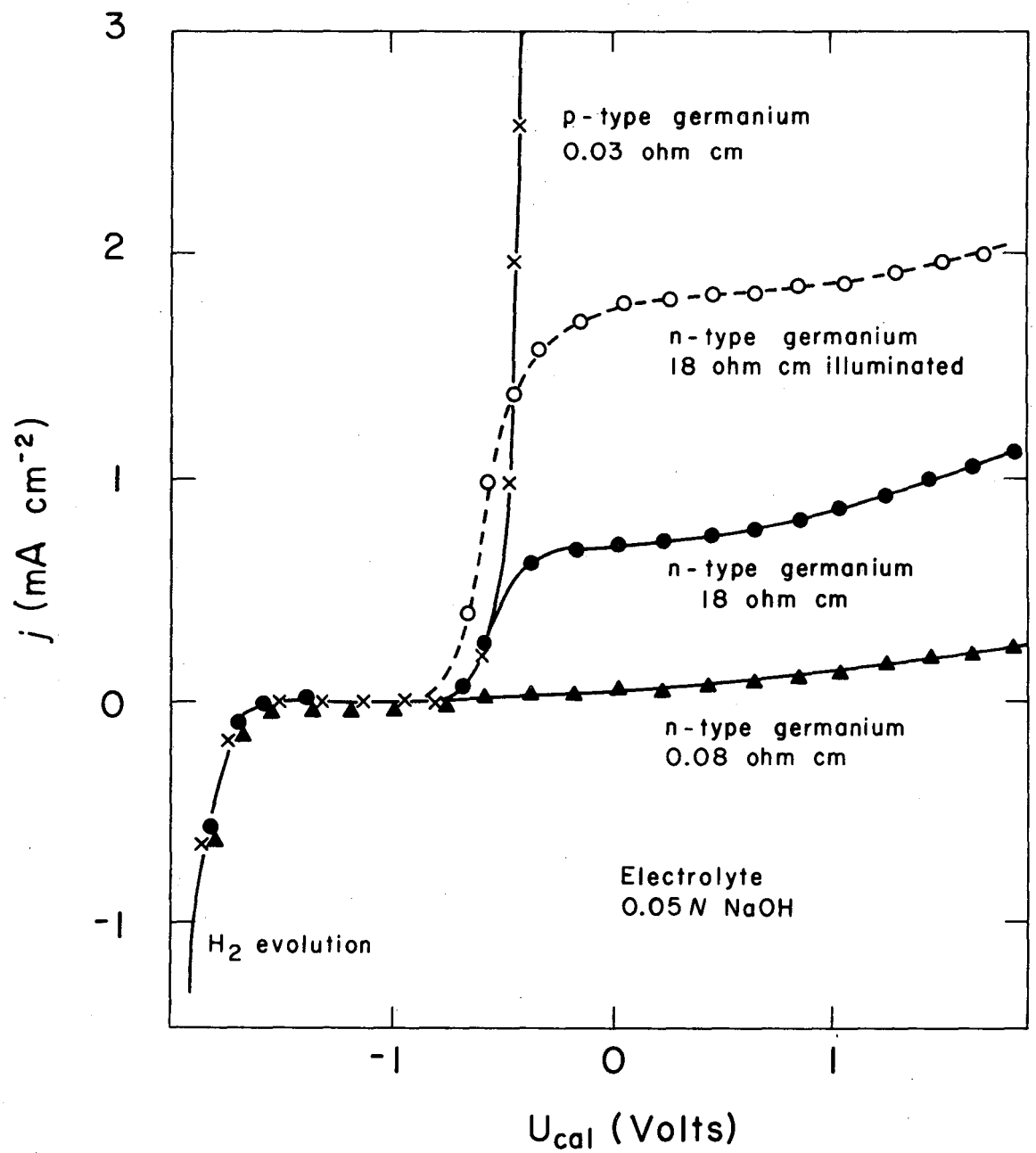
3
2
1
0
-1
j (mA cm-2)
p-type germanium
0.03 ohm cm
n-type germanium
18 ohm cm illuminated
n-type germanium
18 ohm cm
n-type germanium
0.08 ohm cm
Electrolyte
0.05 N NaOH
H2 evolution
-1
0
1
Ucal (Volts)
XBL684-2344

Fig. 39

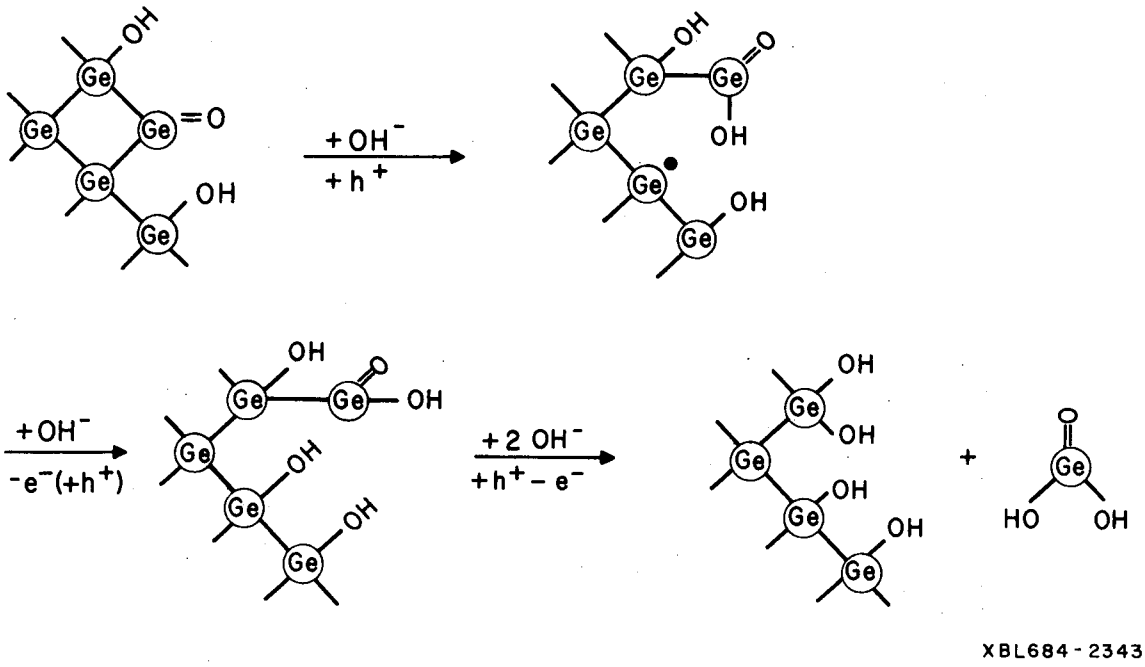

Fig. 40

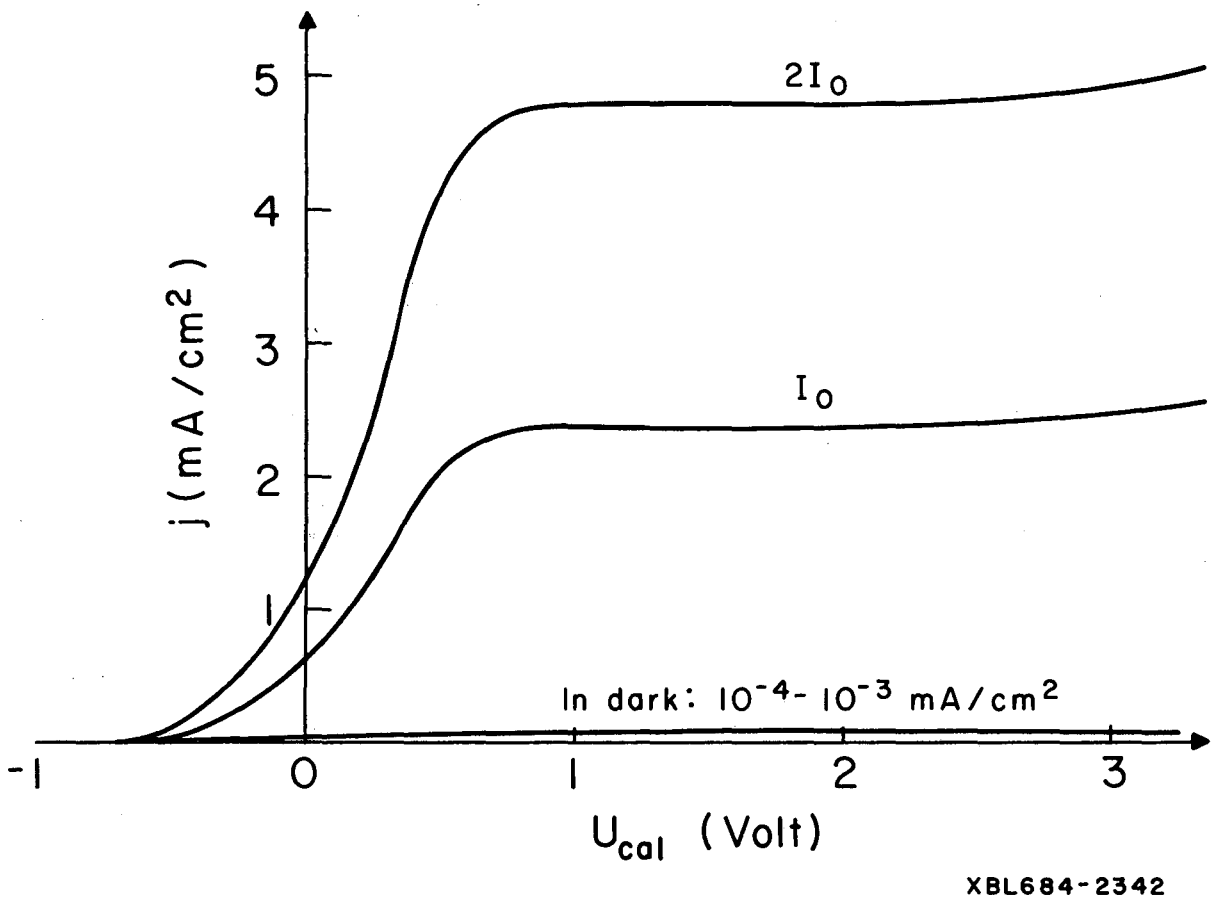
5
4
3
2
1
j (mA/cm²)
2I₀
I₀
In dark: 10⁻⁴- 10⁻³ mA/cm²
-1
0
1
2
3
U_cal (Volt)
XBL684-2342

Fig. 41

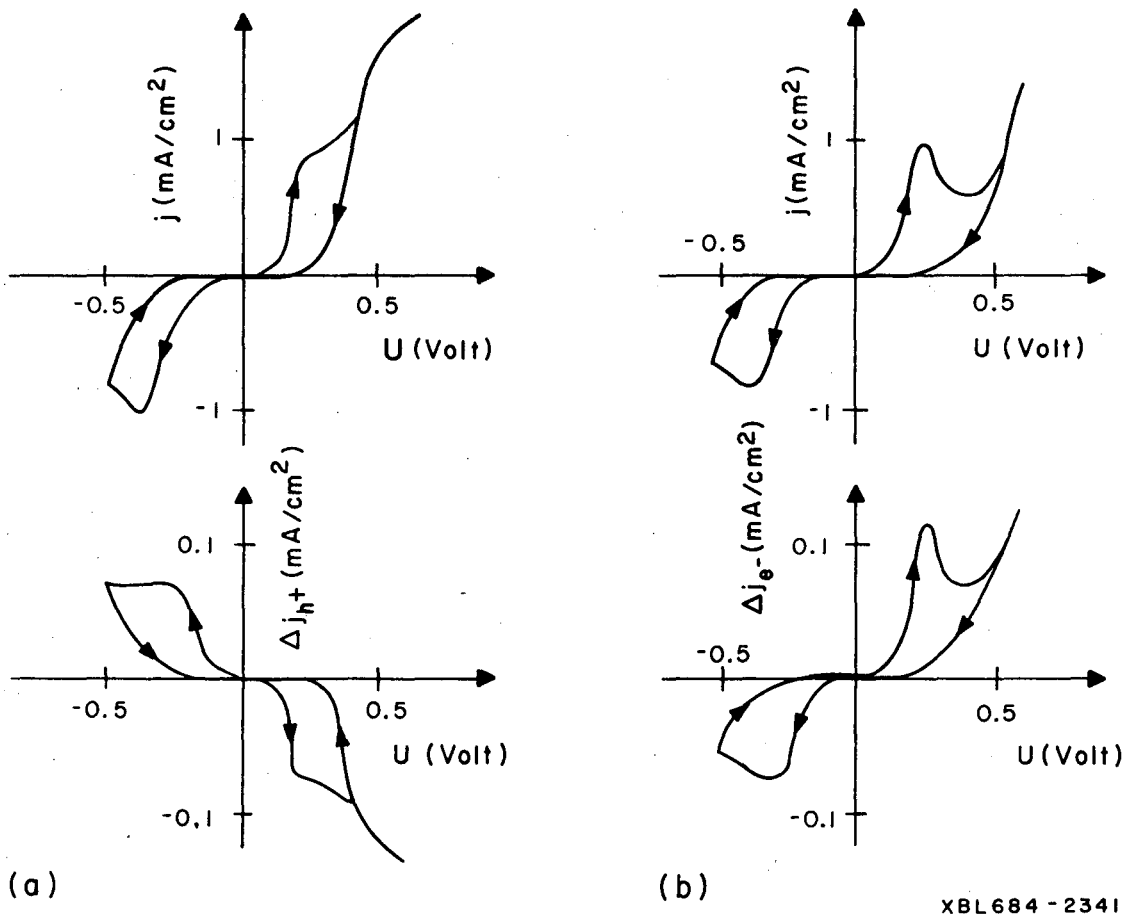
j (mA/cm²)
1
-0.5
0.5
U (Volt)
-1
Δj_h+ (mA/cm²)
0.1
-0.5
0.5
U (Volt)
-0.1
(a)
j(mA/cm²)
1
-0.5
0.5
U (Volt)
-1
Δj_e- (mA/cm²)
0.1
-0.5
0.5
U(Volt)
-0.1
(b)
XBL684-2341

Fig. 42

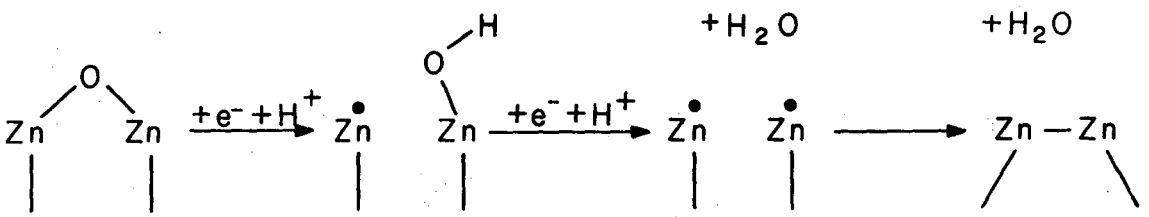

XBL683-2222

Fig. 43

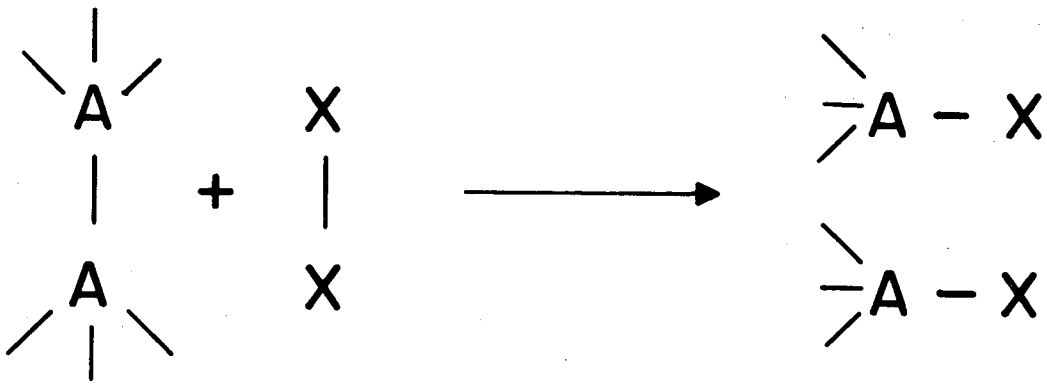

$X_2 = I_2, Br_2, Cl_2, H_2O_2$

XBL684-2340

Fig. 44

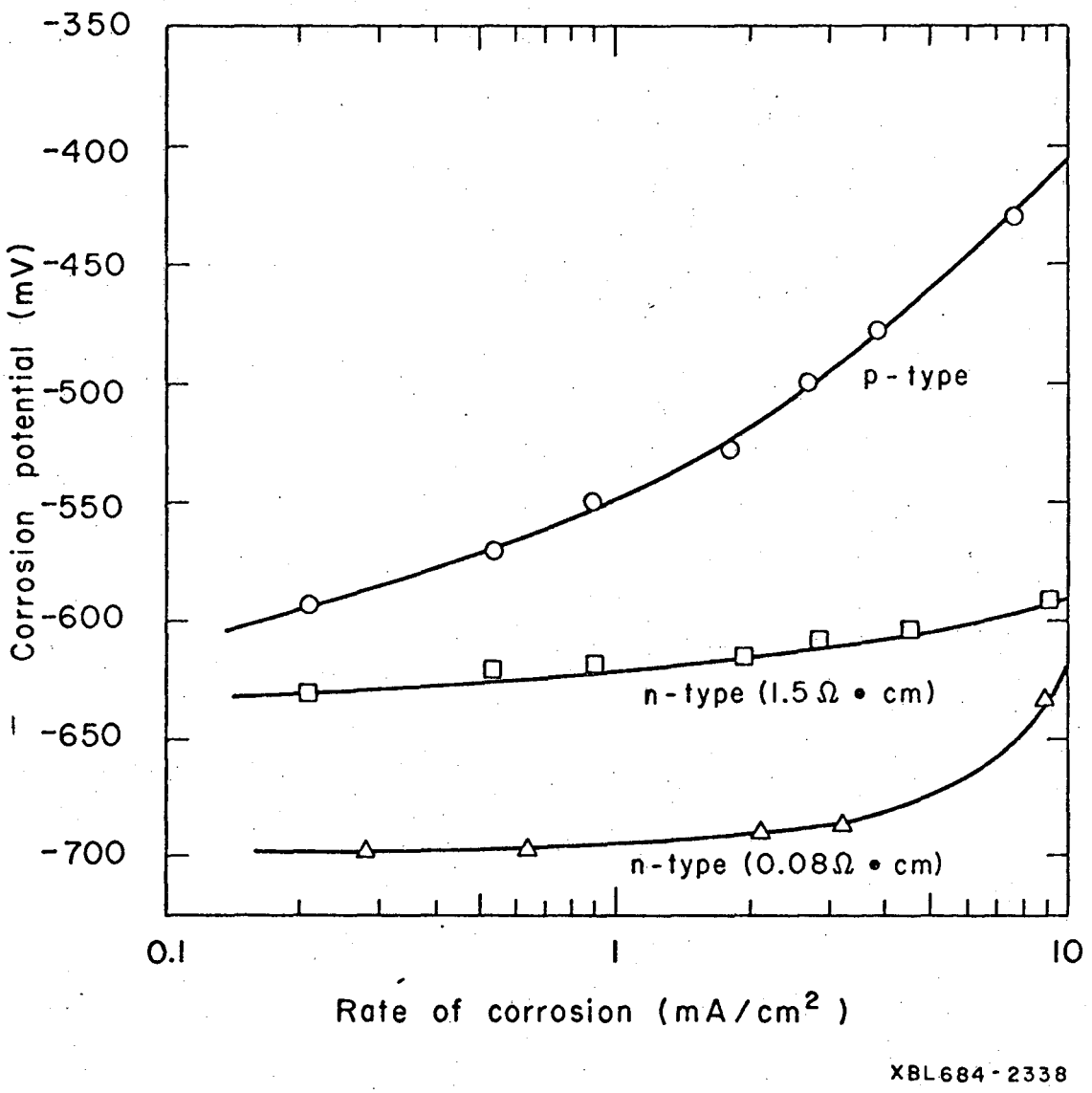
-350
-400
-450
-500
-550
-600
-650
-700
Corrosion potential (mV)
p - type
n - type (1.5 Ω • cm)
n - type (0.08Ω • cm)
0.1
1
10
Rate of corrosion (mA/cm²)
XBL684-2338

Fig. 45

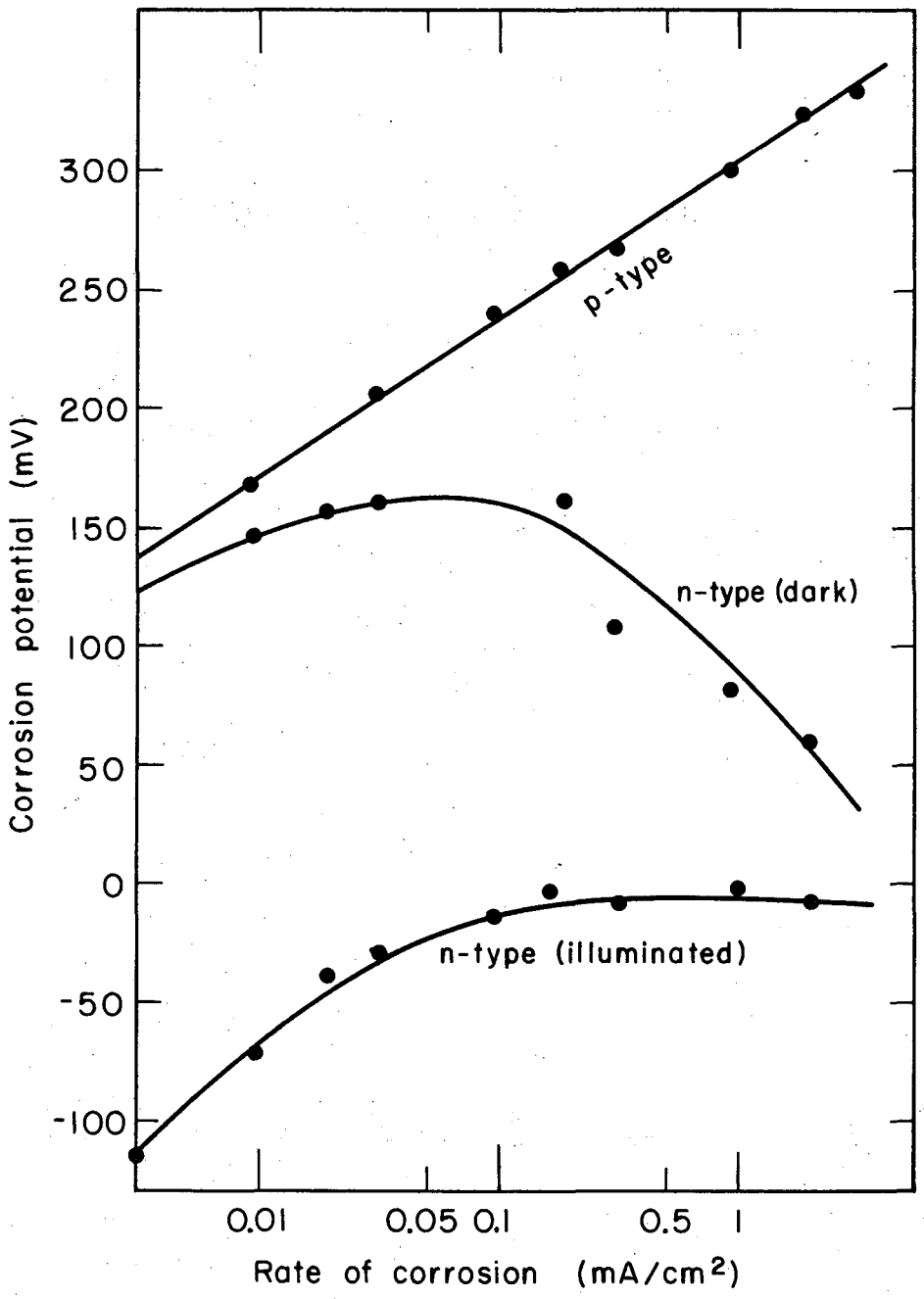
300
250
200
150
100
50
0
-50
-100
Corrosion potential (mV)
p-type
n-type (dark)
n-type (illuminated)
0.01
0.05
0.1
0.5
1
Rate of corrosion (mA/cm²)
XBL689-6980

Fig. 46